Winter 2012

A New Phase Speciation Leaching Procedure for the Determination of Metals in Oxic and Anoxic Sediments

Brandon R. Gipson
Old Dominion University

A NEW PHASE SPECIATION LEACHING PROCEDURE FOR THE DETERMINATION OF METALS IN OXIC AND ANOXIC SEDIMENTS

by

Brandon R. Gipson
B.S. May 2007, Old Dominion University

A Thesis Submitted to the Faculty of
Old Dominion University in Partial Fulfillment of the
Requirement for the Degree of

MASTER OF SCIENCE

OCEAN AND EARTH SCIENCES

OLD DOMINION UNIVERSITY
December 2012

Approved by:

Gregory A. Cutter (Director)

David J. Burdige (Member)

Peter N. Sedwick (Member)

ABSTRACT

A NEW PHASE SPECIATION LEACHING PROCEDURE FOR THE DETERMINATION OF METALS IN OXIC AND ANOXIC SEDIMENTS

Brandon R. Gipson
Old Dominion University, 2012
Director: Dr. Gregory A. Cutter

Toxic trace elements such as cadmium, lead, chromium, and arsenic released by human activities can accumulate in marine and estuarine sediments, where these metals are often sequestered until local environmental changes (e.g., redox, salinity, and/or pH) allow these elements to be reintroduced into the food web. In order to assess the extent of toxic trace element contamination in sediment, numerous leaching schemes have been developed that separate sediment-bound trace metals into operationally defined geochemical phases. These "phase speciation" leaching schemes are typically designed with the purpose of being used on either oxic or anoxic sediments. However, natural sediments often contain prominent redox boundaries; therefore, it is useful to develop a single phase speciation leaching scheme which can be used on both oxic and anoxic sediments.

A six step leaching scheme was developed in order to separate sediment-bound trace elements into five operationally defined phases: exchangeable, oxide, acid volatile sulfide (AVS), organic, and pyrite. The efficacy of five of the six leaching steps (oxide, AVS, organic #1 and #2, and pyrite) was evaluated using standard reference sediments (NIST 2702 and BCR-701) and actual sediment samples. Overall, the results show that the six step leaching process compared well with other frequently utilized phase speciation leaching schemes ("Tessier" and "optimized BCR"). With the exception of

some surface sediment oxides carrying over into the AVS phase, the leach AVS and pyrite results compared well with H_2S generation sediment sulfide analysis methods. The organic phase extractions were about three times more effective (~60% removal efficiency) at removing labile organic material (e.g., proteins and humic and fulvic acids) in sediment than refractory organics (e.g., protokerogens) (~20% removal efficiency). The six step leach method was applied to bulk sediments obtained from three estuaries with differing geochemical environments (salinity and sediment C and S concentrations). The sediment phase speciation results for the major (Fe, Mn, and Ca) and trace metals (Cd, Pb, Cr, and As) of interest are similar to those reported by other workers for similar environments, with the majority of the trace metals being located in the oxide and organic phases.

This thesis is dedicated to my parents, Melvin and Malinda Gipson.

ACKNOWLEDGEMENTS

I would like to thank the numerous graduate and undergraduate students from the Cutter Lab for their help with my project over the years. I also want to thank my advisor, Greg Cutter, for the opportunity to gain valuable experience working in the field of Chemical Oceanography. I am also grateful for the guidance given to me by my committee over the past several months. Finally, I want to thank my parents for their love, patience, and never-ending faith in me and what I can accomplish.

TABLE OF CONTENTS

Page

Chapter Page

LIST OF TABLES

LIST OF FIGURES

Figure Page

Figure

Page

CHAPTER 1

INTRODUCTION AND BACKGROUND

1.1. Introduction

Marine and estuarine sediments can serve as repositories for anthropogenic organic and inorganic contaminants from land-based pollution sources. Many of these substances are toxic metallic and semi-metallic elements that are released through industrial activity and improper disposal of urban waste. Once introduced into a watershed, these elements can become chemically bound to sediment particles, decreasing their overall bioavailability to benthic organisms (Sundelin and Eriksson, 2001; Fan and Wang, 2001). However, these elements can be subsequently reintroduced into the food web by the re-suspension of sediment by anthropogenic changes in the local environment, such as dredging and filling, or by natural forces, such as major storm events. This re-suspension can cause local changes in pH, salinity, redox conditions, and the overall concentration of available organic complexing agents, all of which have the potential to increase the bioavailability of trace metals in sediments (Forstner, and Salomons, 1991; Fan and Wang, 2001; Gambrell et. al., 1980; Morse, 1994).

When released into the environment in sufficient amounts, toxic elements can pose a serious threat to human health via the consumption of contaminated seafood and crops irrigated with polluted water (Von Burg and Greenwood, 1991; Nogawa and Ishizak, 1979; Lui et. al., 2007). Elevated levels of toxic metals such as Cd, Cr, Pb, and As in sediments can lead to increased concentrations of these elements in benthic organisms (e.g., clams, mussels, oysters, polychaete worms) that are frequently consumed by higher organisms (Ke and Wang, 2001; Lee et. al., 2000; Luoma and Bryan, 1978;

Pempkowjak, 1999; Warren et. al., 1998; Oshida and Word, 1982; Casado-Martinez et. al., 2010). In addition, some of these metals can be transferred up trophic levels, causing elevated and potentially toxic concentrations of these elements in the food web (Bull et. al., 1983; Kirby and Maher, 2002) Therefore, it is important to understand how the total exposure to toxic elements in sediments relates to the degree of uptake by benthic organisms. In order to asses this, the phase speciation of these trace metals in sediment must be taken into account.

Not only are the total concentrations of toxic trace elements in sediment important for assessing the degree of exposure for benthic organisms, but also the chemical phases that these elements are associated with in sediment (or phase speciation) are crucial for determining their potential bioavailability (Luoma, 1986; Griscom and Fisher, 2004; Peijnenburg and Jager, 2003). Therefore, numerous leaching methods have been developed to separate trace metals according to operationally defined sediment phases (e.g., Tessier et. al., 1979; Lord, 1982; Salomons and Fortsner, 1984; Huerta-Diaz and Morse, 1990; Krisnamurti et. al., 1995; Sahuquillo et. al., 1999; Arain et. al., 2008). However, the redox conditions of the sediment these methods are applied to can impact the effectiveness of these leaching schemes. In addition, the preservation of in-situ conditions prior to and during the leaching process is crucial for determining the phase speciation of sediment-bound metals (Forstner and Salomons, 1991; Stephens et. al., 2001; Kersten and Forstner, 1986; Rapin et. al., 1986). Therefore, it is important for a leaching scheme to be compatible with the local redox conditions of the sediment being analyzed, either oxic or anoxic.

The goal of this research project was to develop a sequential leaching method that can be applied to both oxic and anoxic sediments. This leaching scheme was then applied to sediments obtained from three estuaries with recent histories of significant industrial pollution and with differing geochemical conditions. The metal phase speciation data from these sediments was then combined with the corresponding total sediment metal concentrations to estimate the degree of trace metal contamination at each of the selected coring sites. In addition, the phase speciation distributions of the major metals (Fe, Mn, and Ca) and trace metals (Cd, Cr, Pb, and As) were compared to the total carbon, nitrogen, and sulfur data from the corresponding sediment cores in order to identify the geochemical relationships between these elements in the different estuarine environments.

1.2. Background

Phase Speciation Leaching Techniques. The history of the development of phase speciation leaching techniques for determining the geochemical associations of trace metals in soil and sediment is quite extensive. Numerous methods have been developed that utilize different leaching reagents in an effort to quantify the metal content in these materials according to operationally-defined geochemical phases. However, all of these methods are similar in that they divide the chemical elements within soils or sediments into geochemical phases or fractions that are defined by the treatment used to extract the metals (i.e., the leach phases are operationally-defined). This stands in contrast to the classical concept of phase speciation, which relates metal location/association to specific minerals with definite chemical compositions (e.g., greenockite (CdS) vs. otavite

($CdCO_3$) (Bacon and Davidson, 2008). However, the degree of specificity associated with classical metal speciation is not possible with most soil and sediment leaching methods, given the complexity of these substances and the fact that no chemical leaching reagent is entirely specific (i.e., a high likelihood of side-reactions to occur during the leaching process) (Chao, 1984). Despite the numerous published operationally defined leaching methods, the goal of all of these phase speciation leaching methods is to be as specific as possible in geochemically fractionating the metals in soils and sediments.

An example of an early study that utilized operationally defined extraction techniques to determine metal concentrations in marine sediments was that of Goldberg and Arrhenius (1958). These workers utilized a combination of dialysis, ion exchange, and ethylene diamine tetra-acetic acid (EDTA) to separate the different geochemical phases in Pacific pelagic sediments. Major developments in geochemical phase speciation leaching techniques continued throughout the late 20^{th} and early 21^{st} centuries (e.g., Tessier et. al., 1979; Lord, 1982; Salomons and Fortsner, 1984; Huerta-Diaz and Morse, 1990; Krisnamurti et. al., 1995; Sahuquillo et. al., 1999; Arain et. al., 2008). Most of these leaching methods consist of at least three steps dividing the trace metals in sediment, soil, or sewage sludge into different geochemical phases. These methods are all similar in that they are usually performed in sequence and typically start with the easiest extracted metals (e.g., metals released by cation exchange processes), which are often the most bioavailable, and end with the metals in the more refractory fractions (e.g., metals bound within framework silicate minerals), which are generally the least bioavailable (Filgueiras et. al., 2002).

Determining the actual bioavailability of trace metals in sediment to benthic organisms is a complex issue. Various workers have noted that the total concentrations of trace metals in benthic organisms often do not directly correlate with the total concentrations of these elements in sediment (Luoma, 1986; Bryan and Langston, 1992). Instead, investigators have concluded that the overall bioavailability (therefore toxicity) of trace metals is closely related to the chemical phases with which these elements are associated in the sediment (Griscom et. al., 2000; Griscom et. al., 2002; Griscom and Fisher, 2004). In addition, different species of benthic organisms have different feeding habits and digestion mechanisms, which also play important roles in the bioavailability of sedimentary trace metals (Amiard et. al., 1986; Warren et. al., 1998; Lee et. al., 2000; Griscom et. al., 2002). Therefore, in order to assess the overall toxicity of trace metals in sediment, it is crucial to know both the geochemical phase speciation of the trace metals and determine the assimilation efficiency of various chemical species of trace elements by benthic organisms. Determining the assimilation efficiency (AE) of the trace element species for an organism is usually accomplished through empirical studies, often through the use of radioactive isotopes. Despite limitations, sequential leaching techniques are still an important tool because they offer one of the few ways of obtaining information relating to the geochemical associations of various trace and major elements in sediments. However, by themselves (i.e., without AE data related to a specific organism) sequential leaches can only provide information regarding the likely bioavailability of trace metals to benthic organisms.

Phase speciation leaching methods are similar in that they all chemically fractionate metals associated with sediment. However, the number of operationally

defined phases, the types of leaching reagents, and the overall efficacy of these methods often vary significantly. For example, Tessier et. al. (1979) divide trace metals in sediment into five fractions: loosely bound or exchangeable, carbonate bound, iron and manganese oxide bound, those bound to organic matter such as humic or fulvic acids, and residual which consist mainly of metals bound to silicates. In contrast, Huerta-Diaz and Morse (1990) define only three fractions: reactive, silicate and pyrite. Both methods are useful for characterizing trace metals and their geochemical associations in sediment. However, the more complex leaching methods are likely to have greater analytical error associated with them due to some degree of inherent chemical non-specificity or overlap (Martin et. al., 1987; Gleyzes et. al., 2002). While less complex leaching schemes tend to partition metals more effectively, due to overall method simplicity they provide less information about the trace metals and their related geochemical phases within the sediment.

All sequential leaching methods are plagued by problems that are inherent to the leaching processes themselves. Some of these issues include: lack of chemical specificity, lack of leaching reagent compatibility, and re-adsorption of trace metals onto sediment during the leaching process. Perhaps the most significant problem associated with sequential leaching methods is the fact that the sediment phases for each method are operationally defined, making the results from different leaching methods difficult to compare directly (Martin et. al., 1987; Filgueiras et. al., et. al., 2002; Gleyzes et. al., 2002). In addition to the numerous problems related to sequential leaching schemes, the type of leaching method used also varies with the redox state of the sediment. For example, the leaching method by Tessier et. al. (1979) is designed to be used on oxic

sediments, while the Huerta-Diaz and Morse (1990) method should be used on anoxic sediments. This becomes problematic when working with sediment columns that contain prominent redox gradients, which is a common occurrence in estuarine sediments. Therefore, it is desirable to develop a single leaching scheme that can be used for both anoxic and oxic sediments.

1.2.1. Sediment Geochemistry of Major Elements

The major elements of concern in this project (Fe, Mn, Ca, C, N, and S) are important indicators of local sediment redox conditions and the nature and sources of organic matter in the sediment column. All of these major elements are geochemically related through both biotic and abiotic reactions in sediments, and impact the pathways through which introduced trace elements are cycled through marine and estuarine systems.

Iron. Iron is a Group 8 d-block transition element. The Fe cycle in estuarine sediments is closely linked to other major elements (Mn, C, N, and S) and trace metals. The speciation of Fe in sediments is chiefly dependent on local redox conditions. In reducing sediment conditions, Fe is readily reduced by microorganisms forming Fe^{2+} ions, which can quickly react with any available oxygen to form insoluble ferric (Fe^{3+}) oxides and hydroxides in oxidizing conditions (Burdige, 2006). These ferric oxide and hydroxide particulates offer ideal locations for the adsorption of various other trace metals such as Cr and As (Crecelius et. al., 1975; Nakayama et. al., 1981a; Warren and Zimmerman, 1994; Sullivan and Aller, 1996). If Fe^{2+} remains in reducing conditions in the presence of biological sulfate reduction, it will combine with ambient S^{2-}, forming

first FeS, then the meta-stable minerals $FeS_{(1-x)}$ (makinawite), Fe_3S_4 (greigite), and finally FeS_2 (pyrite) (Wang and Morse, 1996).

Manganese. Manganese is a Group 7 d-block transition element. The geochemistries of Mn and Fe are similar, in that Mn forms insoluble oxides in oxidizing conditions and soluble cations in reducing conditions (Burdige, 2006). Like Fe, Mn oxides play a crucial role in the scavenging of dissolved trace metals by providing a reactive surface for adsorption or through the process of coprecipitation (Sadiq, 1992). Under certain conditions, Mn oxides can also act as oxidizing reagents for the trace metal Cr, increasing its bioavailability and toxicity (Nakayama et. al., 1981b). In low oxygen conditions, Mn oxides such as vernadite (δ-MnO_2) are reduced by microorganisms, forming Mn^{2+}, which is readily soluble in water (Burdige, 2006). In suboxic sediment conditions, reduced Mn oftentimes precipitates as rhodochrosite ($MnCO_3$) (Sadiq, 1992). In anoxic sediment conditions, reduced Mn can absorb to meta-stable Fe minerals such as makinawite, forming small amounts of MnS (Arakaki and Morse, 1993). However, in anoxic sediments with high degrees of pyritization, this element is more likely to be incorporated into pyrite minerals (Huerta-Diaz and Morse, 1992).

Calcium. Calcium is a Group 2 s-block element, which is one of the alkaline earth metals. The calcium cycle is linked with magnesium, oxygen, and carbon, forming an integral part of the carbonate cycle. Trace metals such as Pb and Cd, which form divalent cations like alkaline earth metals, often adsorb onto calcite ($CaCO_3$) mineral surfaces, forming trace metal carbonates that serve as sinks for these trace metals in oxic sediment conditions (Davis et. al. 1987; Fulgum et. al., 1988). However, these carbonates

are readily solublized in low pH conditions, in which case these carbonate minerals can act as sources of trace metals to benthic organisms.

Carbon. Carbon is a Group 14 p-block nonmetal. Carbon, in the reduced form of organic matter, plays a crucial role in redox cycling in estuarine sediment systems, by serving as the chief reducing reagent. Organic matter is oxidized via aerobic respiration, denitrification (NO_3 reduction), Mn reduction, Fe reduction, sulfate reduction, and methanogenesis by microorganisms, producing CO_2, N_2, Mn^{2+}, Fe^{2+}, H_2S, and CH_4, respectively (Burdige, 2006). Three of these biogenic respiration products (Mn^{2+}, Fe^{2+}, and H_2S) play significant roles in the cycling of major and trace metals in anoxic sediments (Dossing et. al., 2011; Belzile and Lebel, 1986; Patterson et. al. 1997; Chen et. al., 2007). The carbon dioxide produced by aerobic respiration, dissolved in water to form carbonic acid, plays a significant role in oxic sediments by introducing trace elements into the carbonate cycle (Sadiq, 1992).

In addition to driving sediment redox cycling, organic components such as humic and fulvic acids play an important role in the cycling of metals by forming complexes which can act as both sinks or sources for toxic elements in sediment systems (Jones and Huang, 2003; Kyziol et. al., 2006; Lin and Chen, 1998; Wu et. al., 2012). Because of its involvement in numerous biotic and abiotic reactions in sediment, and its tendency to complex with trace metals, organic carbon is arguably the most important element in terms of the cycling of both major and trace metals in estuarine sediment systems.

Nitrogen. Nitrogen is a Group 15 nonmetal. Nitrogen in the form of nitrate (NO_3^-) serves as the terminal electron acceptor for the nitrate-reducing microorganisms that remineralize organic carbon in sediments with low oxygen concentrations (Burdige,

2006). During this mineralization process, known as denitrification, nitrogen gas (N_2), which is quite chemically unreactive, is released to the atmosphere.

Sulfur. Sulfur is a Group 16 nonmetal. Sulfur, like nitrogen, when combined with oxygen in the form of the oxyanion sulfate (SO_4^{2-}), serves as the terminal electron acceptor for sulfate-reducing microorganisms. Sulfate reducers use this anion much like nitrate reducing microorganisms use NO_3^-, in order to remineralize organic carbon compounds in anoxic sediments (Burdige, 2006).

In addition to its role in metal cycling as an oxidant in the form of sulfate, sulfur also plays an important role in the geochemical cycling of metals, in particular the so-called chalcophilic elements. In anoxic sediments, hydrogen sulfide (H_2S), which is produced as a result of sulfate reduction, reacts with many major and trace elements producing a range of sulfide minerals from metal monosulfides (e.g., FeS, CdS, PbS, CuS and HgS) to pyrites (e.g., FeS_2 and FeAsS) to arsenic sulfides such as realgar (AsS) and orpiment (As_2S_3). (Sadiq, 1992). These sulfide minerals act as both sinks and sources for trace elements in sediments, depending on the redox conditions (Belzile and Lebel, 1986; Morse and Arakaki, 1993; Guo et.al., 1997; Stephens et. al., 2001).

Much like carbon, sulfur plays several important roles in the cycling of major and trace metals in sediments. Oxidized sulfur compounds help drive sediment redox reactions in low O_2 environments, while reduced sulfur reacts with metals to form important sulfide minerals that can control overall trace metal bioavailability in marine and estuarine systems.

1.2.2. Sediment Geochemistry of Trace Elements

The trace elements of concern in this project (Cd, Pb, Cr, and As) all exhibit different chemical properties that impact on their bioavailability to benthic organisms. Because of this, the geochemical mobility of each element must be taken into account.

Cadmium. Cadmium is a Group 12 d-block metal, which also includes Zn and Hg. Unlike Zn, but much like Hg, Cd serves almost no biological function and is toxic to most organisms. The only known exceptions to the almost universal toxicity of Cd is for some species of diatoms that live in environments with extreme nutrient deficiency and use Cd in place of Zn in essential enzymes (Lane and Morel, 2000; Park et. al., 2007).

In oxic conditions, a significant amount of Cd is often associated with the water soluble/exchangeable and carbonate fractions in marine and estuarine sediments (Guo et.al., 1997; Rifaat et. al., 1992; Riba et. al., 2002; Abaychi and Douabul, 1986; Larner et. al., 2008; Passos et. al., 2011; Sundary et. al., 2011). However, some workers have noted that the Fe and Mn oxide phases can also contain a substantial percentage of this metal (Riba et. al., 2002; Guo et. al., 1997; Amiard et. al., 2007). Nonetheless, the amounts of Cd in the water soluble/exchangeable and carbonate phases are important, because they are readily available. Cadmium in the water soluble/exchangeable fraction is very mobile, and readily exchanges across the sediment-water interface with changes in the salinity of the overlying seawater (Filgueiras et. al., 2002). Cadmium in the carbonate fraction is also quite mobile (although not as much as the water soluble/exchangeable Cd), and can be released in low pH conditions (Filgueiras et. a., 2002). The close association of Cd and carbonates in sediments appears to be due to the ready adsorption of dissolved Cd^{2+} ions in seawater onto calcite in oxic conditions (Davis et. al., 1987; Chada et. al., 2005). Like

other sediment-bound trace metals, Cd in the Fe and Mn oxide and organic fractions is generally less available than Cd in the water soluble/exchangeable and carbonate fractions (Filgueiras et. al., 2002). Overall, Cd tends to concentrate in the more labile geochemical phases in oxic sediment conditions.

Much like other chalcophiles such as Zn, Cd tends to be sequestered in anoxic conditions in the form of a monosulfide (CdS), which is relatively insoluble in water and stable in low oxygen sediments (Guo et. al., 1997; Kersten and Forstner, 1986; Morse and Luther, 1999). Due to this stability and the chemical kinetics related to the formation of CdS, Cd is rarely incorporated into the pyrite phase of sediments (Kluckohn, 1990; Huerta-Diaz and Morse, 1992; Morse and Luther, 1999). Because of this, Cd tends to associate with the "reactive" non-pyrite sulfide phase of anoxic marine sediments (Huerta-Diaz and Morse, 1992). Cadmium concentrations in pristine/uncontaminated sediments are relatively low (less than 0.5 ppm), due to this elements uniformly low crustal abundance; therefore, higher concentrations than this are typically due to anthropogenic influences (Nriagu, 1980).

Lead. Lead is a Group 14 element p-block metal, which includes nonmetals such as C and Si and other p-block metals such as Sn. Like Cd, Pb is a chalcophile element; however, Pb serves no known useful purpose in biochemistry, and is toxic to most organisms (Ulrich and Schlipkoter, 1991). Lead is present in the environment in both organic and inorganic compounds. Organic Pb compounds are generally more bioavailable (due to their high lipid solubility) and therefore extremely toxic (Mahaffey, 1977). This stands in contrast to inorganic lead compounds or elemental lead, which are often poorly water soluble (with the exception of low pH conditions); therefore, they are

generally slowly absorbed by most organisms (Bryan and Langston, 1992; Ulrich and Schlipkoter, 1991).

In oxidizing sediment conditions, Pb readily adsorbs onto Fe and Mn oxides and hydroxides, with strong correlations being found between extractable Fe and total Pb concentrations in sediment (Balistrieri and Murray, 1982, 1984; Langston, 1986). Under these conditions, Pb can also adsorb to calcite forming a layer of $PbCO_3$ on the mineral surface (Chada et. al., 2005). Because of this, the majority of the total Pb in marine and estuarine environments is often associated with the Fe and Mn oxides and carbonate phases in oxic sediments (Abaychi and Douabul, 1986; Riba et. al., 2002; Purchase and Fergusson, 1986; Langston, 1986; Sundary et. al., 2011). However, some workers have reported a significant percentage of Pb associated with the organic/sulfide phases in marine and estuarine sediments (Scoullos, 1986; Passos et. al., 2010; Sundary et. al., 2011). Nevertheless, these results are inconclusive due to the fact that the leaching schemes they used could not distinguish between sulfides and organics.

In reducing conditions, Pb is likely converted to a monosulfide mineral (PbS) and is only gradually incorporated into the pyrite phase of sediments (Purchase and Fergusson, 1986; Davis et.al., 1996; Huerta-Diaz and Morse, 1992). Because of this, like Cd, Pb in anoxic marine and estuarine sediments is mainly associated with the "reactive" or non-pyrite sulfide fraction (Huerta-Diaz and Morse, 1992). It is generally accepted that sediments lacking anthropogenic contamination by this element contain less than 5 ppm Pb by dry weight (Sadiq, 1992).

Chromium. Chromium is a Group 6 element with a complex geochemistry that involves several different oxidation states. Unlike the other trace metals studied in this project, chromium is an essential trace element for numerous organisms (Gauglhofer and Bianchi, 1991). The two most common oxidation states of chromium in sediments and the overlying water column are Cr^{3+} and Cr^{6+} (Richard and Bourg, 1991; Sadiq, 1992). These two oxidation states are stable in different redox conditions and have very different geochemical properties.

In oxic marine and estuarine environments, Cr^{3+} is a cation that either rapidly coprecipitates with Fe oxides or forms complexes with organic matter (Nakayama et. al., 1981a). Because of this, the concentration of free Cr^{3+} is expected to be quite low in most oxic seawater environments (Sadiq, 1992; Rai et. al., 1989). On the other hand, Cr^{6+} in the form of the chromate anion (CrO_4^{2-} or $HCrO_4^-$) is generally stable in seawater in oxic conditions and does not readily absorb onto Fe oxides (Richard and Bourg, 1991; Nakayama et. al., 1981c). However, workers have noted that chromate can absorb onto Mn oxides (Eray and Rai, 1987). Because of the tendency for Cr^{3+} to coprecipitate with Fe oxides or complex with organic matter, and the tendency of chromate to adsorb onto Mn oxides, the majority of the total Cr content in oxic sediments is usually associated with the Fe and Mn oxide-bound and organic-bound metal fractions (Kersten and Forstner, 1986; Guo et. al., 1997; Larner et. al., 2008; Sundary et. al., 2011). The oxidation state of Cr is highly variable and it can readily change from the generally unavailable Cr^{3+} form to the highly available toxic Cr^{6+} form in oxic sediment environments. This change in Cr oxidation states is closely tied to sediment Mn redox reactions and normally does not occur through reaction with O_2 alone. This Cr-Mn

coupling is due to the slow chemical kinetics associated with the direct oxidation of Cr^{3+} by dissolved O_2, and the fact that other reactions, such as the adsorption of Cr^{3+} onto oxides or organic material, occur at a faster rate (Richard and Bourg, 1991). Instead, Mn oxides act as catalysts driving the reaction between Cr^{3+} and dissolved O_2, producing Cr^{6+} in the form of readily soluble chromates (Nakayama et. al., 1981b). This oxidation of Cr^{3+} in the presence of Mn oxides occurs relatively rapidly over a wide range of pH and ionic strengths (Johnson and Xyla, 1991). However, this process can be inhibited by the presence of organic substances, due to the tendency of Cr^{3+} to form stable complexes with organic ligands (Douglas et. al., 1986; Nakayama et. al., 1981b; Johnson and Xyla, 1991). In oxic sediments, the readily available Cr (that not bound to oxide minerals or insoluble organic material) consists mainly of chromate, which is very soluble in seawater and highly toxic to most organisms (Sadiq, 1992; Gauglhofer and Bianchi, 1991).

In reducing environments, Cr exists mainly in the +3 oxidation state as a sparsely soluble compound (such as $Cr(OH)_3$), or it is complexed with high molecular weight (i.e., insoluble) humic material (Richard and Bourg, 1991; Guo et. al., 1997). Both of these forms are only slightly incorporated into the sediment pyrite phase (Huerta-Diaz and Morse, 1992). Like Cr^{3+} bound to Fe oxides in oxic sediments, Cr in anoxic sediments is generally not available due to the low solubility of the compounds and complexes that it forms under these conditions (Sadiq, 1992; Guo et. al., 1997). Because of this, Cr is mainly bioavailable in oxic sediments and sequestered in anoxic sediments. Finally, uncontaminated sediment generally contains less than 20 ppm of this element (Sadiq, 1992).

Arsenic. Arsenic is a Group 15 element along with nitrogen and phosphorus, but unlike these nonmetallic nutrient elements which are both crucial for protein synthesis, As is a metalloid that is well known to be toxic to living organisms (Sharma and Sohn, 2009).

Much like Cr^{6+}, arsenic in marine and estuarine environments is usually associated with oxygen in the form of arsenite and arsenate, which are arsenic in the form the 3+ and 5+ oxidation states, respectively (Sadiq, 1992). Generally, arsenite compounds are more toxic than arsenate compounds for most organisms, due to arsenite's strong affinity for thiol groups; however, arsenate compounds generally have a greater tendency to bioaccumulate in marine organisms (Sadiq, 1992; Sharma and Sohn, 2009). A significant amount of As in marine and estuarine environments also exists as organic arsenic compounds, but the toxicity of these compounds tends to be relatively low compared to the inorganic species (Neff, 1997; Sharma and Sohn, 2009).

In oxic marine and estuarine environments, arsenic is chiefly present in the form of the arsenate anion (Sadiq, 1992; Neff, 1997). Much like Cr in the 3+ form, arsenate also has a high affinity for Fe oxides. Workers have observed a close relationship between Fe oxides and As concentrations in marine and estuarine sediments (Crecelius et. al., 1975; Langston, 1986; Sullivan and Aller, 1996). The reason for this close relationship appears to be due to the rapid adsorption of both arsenate and arsenite, which occurs on the surfaces of Fe oxides under oxic conditions (Pierce and Moore, 1982; Wilkie and Hering, 1996). On the other hand, the adsorption of arsenate and arsenite onto Mn oxides in sediments is much less significant than for Fe oxides, due to the net charge similarities of these anions and the surfaces of Mn oxides under common marine and

estuarine pH conditions (Sadiq, 1992). Due to the tendency of arsenate and arsenite to adsorb onto Fe oxides, many workers have noted that the majority of the total As in oxic marine and estuarine sediments is often associated with the Fe and Mn oxide phases (Guo et. al, 1997; Whiteley and Pearce, 2003; Lopez-Gonzales et. al., 2006; Larner et. al., 2008).

In marine or estuarine anoxic environments, arsenic usually behaves like other chalcophilic elements (such as Cd or Pb) by readily reacting with dissolved sulfide species. However, unlike Cd or Pb, which normally form metal monosulfides in anoxic sediments, arsenic is often associated with the pyrite fraction, likely in the form of arsenopyrite (FeAsS) (Belzile and Lebel, 1986; Huerta-Diaz and Morse, 1992). Under these conditions, As can also be incorporated into the minerals orpiment (As_2S_3), realgar (AsS) or other compounds with trace metals such as zinc and copper (Huerta-Diaz and Morse, 1992; Neff, 1997; Sadiq, 1990). Once in these diagenetic forms, arsenic is not generally mobile, due to the low solubility of these minerals, unless the local redox conditions change in the sediment (Morse, 1994; Neff, 1997). However, some workers have failed to observe the formation of insoluble sulfides in anoxic conditions (Guo et.al., 1997). In this case, As becomes highly soluble in anoxic conditions. Examples of redox changes that make pyrite-bound metals such as As available occur by physical mixing (e.g., storm events, intensive bioturbation, dredging) or without physical mixing due to seasonal variations in sediment redox potential (Morse, 1994; Neff, 1997). Finally, uncontaminated sediment typically contains less than 10 ppm of this highly toxic element (Sadiq, 1992).

1.3. Research Objectives

The goals of this research project were two-fold. The first was to develop a sequential leaching method that is effective for both anoxic and oxic sediment. To accomplish this, a six step leaching process was utilized in order to extract elements associated with five major operationally defined components of the leached sediments: exchangeable, oxide, acid volatile sulfide (AVS), organic, and pyrite fractions. The second goal was to apply this leaching scheme to sediment samples taken from three estuaries with significant anthropogenic metal loadings and differing environments (overall salinity and sediment carbon, nitrogen, and sulfur concentrations). The overall goal of this research was to describe the phase speciation distributions of three major sediment bound metals (Fe, Mn, and Ca) and four potentially toxic trace elements (Cd, Pb, Cr, and As), and examine how they relate to total sediment carbon, nitrogen, and sulfur concentrations in different estuarine environments.

CHAPTER 2

SAMPLING AND ANALYTICAL METHODS

2.1. Sampling Locations and Methods

The sediments analyzed for elemental phase speciation leaching and bulk composition were collected from three locations: Elizabeth River, in Norfolk Virginia (designated as ER), Baltimore Harbor in Baltimore, Maryland (designated as BH), and Napa River near Mare Island in San Francisco Bay, California (designated as MI). These areas were chosen for this study because they offered different levels of anthropogenic metal contamination with varying estuarine conditions related to salinity and sediment organic carbon content, which allowed the testing of the leaching method under varying geochemical regimes. The Elizabeth River represented an estuarine environment with relatively high sedimentary organic carbon and salinity. Baltimore Harbor represented an estuarine environment with high sedimentary organic carbon and low salinity. The Napa River represented an estuarine environment with relatively low sedimentary organic carbon and high salinity. Individual coring sites, designated as ER1 (36° 52.32' N, 76° 20.09' W), ER2 (36° 48.39' N, 76° 17.36' W), BH1 (39° 12.25' N, 76° 31.41' W), BH2 (39° 15.27' N, 76° 35.89' W), MI1 (38° 04.23' N, 122° 14.91' W), and MI2 (38° 05.20' N, 122° 15.30' W), were chosen in an effort to get an overall picture of the trace metal contamination related to local anthropogenic inputs into the watershed of each estuary. Cores were collected in May 2006 for the Elizabeth River, June 2007 for Baltimore Harbor, and October 2007 for the Napa River near Mare Island.

Two sediment cores were collected in each of the three estuaries using box coring methods. Sub-cores 20-30 cm in length were taken by hand using polycarbonate tubes

from the box corer. During this process, care was taken to ensure that a layer of water remained on the surface of the sediment in order to preserve in-situ sediment redox conditions. These 10 sub-cores were then immediately sectioned on-site into 1 cm sections over the upper 10 cm inside a N_2-purged glove bag using polycarbonate sectioning tools in order to prevent both sediment oxidation and metal contamination. The 1 cm core sections were then placed into acid cleaned Ziploc bags and immediately frozen at 0°C. Back at the shore lab, aliquots of these core sections were thawed, weighed wet, oven dried, and then weighed again to obtain the sediment wet/dry ratios; the remaining sediment subsamples were kept frozen and used later for the phase speciation leaches.

2.2. Phase Speciation Leach Sample Processing

In order to determine the concentrations of major and selected trace elements in the sample sediments, the sequential leaching method was performed on one centimeter intervals of each of the two cores taken from the three estuaries. Numerous workers have noted that the extensive processing of sediment prior to leaching, such as oven-, freeze-, or even air-drying, tends to alter the chemical speciation of sediment bound metals (Forstner and Salomons, 1991; Stephens et. al., 2001; Kersten and Forstner, 1986; Rapin et. al., 1986). Therefore, sediment samples were processed wet and frozen, in an effort to preserve the in-situ redox conditions and keep the sediment bound metals in their in-situ oxidation states. Frozen wet sediment (about 2 grams wet weight for each tube) was weighed out in a glove box under a nitrogen atmosphere into Teflon centrifuge tubes as

triplicate two gram aliquots immediately prior to each batch of leaches. The first three steps of the phase leaching process were performed inside the nitrogen-purged glove box, in an effort to prevent sediment oxidation, while the last three steps were done outside of the box due to the chemical stability of the organic and pyrite phases.

2.3. Phase Speciation Leaches

The first step of the leaching process extracts metals associated with the ion exchangeable fraction, and uses a magnesium chloride leaching solution as described by Tessier et. al. (1979). The second step of the leaching process utilizes an oxalate reagent to extract trace metals associated with Fe and Mn oxides. The solution is adjusted to a pH of 6 with ammonium hydroxide, in an effort to maximize both selectivity and efficiency. This oxalate reagent is similar to the solution utilized by Tovar-Sanchez et. al. (2003) to remove trace amounts of iron oxides from phytoplankton. In addition, similar oxalate solutions have been used with success to remove moderately reducible iron oxide-bound trace metals in soils by various workers (Gleyzes et. al. 2002, and references therein). The third step of this leaching method utilizes a weak HCl solution to liberate trace metals associated with metal monosulfides, also known as the AVS (Acid Volatile Sulfide) phase. This step is similar to a leaching method utilized by Cooper and Morse (1998). The fourth and fifth steps of this phase speciation leach remove metals bound to the organic fractions of the sediment. The fourth step utilizes a 1M NaOH solution, to remove the metals associated with both the humic and fulvic fractions in the sediments. The fifth step consists of a strong HCl leach, to remove metals associated with proteins and carbohydrates. Both of these steps are similar to methods that have been utilized by

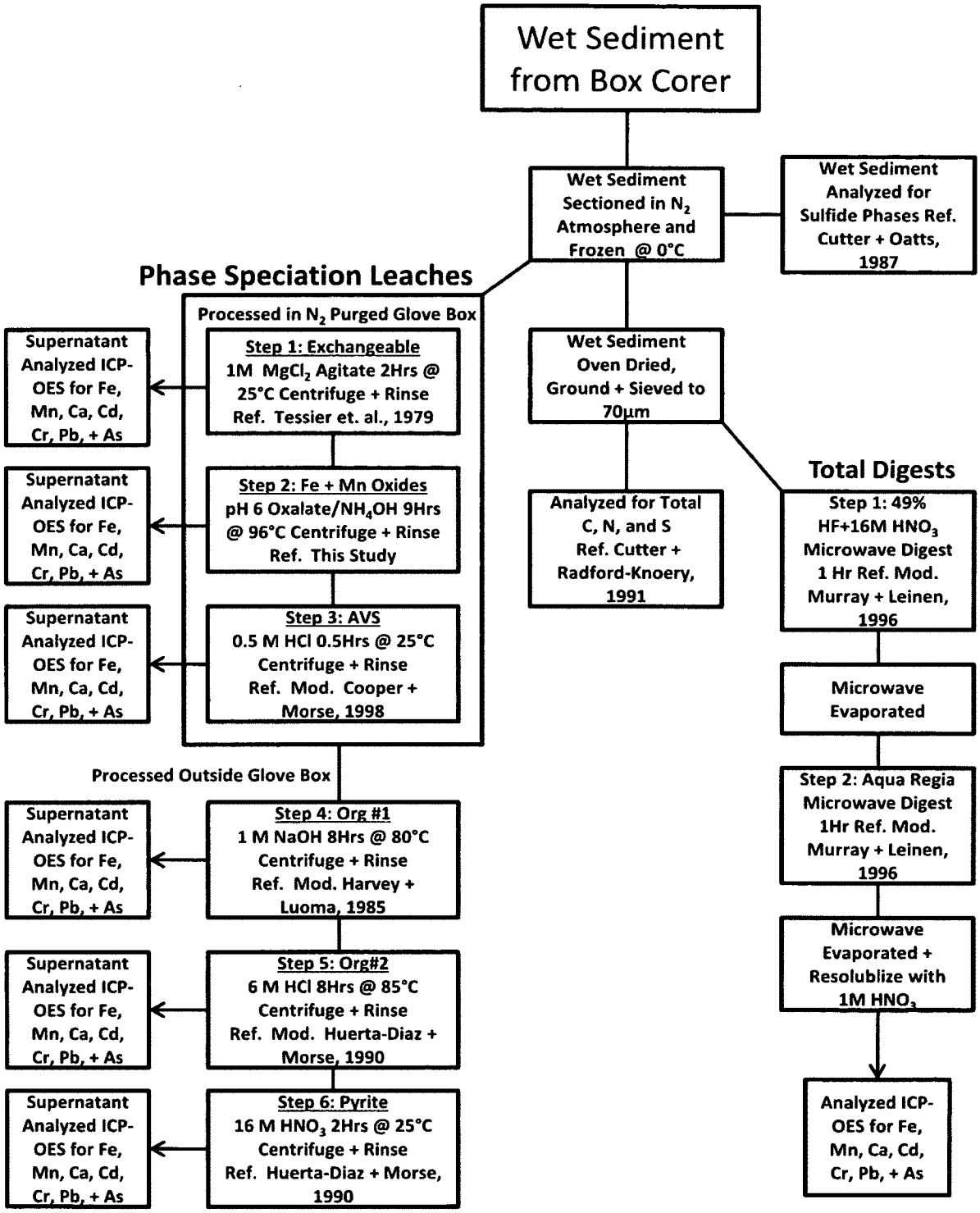

Fig. 1. Box Diagram Describing this Entire Project Including the Six Step Phase Leaching Method and the Total Digestion Process. Mod. = Modified.

various workers to remove metals associated with organic fractions without oxidizing the pyrite fraction in the sediment (Harvey and Luoma, 1985; Huerta-Diaz and Morse, 1990). Finally, in step six, the metals associated with the pyrite fraction are extracted using concentrated HNO_3, following the method used by Huerta-Diaz and Morse (1990). The box diagram (Fig. 1) summarizes all of the sediment processing steps. It describes the leaching scheme, including the conditions, time durations, and relevant references for each of the six steps. In addition to this, the "cookbook" for the phase speciation leaches is presented in Appendix A.

2.4. Phase Speciation Leach Tests

In order to verify leach efficiency, the results obtained from the six step leaching process were compared to several published methods using Fe and Mn as a tracer elements, due to their relatively high sedimentary abundances and tight couplings with local sediment redox conditions. In order to circumvent possible sediment homogeneity issues associated with the wet frozen core sections, many of these tests were also performed using NIST 2702 (Inorganics in Marine Sediment) standard reference sediment, which was generally representative of the actual sample materials.

2.4.1. Exchangeable Leach

This part of the leaching process utilizes a simple and well known Tessier et. al. (1979) method for removing readily extracted metals released by ion exchange. Therefore, the efficiency of this step was assumed and not evaluated.

2.4.2. Oxide Leach

In order to develop an effective leaching method that was efficient at removing sediment bound oxides, but did not attack the AVS phase in sediment, both the Tovar-Sanchez et. al. (2003) oxalate and Tessier et. al. (1979) hydroxylamine/acetic acid oxide leaching methods were assessed for specificity and efficiency. These oxide leaching methods were first evaluated for specificity using the cryo-trapping and GC-PID (Gas Chromatograph-Photo Ionization Detection) method utilized by Cutter and Oatts (1987) to quantitatively determine AVS content in sediments. However, instead of injecting HCl into the gas stripper containing an aliquot of frozen anoxic sediment, either the Tovar-Sanchez et. al. (2003) oxalate reagent at various pH conditions (the original leach is at pH 8) , or the Tessier et. al. (1979) hydroxylamine/acetic acid oxide leaching reagent, were injected into the gas stripper. After multiple tests, it was determined that only the Tovar-Sanchez et. al. (2003) oxalate reagent with a pH of 6 or greater did not produce detectable sulfide. Therefore, an oxalate reagent with a pH of 6, which should give the maximum Fe and Mn oxide leaching efficiency without attacking the AVS phase, was selected.

Next, the efficiency of the modified Tovar-Sanchez et. al. (2003) oxide leach was evaluated. This was done by comparing the Fe and Mn recoveries for NIST 2702 and two core samples (dried, ground, and sieved aliquots of ER 1 1-2 cm and MI 1 1-2 cm) using pH 6 buffered oxalate leach and the well established Tessier et. al. (1979) hydroxylamine/acetic acid oxide leach. Near-surface core samples were chosen for this test, as they should contain the highest Fe and Mn oxide concentrations in each core. The results of these comparisons (Fig. 2) indicate that the overall efficiencies of the two leaching methods for removing Fe and Mn oxides are statistically equivalent.

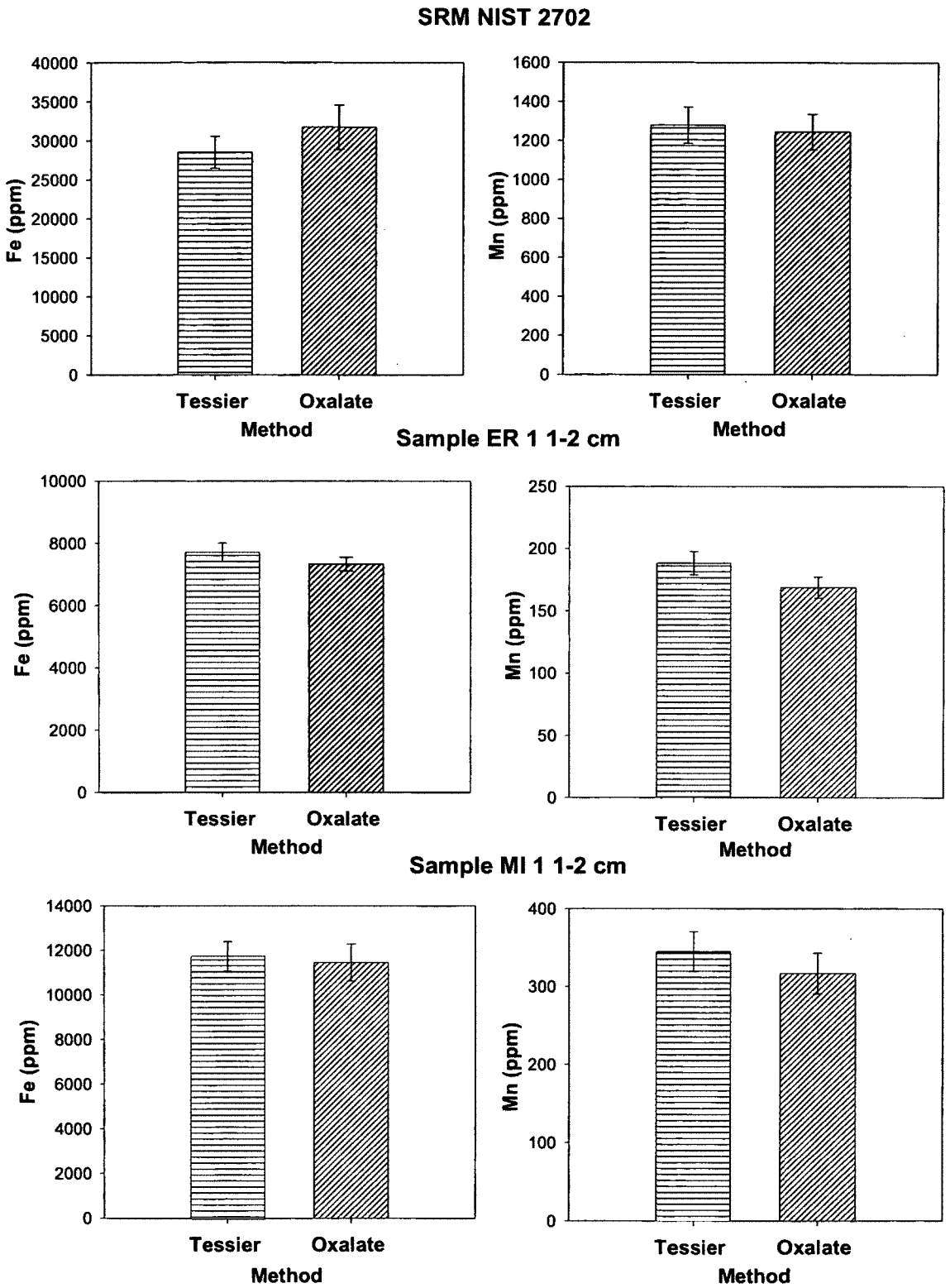

Fig. 2. Fe and Mn Recoveries for Oxides Using the Tessier et. al. (1979) and the pH 6 Oxalate Reagent Using NIST 2702, ER 1 1-2 cm, and MI 1 1-2 cm. Recoveries obtained using both methods are statistically identical for all the samples (n = 3 for all samples).

In order to compare the results obtained using these two oxide leaching methods, either the Student's t-Tests or Mann-Whitney Tests (Table 1) were performed on each data set. Student's t-Tests were utilized to compare normally distributed data sets, while Mann-Whitney nonparametric tests were utilized to compare data sets lacking normal distributions.

Table 1. Results of Parametric and Nonparametric Statistical Tests to Determine Whether Tessier et. al. (1979) and Modified Tovar-Sanchez et. al. (2003) Oxide Leaches are Statistically Different. SD = Data Sets Statistically Different; NSD = Data Sets Not Statistically Different; NA = Not Applied

Hydroxylamine vs. pH 6 Oxalate Oxide Phase Leaches (n = 3)								
	Fe Recovery in Oxide Leaches				**Mn Recovery in Oxide Leaches**			
	Mann-Whitney		**Student's t-test**		**Mann-Whitney**		**Student's t-test**	
Sample	**p-Values**	**SD/NSD**	**p-Values**	**SD/NSD**	**p-Values**	**SD/NSD**	**p-Values**	**SD/NSD**
NIST 2702	NA	NA	0.186	**NSD**	NA	NA	0.674	**NSD**
ER1 1-2 cm	NA	NA	0.145	**NSD**	0.100	**NSD**	NA	NA
MI1 1-2 cm	NA	NA	0.695	**NSD**	NA	NA	0.268	**NSD**

In addition to this, the efficiency and specificity of the oxide leach step was determined by analyzing the mineralogy of the NIST 2702 reference sediment both before and after an oxalate leach using X-Ray Diffraction (XRD), in concert with the Rock Jock software package. X-ray diffraction analysis indicated that the majority of the ferrihydrite was removed after pH 6 oxalate leaching (a relatively small yet unquantifiable amount of ferrihydrite remained after leaching). Overall, the modified Tovar-Sanchez (2003) leaching reagent developed in this project appears to be as effective as the frequently used Tessier et. al. (1979) hydroxylamine/acetic acid method in solublizing Fe and Mn oxides in a variety of sediments. However, unlike the

hydroxylamine/acetic acid reagent, the oxalate reagent developed in this project extracts oxide-bound elements in sediments without attacking the AVS phase.

2.4.3. AVS Leach

Because acid volatile sulfides are virtually absent from dried oxidized sediment, such as a standard reference material, the efficacy of the AVS phase was assessed using the frozen bulk sediment from the sampling locations. The Fe recovery from this phase of the leaching process was compared to the total AVS sulfur recovered using the Cutter and Oatts (1987) method after a stoiciometric correction (i.e., for AVS, FeS, the ratio is 1:1). The Fe sediment profiles obtained from the leach AVS step and the Fe:S molar ratio corrected data from the Cutter and Oatts (1987) AVS analysis method (Fig. 3) are illustrated on the following page. For this discussion, AVS calculated Fe will be defined as the Fe predicted from the S stoichiometry, while AVS leach Fe is the Fe solublized directly from the AVS leaching step. Some of the prominent features in the profiles obtained using the Cutter and Oatts (1987) method are the low concentrations (or in some cases nondetectable concentrations) of AVS calculated Fe in the surface samples of most of these cores and a general trend of increasing AVS calculated Fe concentrations down core until a plateau is reached. After this plateau in concentration, most profiles show what appears to be a decreasing trend in AVS calculated Fe. These trends are likely diagenetic signatures indicating redox transitions in the sediment columns. Most of the AVS leach Fe profiles also show a somewhat similar trend; however, all of the AVS leach Fe profiles lack the extreme surface minimum seen in the Cutter and Oatts (1987) AVS calculated Fe profiles.

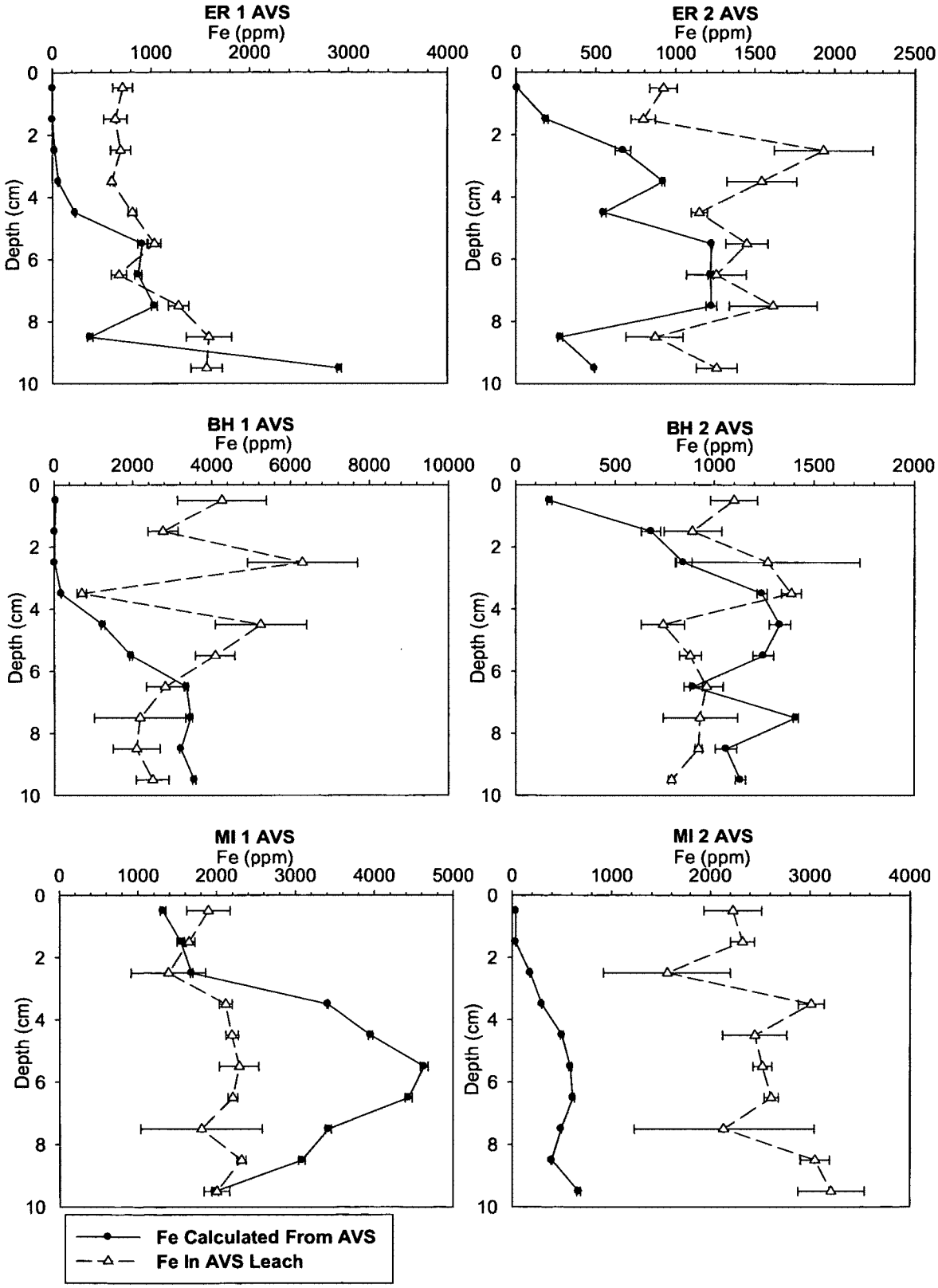

Fig. 3. Stoichiometrically Corrected Cutter and Oatts (1987) AVS Sulfide Data Profiles vs. AVS Leach Fe Profiles for All Sediment Cores Taken from the Elizabeth River (ER1+2), Baltimore Harbor (BH1+2) and Mare Island (MI1+2).

This difference between the two data sets is likely due to some lack of extraction efficiency by the oxide leaching step. This apparent lack of efficiency was seen in the results of the XRD analyses performed on the NIST 2702 standard reference sediment in order to test the efficiency of the pH 6 oxalate leach. X-ray diffraction analysis showed a relatively small yet unquantifiable amount of ferrihydrite remained in the sediment after applying the pH 6 oxalate oxide leach. However, due to the high concentrations of Fe and Mn oxides in these sediments, even a relatively small degree of inefficiency could result in a significant amount of Fe "carryover" into the AVS fraction (AVS leach Fe fraction considerably smaller than the oxide leach Fe for all sediments) as the 0.5M HCl AVS leach would likely attack any leftover oxide (Chao and Zhou, 1983; Huerta-Diaz and Morse, 1990). This would be especially significant in the surface sediments, where the Fe oxide concentrations tend to be the highest. This carryover effect would likely be more significant in the bulk frozen sediment samples than for the NIST 2702 reference sediment used in the oxide leach tests (Section 2.4.2.). This is due to the fact that the homogeneous small sediment grains (sieved at 70μm) which constitutes the NIST 2702 reference sediment would have dissolved more readily in the oxide leaching step than the heterogeneous bulk sediment from the sampling cores (Martin et. al., 1987; Pickering, 1986).

Student's t-Tests and Mann-Whitney Tests were applied to the AVS calculated Fe and AVS leach Fe data sets from each core, in order to determine if the results from these methods are statistically different (Table 2). These tests were applied separately to the complete data sets from the entire core profiles (left side of Table 2) and to the data from

Table 2. Results of Parametric and Nonparametric Statistical Tests to Determine Whether Results from Different Methods for Fe Associated AVS Determination are Statistically Different. SD = Data Sets Statistically Different; NSD = Data Sets Not Statistically Different; NA = Not Applied

AVS Leach vs. Cutter and Oatts (1987)								
	Entire Cores				**Anoxic Sections Only**			
	Mann-Whitney		**Student's t-test**		**Mann-Whitney**		**Student's t-test**	
Profiles	**p-Values**	**SD/NSD**	**p-Values**	**SD/NSD**	**p-Values**	**SD/NSD**	**p-Values**	**SD/NSD**
ER1	0.01	**SD**	NA	NA	0.169	**NSD**	NA	NA
ER2	NA	NA	<0.001	**SD**	NA	NA	<0.001	**SD**
BH1	NA	NA	0.003	**SD**	0.449	**NSD**	NA	NA
BH2	NA	NA	0.961	**NSD**	NA	NA	NA	NA
MI1	0.04	**SD**	NA	NA	NA	NA	NA	NA
MI2	<0.001	**SD**	NA	NA	<0.001	**SD**	NA	NA

only the anoxic regions of the sediment cores (right side of Table 2), with sediment redox zones being defined by the visual observation of the color transition from brown to black in the cores. These separate statistical tests were performed on the data from the anoxic regions only and were applied to all of the cores except BH 2 and MI 1, which were entirely anoxic. These tests showed that the apparent carryover of oxic sediment oxide Fe into the AVS phase was a significant source of error ($p > 0.050$) in the AVS phase for at least two (ER 1 and BH 1) of the six cores. This apparent oxic region carryover effect for the cores with significant oxic sediment zones (ER1, ER2, BH1, and MI2) resulted in a 93.1 ±10.8% overall average percent error for the AVS leach Fe. In addition, the AVS profiles (Fig. 3) show that results from cores ER2 and MI2 also appear to be reflect an appreciable amount of Fe oxide carryover. However, these profiles show a considerable amount of Fe carryover occurring in samples from both the oxic and anoxic regions of these cores. Overall, the AVS leaching step is generally effective in removing AVS-bound metals in the anoxic regions of these cores. However, there are apparent carryover

issues associated with some degree of oxide leach inefficiency, which appear to be restricted mainly to the oxic regions of these sediment cores.

2.4.4. Organic Leaches

The efficiency of the organic phase leaching steps were assessed by comparing the carbon content of NIST 2702 (n = 3) before and after performing steps 1 through 5 of the six step leaching scheme. Total carbon, nitrogen, and sulfur were determined by oxidative pyrolysis using the Cutter and Radford-Knoery (1991) method. The total mineral carbonate (excluding shell material) in all sample sediments and NIST 2702 was insignificant (< 0.2%); therefore, no carbonate leaching phase was used in this leaching scheme, and the total sediment carbon concentration is assumed to be all in the form of organic material. The total organic carbon removal efficiency of the organic leaches for NIST 2702 were quite low (20.8 ±0.9% total C removal efficiency). However, the organic leaches were about three times more effective at removing total nitrogen from this sediment (63.5 ±2.2% total N removal efficiency). This suggests that the organic leaching steps are much more effective at solublizing the labile organic material (and the metals associated with them) than the more refractory organic substances, because labile organic material (such as proteins and humic and fulvic acids) tend to be relatively rich in nitrogen compared to refractory organic matter (such as protokerogen) (Schultz and Miller, 1986; Burdige, 2006). Therefore, this leaching scheme is mainly effective in removing the metals bound to the labile organic fractions (e.g., proteins and humic and fulvic acids) of the sediments.

2.4.5. Pyrite Leach

Much like the AVS step, the efficacy of the pyrite step of my leaching scheme was evaluated by comparing the leach Fe data to the Cutter and Oatts (1987) method. However, for this comparison, the sulfide recovery from the last step of the Cutter and Oatts (1987) method, which selectively reduces pyrite in sediment using Cr^{2+}, was stoichiometrically corrected using a 1:2 ratio (FeS_2) to obtain expected pyrite Fe values. The results of this comparison between the Fe recoveries of the two methods for the NIST 2702 reference sediment are presented below (Fig. 4).

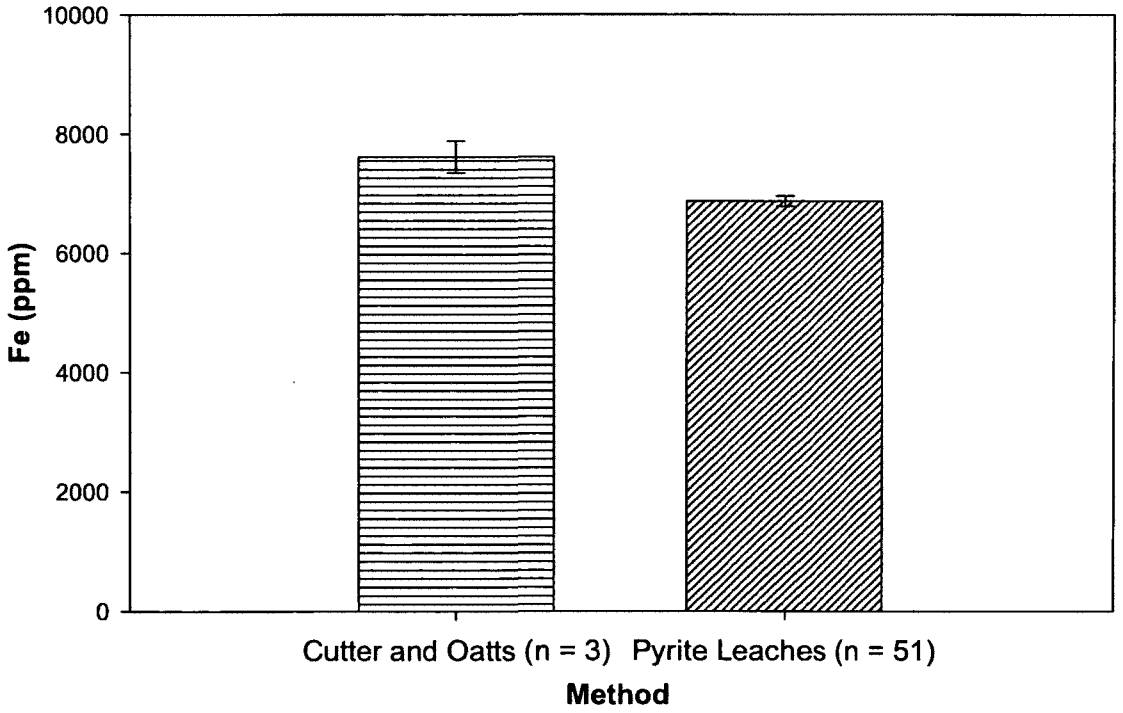

Fig. 4. Stoichiometrically Corrected Cutter and Oatts (1987) Pyrite Sulfide Data Showing Fe Equivalence vs. Pyrite Leach Step Fe Recoveries for NIST 2702 in All the Leach Batches.

The graph on the previous page (Fig. 4) shows that the results from these two methods are not within the average error, with the pyrite Fe results obtained Cutter and Oatts (1987) method being consistently higher than the pyrite leach Fe. In addition to this, a Mann-Whitney Test showed that the results from these two methods are statistically different with a p-value of 0.004. Nevertheless, the mean values for these very different analytical methods are within about 10% of each other.

Table 3. Results of Parametric and Nonparametric Statistical Tests to Determine Whether Results from Different Methods for Fe Associated with Pyrite are Statistically Different. SD = Data Sets Statistically Different; NSD = Data Sets Not Statistically Different; NA = Not Applied

Pyrite Leach vs. Cutter and Oatts (1987)								
	Entire Cores				**Anoxic Sections Only**			
	Mann-Whitney		**Student's t-test**		**Mann-Whitney**		**Student's t-test**	
Profiles	**p-Values**	**SD/NSD**	**p-Values**	**SD/NSD**	**p-Values**	**SD/NSD**	**p-Values**	**SD/NSD**
ER1	0.247	**NSD**	NA	NA	0.568	**NSD**	NA	NA
ER2	0.001	**SD**	NA	NA	0.004	**SD**	NA	NA
BH1	0.308	**NSD**	NA	NA	0.556	**NSD**	NA	NA
BH2	0.201	**NSD**	NA	NA	NA	NA	NA	NA
MI1	0.247	**NSD**	NA	NA	NA	NA	NA	NA
MI2	NA	NA	<0.001	**SD**	NA	NA	0.002	**SD**

In addition to the NIST 2702 reference sediment, the sediment samples from the three estuaries studied in this project (the Elizabeth River, Baltimore Harbor, and Napa River) were also analyzed for pyrite using the Cutter and Oatts (1987) method. The sulfide recoveries for the samples were stoichiometrically corrected to obtain the Fe equivalences using the same process used for the NIST 2702 reference sediment. Depending on whether the profile data sets were normally distributed or not, either Student's t-Tests or Mann-Whitney Tests were performed in order to assess whether the

results from the pyrite leach and the Cutter and Oatts (1987) method were significantly different. Like the AVS Fe tests illustrated in Section 2.4.3., these statistical tests were performed separately on the entire Fe data sets from each core and on the Fe data from the anoxic sections of each core only (Table 3). Again, separate statistical tests for anoxic sections only were not performed on BH 2 and MI 1, as these cores were entirely anoxic.

In contrast to the comparisons made between the leach and Cutter and Oatts (1987) AVS profiles (Fig. 3), the Fe concentrations for the two pyrite methods (Fig. 5) generally agree more closely. This is reflected in the results from the Student's t-Tests and the Mann-Whitney Tests results. Only two out of the six statistical tests performed on the entire data sets were statistically different. The statistical test results for the entire data sets were similar to the results obtained from the anoxic sections only. This indicates that the pyrite leaching step of this scheme does not suffer from the same degree of Fe oxide carryover (overall average percent error = 26.5 ±25.1% for pyrite leach in oxic regions of cores) in the surface sediments as the AVS leaching phase. The reason (or reasons) why the Fe data from two of these cores (ER2 and MI2) are statistically different is unclear. However, these differences between the pyrite leach Fe recoveries and the Cutter and Oatts (1987) pyrite results could reflect sediment heterogeneity issues associated with the use of bulk sample sediment. These issues are discussed in detail in Section 2.7. Overall, the pyrite leaching step of this method appears to be effective in extracting the pyrite-bound metals in these sediments.

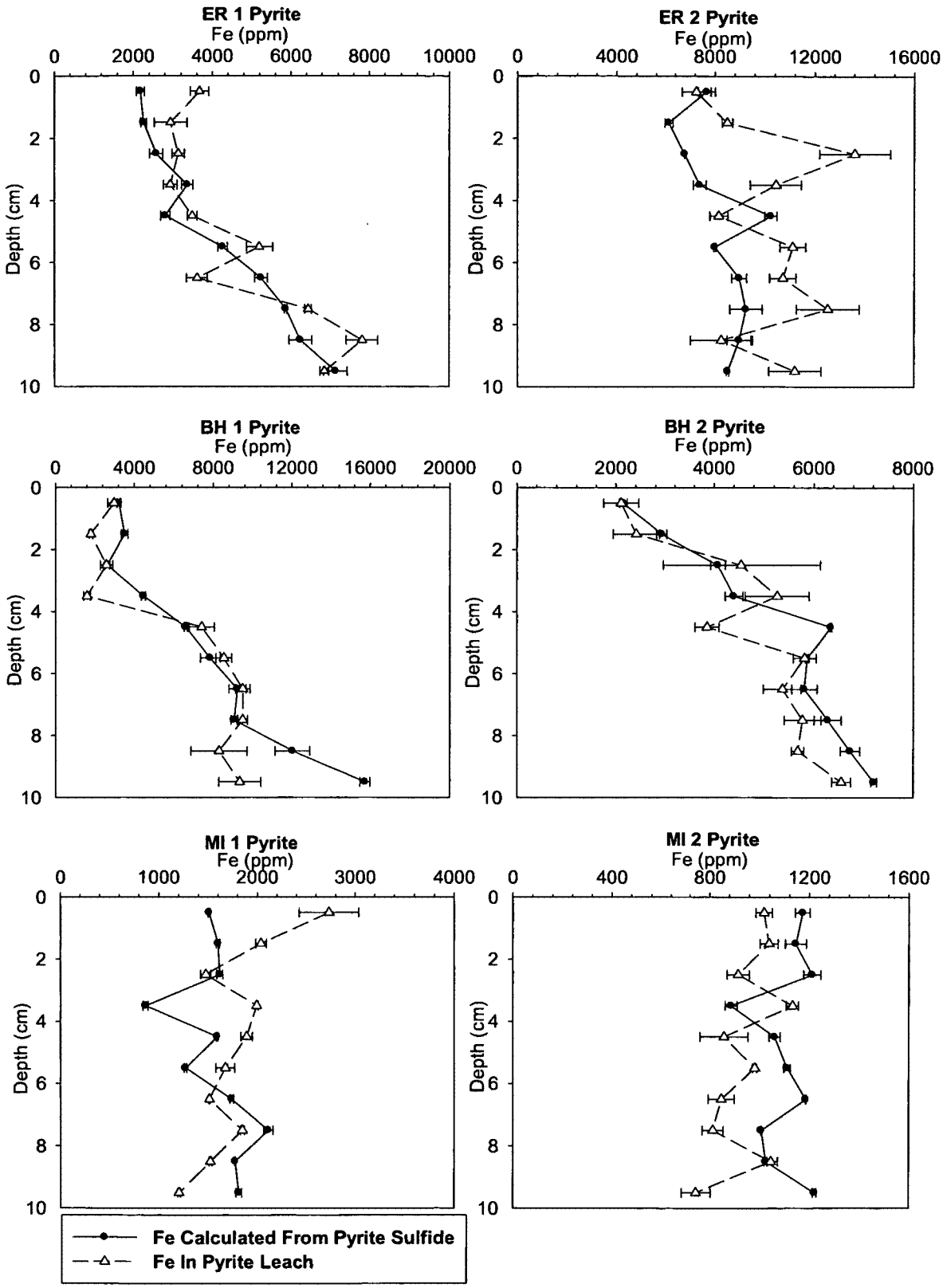

Fig. 5. Stoichiometrically Corrected Cutter and Oatts (1987) Pyrite Sulfide Data Showing Fe Equivalence for All Sediment Cores Taken from the Elizabeth River (ER1+2), Baltimore Harbor (BH1+2) and Mare Island (MI1+2) vs. Pyrite Leach Fe Recoveries.

2.4.6. Six Step Phase Leach vs. Optimized BCR Phase Leach

In addition to the individual tests done on 5 of the 6 steps of this leaching scheme, a sediment phase speciation standard reference material (BCR-701) was analyzed in an effort to compare the specificity and efficiency of the six step leaching scheme developed in this project to the widely-used, optimized BCR (Community Bureau Reference) phase speciation leaching method. The optimized BCR method was developed in an effort to create a standardized phase speciation leaching scheme that can be used on multiple types of samples (Sahuquillo et. al., 1999; Sutherland, 2010). The optimized BCR method consists of three leaching steps: the acid extractable step (0.11 M acetic acid leach at 22 ±5°C for 16 hrs), the reducible step (0.5 M hydroxylamine hydrochloride leach at pH 1.5 and 22 ±5°C for 16 hrs), and the oxidizeable step (30% H_2O_2 at pH 2 and 22 ±5°C for 1 hr, then heat to 85 ±5°C for 1 hr) (Usero et. al., 1998; Sutherland and Tack, 2003). The BCR-701 standard reference material is a contaminated lake sediment with certified concentrations of elements in the sediment phases obtained using the optimized BCR leaching scheme for three of the four trace elements (Cd, Cr, and Pb) analyzed in this study. The certified concentrations of these three elements as reported by Sutherland (2010) are presented in Table 4. The certified values from the first two phases of the BCR scheme are summed in order to compare the BCR-701 phase speciation results obtained using the six step leach to the certified results obtained using the optimized BCR leaching method. The sums of these two BCR steps should be roughly equivalent to the sums of the first three steps of the six step leach.

Table 4. Results Obtained by Sutherland (2010) for BCR-701 Using the BCR Phase Speciation Leaching Method.

Sutherland (2010)										
BCR-701 (ppm)	**Acid Extractable**	**SD**	**Reducible**	**SD**	**Acid Extractable + Reducible**	**Oxidizable**	**SD**	**Total Sum Phases**	**Aqua Regia Leach**	**SD**
Cd	7.34	0.35	3.77	0.28	**11.11**	0.27	0.06	**11.38**	**11.7**	**0.6**
Cr	2.26	0.16	45.7	2.0	**47.96**	143	7	**191.0**	**272**	**12**
Pb	3.18	0.21	126	3	**129.18**	9.3	2	**138.5**	**143**	**3**

Table 5 on the following page shows the phase speciation results for the BCR-701 reference sediment that were obtained using the six step phase speciation leaching method developed in this project. A comparison between Tables 4 and 5 reveals that the sums of the first three phases in the six step leach were within 10% of the sums of the Cd and Pb recoveries from the first two phases of the BCR Leach. However, Cr does not follow this trend. The amount of Cr removed in the first three steps of the six step leaching process greatly exceeds what was extracted in the first two BCR phases (over 378% greater recovery). Nonetheless, the sums of concentration in all the six phases from the six step leaching scheme were well within the standard deviations for all of the aqua regia digest bulk sediment metal recoveries, as reported by Sutherland (2010).

Table 5. Results Obtained Using the Six Step Leaching Method for Standard Reference Material BCR-701.

Six Step Leach (n =3)								
BCR-701 (ppm)	**Exchangeable**	**SD**	**Oxides**	**SD**	**AVS**	**SD**	**Sum of First Three Steps**	**SD**
Cd	6.19	0.13	5.26	0.01	0.02	0.00	**11.47**	**0.08**
Cr	0.07	0.01	175.10	5.09	6.31	1.01	**181.48**	**3.00**
Pb	0.43	0.09	137.82	1.27	1.12	0.11	**139.37**	**0.74**
	Org #1	**SD**	**Org #2**	**SD**	**Pyrite**	**SD**	**Total Sum Six Phases**	**SD**
Cd	0.13	0.02	0.08	0.02	0.08	0.02	**11.68**	**0.05**
Cr	6.31	0.86	91.26	3.07	0.38	0.07	**279.43**	**2.49**
Pb	ND	NA	5.04	0.33	ND	NA	**144.41**	**0.66**

The reason for the much higher Cr recovery in the first three steps of the six step leach process is unclear (Table 5). It does appear that the modified Tovar-Sanchez et. al. (2003) oxalate oxide leach was much more effective than the optimized BCR hydroxylamine leach at removing oxide bound Cr in this sediment. However, it is very difficult to directly compare the results from these two very different leaching schemes, due to the fact that the steps from each method are strictly operationally defined, as different reagents attack sediment bound metals in different ways (Sutherland and Tack, 2003; Anju et. al. 2010). In addition, small differences between phase speciation leaching methods (e.g., temperature, leaching time, reagent pH, ratio of solid material being leached to reagent) can have a large effect on metal recoveries (Martin et. al., 1987). Overall, the BCR-701 leaching results from the six step leaching scheme were similar to the certified phase speciation concentrations for two (Cd and Pb) of the three metals as reported by Sutherland (2010). The greater Cr recovery for the first 3 steps of the six step leach was likely due to the use of a much more efficient oxide leaching step (perhaps due

to higher temperature leaching conditions) relative to the reducing step (performed at room temperature) used in the modified BCR leaching scheme.

2.5. Total Sediment Digests

In addition to the phase speciation leaches, total sediment digests were performed via microwave-assisted digestion in order to obtain total bulk concentrations of the major and target trace metals in each interval of the sediment cores. The total digestion process used was a modified version of the microwave-assisted digestion method utilized by Murray and Leinen (1996).

Aliquots of dried, ground, and sieved (< 70 μm) sediment (~100 mg) were taken from each section of the six sampled cores and digested (n = 2 for each core section) via a two step process. The first step of this digestion process was a concentrated hydrofluoric and nitric acid digest, which involved 12 ml 49% HF and 3 ml concentrated HNO_3 added to each of the samples in Teflon microwave reaction vessels and held at 175° C for 1 hr, in an effort to solublize metals associated with silicate minerals (Murray and Leinin, 1996). After this, the samples were fully dried using a microwave accelerated process and a second digestion was performed. This step utilized 16 ml of aqua regia (1:3 ratio 16M HNO_3 to 12M HCl) which was added to each reaction vessel in an effort to oxidize any organic matter and digest any remaining mineral material. The entire total digestion process is described in the right side of the box diagram introduced in Section 2.3. (Fig. 1), and the details related to this process are included in Appendix B.

2.6. Sample Analysis

The supernatants collected from each step of the phase leaches and the total digests were filtered using 25 mm diameter 1.0 μm pore acid-cleaned, polycarbonate filters and then diluted with 18 MΩ-cm deionized H_2O (10-fold or 2.5-fold), depending on the anticipated major and trace metal concentrations. Next, the filtered and diluted supernatants from each step of the phase speciation leaches and the total digests were analyzed using ICP-OES (Inductively Coupled Plasma Optical Emission Spectroscopy) to determine the concentrations of major elements (Fe, Mn, and Ca), and the target trace elements (Cd, Cr, Pb, and As). Solution concentrations were then used to calculate sediment metal concentrations.

2.7. Sources of Error

Generally speaking, the sums of the concentrations in the geochemical phases for the major and trace elements for the majority of the sediment samples are either less than or statistically identical to total bulk sediment element concentrations (Appendix C). This is to be expected, as the total sum of elements in these phases should be either equal to or at the very least be roughly equal (i.e. ~±10% of error) to the amount solublized during the total digest. It is also acceptable for the phase sums to be less than the total digest recovery, due to these elements being associated with refractory silicate minerals that are not solublized. The chief exception to this trend is the Cd phase speciation and total digest data. The sum of the Cd data from the phase speciation leaches exceeds the total digest recoveries for over three quarters of all of the core sections (46 out of a total of 60 core samples). In addition to this issue, the standard deviations for the sums of the phase

leaches (especially for Ca) are much larger than the standard deviations for the total digests. The discrepancies in the Cd concentrations appears to be mainly due to analytical issues associated with using ICP-OES to analyze low level (ppb after sample dilutions prior to analysis) Cd concentrations. The large error bars in the Ca phase data sums appear to be due sediment heterogeneity issues, related to the use of wet-bulk sediment samples for the phase speciation leaches.

Sediment Heterogeneity. Overall, the precision associated with the phase speciation leaches were generally worse than that for the total digests. One of the reasons for this appears to be sediment heterogeneity associated with the use of wet-bulk sediment for the phase speciation leaches. This becomes evident when the pooled standard deviations from the sums of the phase concentrations in the NIST 2702 reference sediment are compared to the pooled standard deviations from the sums of the phase concentrations from all of the wet-bulk sediment samples obtained from the Elizabeth River, Baltimore Harbor, and Napa River (Table 6). NIST 2702 is a dried, sieved (< 70μm), and fully homogenized standard reference sediment that was analyzed in triplicate during each batch of the phase speciation leaches, in order to monitor for batch consistency. Table 6 shows that, with the exceptions of As and Cd, the pooled standard deviations are over twice as large for the wet-bulk sediment samples than for the NIST 2702 reference sediment. This indicates a significant degree of sediment heterogeneity in the wet-bulk sediment samples, which is a major source of error for 6 of the 7 elements examined in the phase speciation leaches. Data in Table 6 suggest that sediment heterogeneity does not affect all of the elements to the same degree, as RSD varies in the following order: Ca>Pb>Mn≈Fe>Cr>Cd>As. Reasons for these differences

Table 6. Table Comparing the Average Standard Deviations Associated with Wet Frozen Samples vs. NIST 2702.

Pooled Standard Deviations Wet vs. Dry Sediment	Fe (ppm)	Ca (ppm)	Mn (ppm)	As (ppm)	Cd (ppm)	Pb (ppm)	Cr (ppm)
Pooled SD From All Core Samples Sum of Phases (Wet-Bulk Sediments, n = 180)	±3336	±22612	±65.9	±1.64	±0.14	±20.8	±12.1
Pooled SD of NIST 2702 Sum of Phases (Dry Sediment, n = 51)	±1280	±72.7	±24.5	±1.22	±0.08	±2.84	±5.90
Percent Difference Between Dry and Wet Sediment SD's	**61.6**	**99.7**	**62.8**	**25.3**	**44.2**	**86.3**	**51.2**

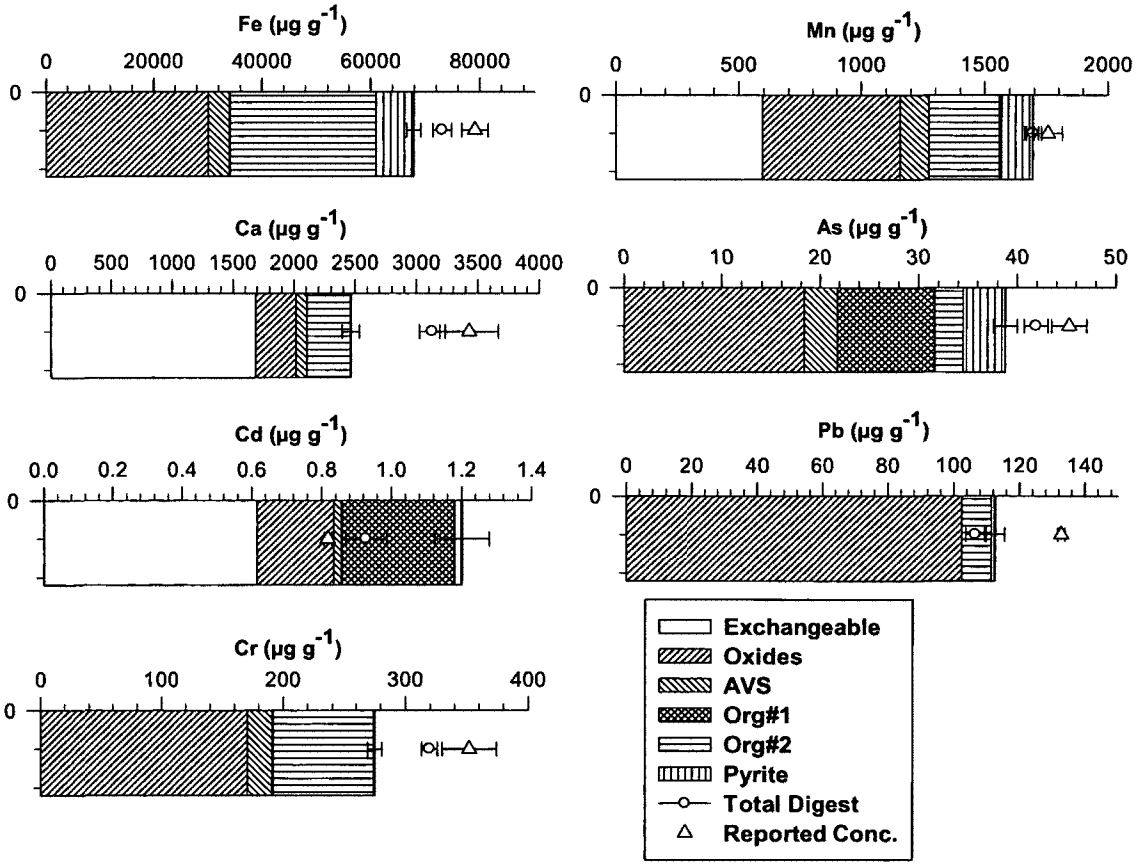

Fig. 6. Average Phase Speciation Concentrations (n = 51) of All of the Elements of Interest for NIST 2702 Standard Reference Sediment. Average total digest recoveries (n =30) and reported concentrations are noted. Error bars for phases note the pooled standard deviation associated with all six steps of the leaching process.

or similarities between elements are clear for some metals such as Ca (e.g., randomly distributed shell material) and Mn and Fe (both precipitate as insoluble oxides in oxic sediments), but not as clear for the other elements.

Cd Spectral Interferences. The average recoveries for the total digestions of the NIST 2702 standard reference sediment (Fig. 6) is not within the reported uncertainty for one of the major elements (Fe) and two of the trace elements (Cd and Pb). Because NIST 2702 is fully homogenized, this discrepancy is likely due to either some lack of efficiency on the part of the total digestion method (likely for Fe and possibly for Pb), or an analytical problem possibly related spectral interferences (likely for Cd, where the average sum of the phase leaches and the average total digests concentrations are greater than the certified value). In order to determine whether the discrepancy between the NIST 2702 reported Cd value and average total digest Cd value is an analytical problem related to the ICP-OES analysis, several NIST 2702 total digest samples (n =6) from multiple digestion batches were analyzed for Cd concentrations using high-resolution ICP-MS (Inductively Coupled Plasma Mass Spectrometry). Total digest samples of NIST 2702 were used in this comparison in order to avoid possible wet-bulk sediment heterogeneity problems, and possible matrix issues associated with the reagents used in the phase speciation leaches. The results of this comparison (Fig. 7) are illustrated in on the following page.

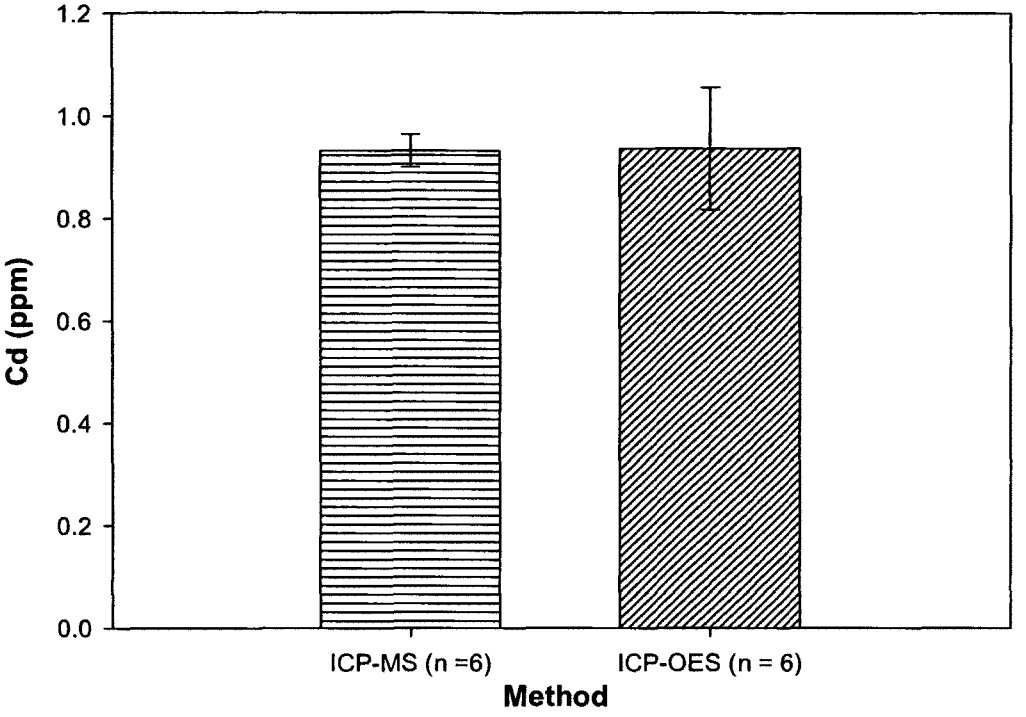

Fig. 7. Cd Concentrations in the Same Total Digest NIST 2702 Samples (n = 6) Using ICP-MS and ICP-OES. Standard deviation associated with ICP-OES is almost four times greater (±0.119 ppm vs. ±0.032 ppm) than ICP-MS analytical method. Nonparametric Mann-Whitney Test results show that both data groups are statistically the same with a p-value of 0.937.

Above shows that the calculated mean Cd concentration values for the six samples are essentially the same for both analytical methods (Fig. 7). However, the standard deviation between each of the samples for ICP-OES analysis is almost four times greater than the ICP-MS method. The greater variability associated with the emission spectroscopy method increases the amount of analytical error, which could cause either an underestimation or overestimation of sediment Cd concentration. Therefore, this does not fully explain why the Cd concentrations for the average sum of the phase leaches and total digests are consistently higher than the reported NIST 2702 Cd concentration. However, the considerably higher Cd concentrations reported in the

phase speciation leach sums (~30%) is likely due to significant matrix effects, caused by leaching reagents used (e.g., 1M NaOH is used in the organic #1 phase leach, 1M $MgCl_2$ is used in the exchangeable phase leach, etc.) compared to the 1M HNO_3 used to solublize the total digest samples. Unfortunately, this could not be confirmed, as ICP-MS analyses were not performed on the NIST 2702 phase digestion samples for comparison due to time constraints.

CHAPTER 3

METAL PHASE SPECIATION IN ESTUARINE SEDIMENTS

3.1. Previous Speciation Studies

The six step leaching process discussed in Chapter 2 was applied to sediments obtained from three estuaries: the Elizabeth River, Baltimore Harbor, and the Napa River near Mare Island in San Francisco Bay. In order to verify some of the overall sediment metal concentrations obtained from the six step phase speciation leaches, comparisons were made to previous leaching studies done on sediments taken from nearby locations in the same three estuaries (Table 7). However, these published studies used techniques that were quite different from the six step phase speciation leaching process. Because of this, the metal concentrations reported in these studies (Rule, 1986, Tsai et. al., 1979, and Lu et. al., 2005) were compared to metal concentrations summed from selected phases obtained from the leaching scheme utilized in this study. All of these previous studies utilized homogenized surface sediments obtained using sediment grabs. Therefore, in order to compare the present results to these studies, the average metal concentrations from each of the six sediment cores studied in this project were calculated with the standard deviations representing the variations in metal concentrations throughout each core.

The total sediment metal concentrations reported by Rule (1986) for the Elizabeth River were obtained using a hot concentrated nitric acid digest followed by the addition of 30% peroxide and additional heating, while the total sediment metal concentrations for Baltimore Harbor from Tsai et. al. (1979) were obtained using a digestion method which utilized a mixture of boiling nitric and sulfuric acids. Both of these methods represent

Table 7. Previous Studies Verses the Average Metal Concentrations from Each of the Sediment Cores Taken from the Northern and Southern Chesapeake Bay Regions and Northern San Francisco Bay. Average metal concentrations that are statistically different from previous study are shown in bold.

Average Metal Concentrations for Cores Used in this Study Verses Previous Studies		Fe (%)	Mn (ppm)	Cd (ppm)	Pb (ppm)	Cr (ppm)	As (ppm)
Elizabeth River	**Mean Lower Elizabeth River (Rule, 1986)**	3.62 ±0.551	398 ±87	2.0 ±1.1	93 ±39	53 ±7	NA
	Avg. Core ER1 (Sum of All Phases)	2.82 ±0.87	307 ±75	1.0 ±0.3	51 ±19	36 ±11	8 ±3
	Mean Mid-Elizabeth River (Rule, 1986)	3.16 ±1.25	251 ±111	2.8 ±0.9	157 ±79	56 ±23	NA
	Avg. Core ER2 (Sum of All Phases)	3.74 ±0.62	308 ±56	0.6 ±0.1	67 ±21	50 ±9	12 ±3
Baltimore Harbor	**Station #8 (Tsai et. al., 1979)**	NA	**650**	**2**	120	**490**	29
	Avg. Core BH 1 (Sum of All Phases)	6.40 ±1.56	**1510 ±391**	**1.1 ±0.3**	120 ±44	**194 ±66**	39 ±11
	Station #10 (Tsai et. al., 1979)	NA	**180**	**4**	170	**190**	**31**
	Avg. Core BH 2 (Sum of All Phases)	4.76 ±1.01	**613 ±142**	**1.6 ±0.7**	135 ±61	**167 ±65**	**18 ±6**
Near Mare Island	**Davis Pt. Core (Lu et. al., 2005)**	1.3 (1.1-1.7)	506 (296-761)	0.28 (0.14-0.74)	24 (21-29)	**16 (12-21)**	NA
	Avg. Core MI 1 (Sum of EX,OX, and AVS)	1.92 ±0.33	489 ±58	0.5 ±0.1	37 ±13	**36 ±5**	8 ±2
	MIC Core (Lu et. al., 2005)	1.8 (0.99-2.9)	637 (282-1136)	0.23 (0.1-0.55)	25 (13-39)	**23 (15-28)**	NA
	Avg. Core MI 2 (Sum of EX, OX, and AVS)	2.08 ±0.28	642 ±229	0.3 ±0.1	21 ±2	**39 ±4**	9 ±1

digestions without a significant dissolution of silicate bound metals. Because of this, the results from these studies were compared to the total metal sums from all six phases of this six step leaching process, which also represent the total non-silicate bound metals in the sediments. The standard deviations reported from Rule (1986) represent the deviations in metal concentrations from numerous sediment grabs taken over the entire length of the lower and mid-Elizabeth River sections. Standard deviation values were not reported by Tsai et. al. (1979), since these values represent individual sediment grabs. However, the sediment metal data reported by Tsai et. al. (1979) are useful because their sediment grabs were taken relatively close to where the Baltimore Harbor cores used in this study were obtained (exact coordinates are not noted by the authors).

In contrast, the sediment metal concentrations reported by Lu et. al. (2005) for cores taken near Mare Island were obtained using a weak (0.5 M HNO_3 at 25°C) nitric acid leach, which would have only removed weakly bound metals. Therefore, the results from Lu et. al. (2005) were compared to the average trace metal sums from the first three leaches of the six step phase speciation leach. These three steps of this leach (which end with the 0.5 M HCl AVS leaching step) should contain the majority of the weakly bound metals in these sediments. The results from Lu et. al. (2005) include the maximum and minimum metal concentration values (shown in parentheses) for individual sediment grabs, which were collected every two months at each location over the course of a year. Like the Tsai et. al. (1979) Baltimore Harbor study, the locations of these sediment grabs appear to have been close to where the MI1 and MI2 cores used in this study were obtained (exact coordinates were not provided by the authors).

Table 7 shows that most of the results from this study are similar to the metal concentrations reported by Rule (1986), Tsai et. al. (1979), and Lu et. al. (2005) for sediments in the Elizabeth River, Baltimore Harbor, and near Mare Island locations. Of the three published studies, the comparison between Tsai et. al. (1979) and the results from cores BH1 and BH2 show the greatest differences in sediment metal concentrations. This is not surprising, given that a significant amount of time has passed since these two studies were performed. The thirty year time difference between this study and the study performed by Tsai et. al. (1979) makes it likely that factors such as dredging and storm events have significantly changed the surface sediment composition in these sampling locations. However, despite the fact that many of the element concentrations reported by Tsai et. al. (1979) are statistically different from the average concentrations found in the Baltimore Harbor cores, the trends in total non-silicate-bound sediment metal concentrations in these two studies are similar. Tsai et. al. (1979) reported higher concentrations of Mn and Cr, and lower concentrations of Cd, Pb, and As in sediment taken from their Station #8 than their Station #10. With the exception of As, this is similar to what is observed in this study for the Baltimore Harbor cores, with core BH1 being approximately near their Station #8 and core BH2 being approximately near their Station #10. The comparison between the MI1 and MI2 core data and the metal concentrations published by Lu et. al. (2005) shows that the results from the sums of the first three steps of the six step leaching scheme is between the minimum and maximum reported metal concentrations published by Lu et. al. (2005) for all of the metals except Cr. The average Cr concentrations measured in cores MI1 and MI2 are almost twice the average reported by Lu et. al. (2005). The reason for these higher average Cr results

likely reflects the relatively high efficiency of the oxalate oxide leach step of the six step leaching process, which is very effective at removing Fe-and Mn-oxide bound Cr in sediments (Discussed in Section 2.4.6.).

3.2. Major and Trace Metals Phase Distributions

In order to compare the six-step phase speciation leach results from the Elizabeth River, Baltimore Harbor, and the Napa River near Mare Island, the concentrations of the major sediment constituents (Fe, Mn, and Ca) and trace metals (As, Cd, Pb, and Cr) in the various leaches were summed and then each was expressed as a percent of the total. This allowed for the comparison of the metal phase proportions between the sediment layers within the cores, between the cores from different parts of the estuaries, and between the estuaries. Total C and S data for each core section are also included on the left side of each profile for comparison.

Iron Phase Speciation Profiles. The phase speciation percentage profiles for Fe (Fig. 8), illustrated on the following page, show clear diagenetic signatures in the Elizabeth River and Baltimore Harbor cores. Overall, these sediment profiles show a lower percentage of pyrite bound Fe at the surface of the sediment columns and higher amounts with depth. The total S concentrations also generally increase down core in all of the sediment profiles, with the most prominent concentration increases occurring in the Elizabeth River and Baltimore Harbor cores (Fig. 8). This shows that there is a significant overall positive correlation (Pearson $r = 0.835$ and $p < 0.001$) between the sediment total S concentrations and the percentages of pyrite associated Fe in these cores. As expected,

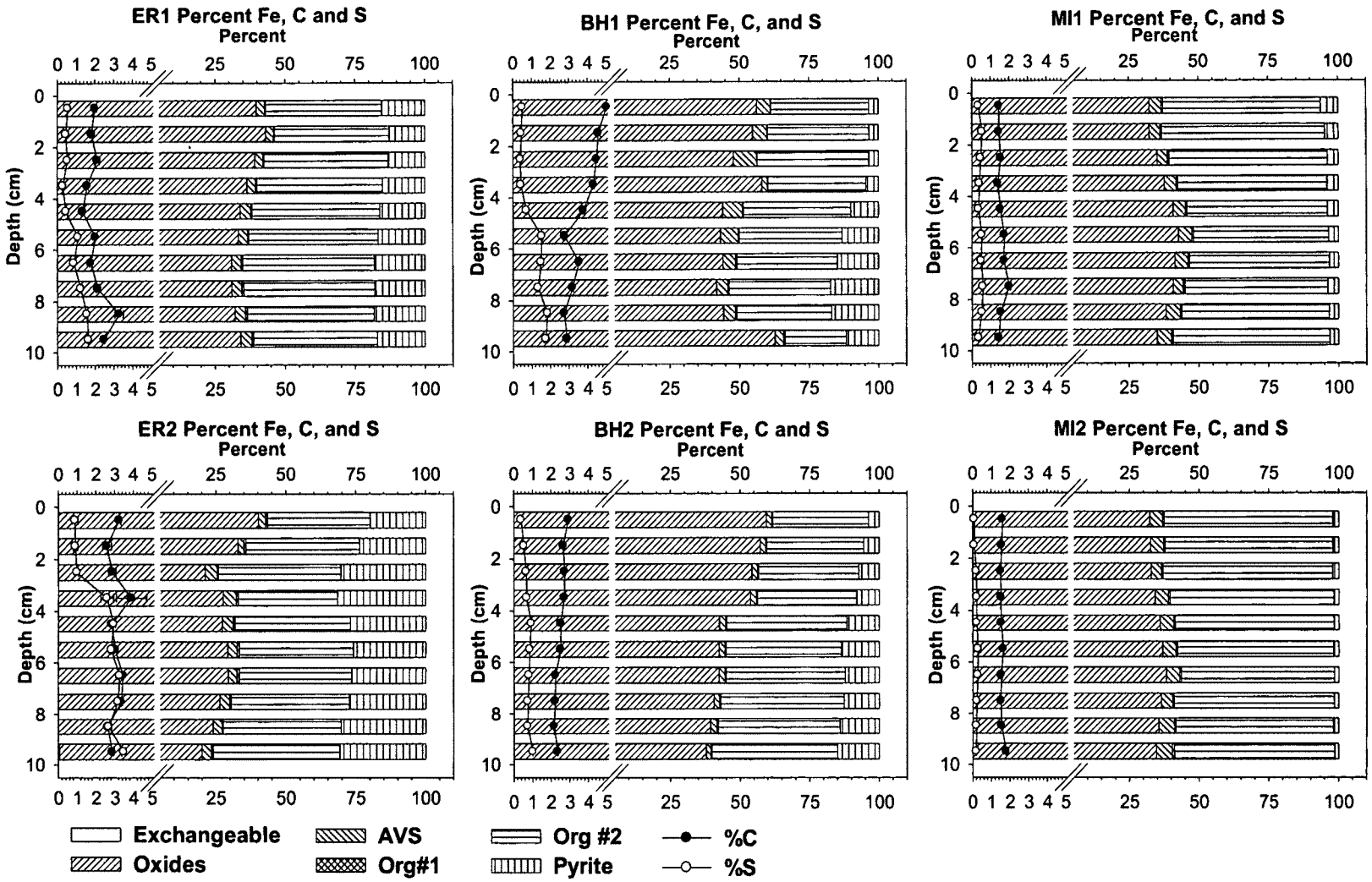

Fig. 8. Sediment Profiles Showing the Total Percentage of Each Phase for Fe Out of the Sum of the Phases in Each of the Six Sediment Cores. Total C and S percents are by total weight of sediment.

the percentages of oxide phase Fe in the Elizabeth River and Baltimore Harbor cores mostly trend in the opposite direction and tend to decrease down core. In contrast to this, the phase speciation percentages in the Mare Island sediment change very little down core, indicating that the redox conditions in the Mare Island cores have minor depth gradients. The AVS phase speciation distribution for Fe also changes very little down core in most of these profiles, with the only exception being Baltimore Harbor core BH1 (Fig. 8). This core shows a slight increase in the AVS phase Fe about half-way through the profile, and then a subsequent decrease toward the base of the core. With the exception of BH2, which shows a general increase in the percentage of organic-bound Fe down core, the overall percentage of organic-bound Fe changes little with depth in the cores (Fig. 8).

Average Iron Phase Speciation. The overall average phase speciation for Fe in each of the sediment cores (Fig. 9), illustrated on the following page, clearly show similarities among sediment cores taken within the same estuaries. The average pyrite Fe proportions significantly correlates with the total proportion of S (Pearson Correlation $r = 0.946$, $p = 0.004$) in these sediment cores. However, the average phase proportions of pyrite Fe does not significantly correlate with the total proportion of C (Pearson Correlation $r = 0.523$, $p = 0.287$). In addition, the average proportion of Fe associated with the oxide phase for each core does not significantly correlate with the average proportion of Fe associated with the pyrite phase (Pearson Correlation $r = -0.454$, $p = 0.366$), as would be expected in systems dominated by diagenetic processes. This suggests that other factors not related to average total organic carbon sediment concentrations, such as salinity differences between the estuaries, different

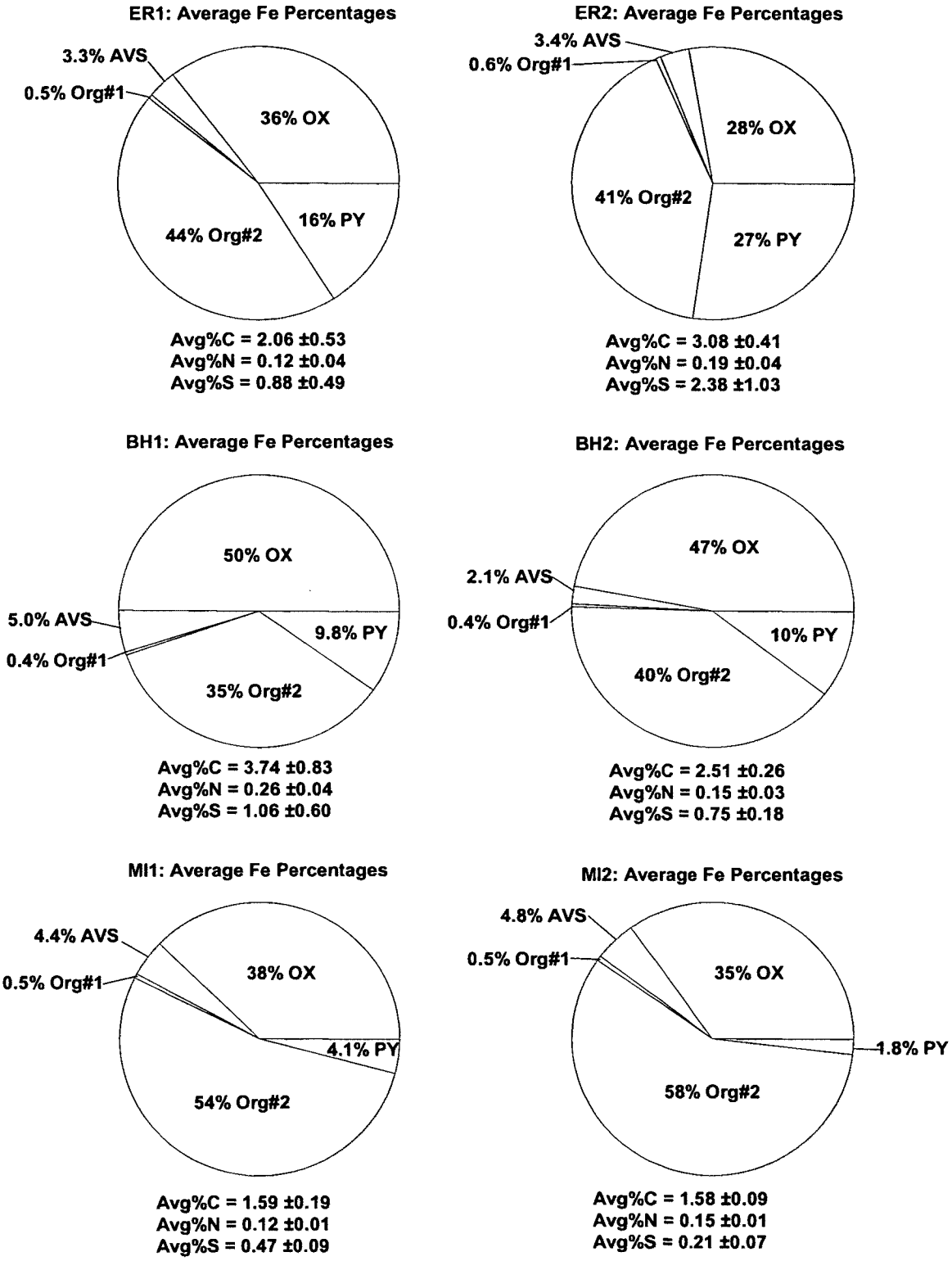

Fig. 9. Pie Graphs Showing the Average Percentages of the Sums of the Phases for Fe in Each Core. Average total carbon, nitrogen, and sulfur percentages for each core are noted below each graph.

sediment oxygen availability due to differing degrees of bioturbation, and/or the type of organic matter in these sediments are dictating the degree of Fe pyritization in these cores. However, salinity (via the concentration of the sulfate ion) usually does not play an important role in the rate of sulfate reduction in most marine and estuarine sediments (Berner, 1984). Therefore, the differing proportions of pyrite-bound Fe, specifically between the Elizabeth River and Baltimore Harbor cores (both with high C and S), is likely due to the type of organic material in each core (sulfate reduction rates in reactive vs. less reactive organic material, as discussed by Westrich and Berner, 1984) or perhaps differing degrees of bioturbation within the sediment cores from each of the estuaries (Luoma and Rainbow, 2008). The fact that the oxide phase is one of the largest reservoirs of Fe in all of these sediments is in agreement with results of numerous other phase speciation studies performed on estuarine or marine sediments (Abaychi and Douabul, 1986; Izquierdo et. al., 1997; Kersten and Forstner, 1986; Riba et.al., 2002; Wiese et. al., 1997; Guo et. al., 1997; Lopez-Gonzalez et. al., 2006; Wang et. al., 2010). The organic fraction of this leach method (organic #2 specifically) also contains a large proportion of Fe in all of the cores, and this result also compares well with other studies (Abu-Hilal, 1993; Wiese et. al., 1997; Guo et.al., 1997). However, the organic leaching steps applied in these studies utilized H_2O_2, which would also solublize Fe associated with pyrite minerals in addition to organic-bound Fe. Therefore, it is difficult to directly compare the organic phase Fe leaching results reported by these authors to the organic phase Fe obtained in this study.

Manganese Phase Speciation Profiles. The phase speciation profiles for Mn (Fig. 10), illustrated on the following page, show that this element only slightly follows the phase speciation of Fe. One of the most significant differences between the profiles of these two elements is the lack of a significant exchangeable fraction in the Fe profiles. This may be due to the relatively rapid formation of low solubility Fe minerals in both oxic (Fe oxides) and anoxic (FeS and FeS_2) marine environments (Burdige, 1993; Sadiq, 1992). However, Mn can exist in the readily soluble form of Mn^{2+} in anoxic and suboxic marine environments (Burdige, 2006). Other researchers have also noted that Mn can be released to the readily exchangeable phase from fully oxidized sediment, due the tendency of this element to loosely adsorb onto its own oxide minerals (Rifaat, et. al., 1992). Half of the Mn phase profiles (Fig. 10) (ER1, ER2, and BH1) show appreciable percentages of pyrite-bound Mn. These three cores also contain the highest average total sulfur concentrations throughout the profiles and some of the highest average pyrite phase Fe speciation percentages (Fig. 9). These observations indicate that appreciable amounts of Mn are incorporated into the pyrite phase of these sediments only when a relatively large percentage of Fe is incorporated into the pyrite phase. This apparent threshold behavior for Mn pyritization seen in these sediment cores is a diagenetic trend that has also been described by other authors (Huerta-Diaz and Morse, 1992).

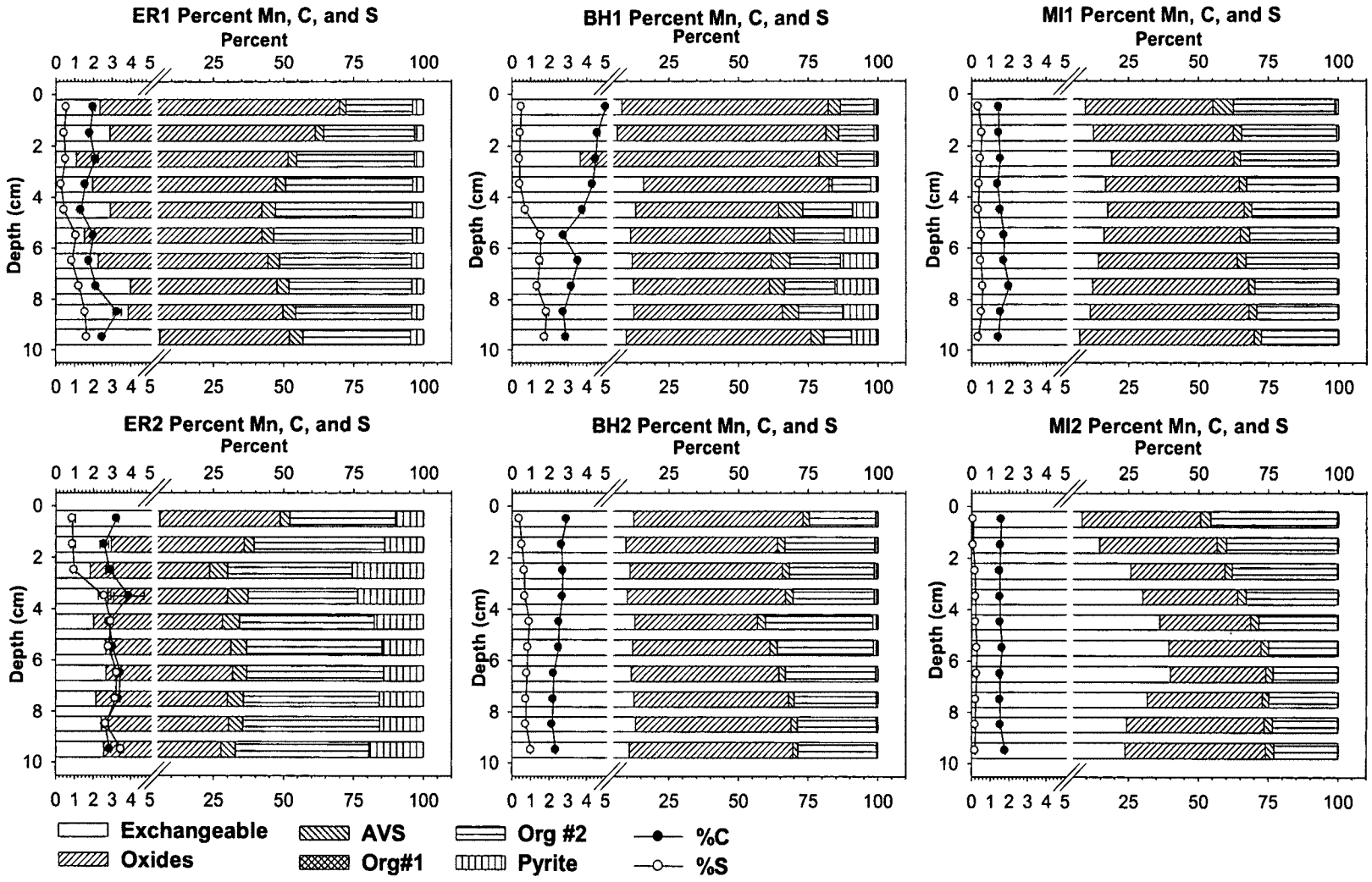

Fig. 10. Sediment Profiles Showing the Total Percentage of Each Phase for Mn Out of the Sum of the Phases in Each of the Six Sediment Cores. Total C and S percents are by total weight of sediment.

Average Manganese Phase Speciation. The average phase speciation distribution for Mn in each of the six sediment cores (Fig. 11) is illustrated on the following page. Unlike Fe, the average Mn phase distribution for cores taken from the same estuaries are not obviously similar. However, some trends do exist, such as the lowest overall percentage of exchangeable Mn being in the Elizabeth River cores, and highest in the Mare Island cores, and the percentage of pyrite associated Mn (ER2 > BH1 > ER1 > BH2 > MI1 > MI2) generally increases as the average total S sediment concentrations increase (ER2 > BH1 > ER1 > BH2 > MI1 > MI2). The proportion of AVS Mn (BH1 > ER2 > ER1 > MI1 > MI2 > BH2) also follows a somewhat similar trend, but only for sediments with relatively high total S concentrations. Overall, the average Mn phase speciation in all of these estuaries shows that the majority of the Mn in these sediments is located in the oxide and organic phases. Many workers have also reported large percentages of Mn in the oxide fractions of estuarine or marine sediments (Abu-Hilal, 1993; Guo et. al., 1997; Wiese et. al., 2003; Riba et. al., 2002; Whiteley and Pearce, 2003; Sundaray et. al., 2011). Workers have also reported a large percentage of Mn being associated with carbonates (Izquirdo et. al., 1997; Riba et. al., 2002; Wiese et. al., 2003; Whiteley and Pearce, 2003; Sundaray et. al., 2011). However, because this study did not utilize a carbonate leaching step, any Mn associated with the carbonate phase of the sediments leached in this study (albeit likely small, given that the total carbonate concentrations for all sediments were < 0.2%) would have been distributed into other phases (likely the AVS phase).

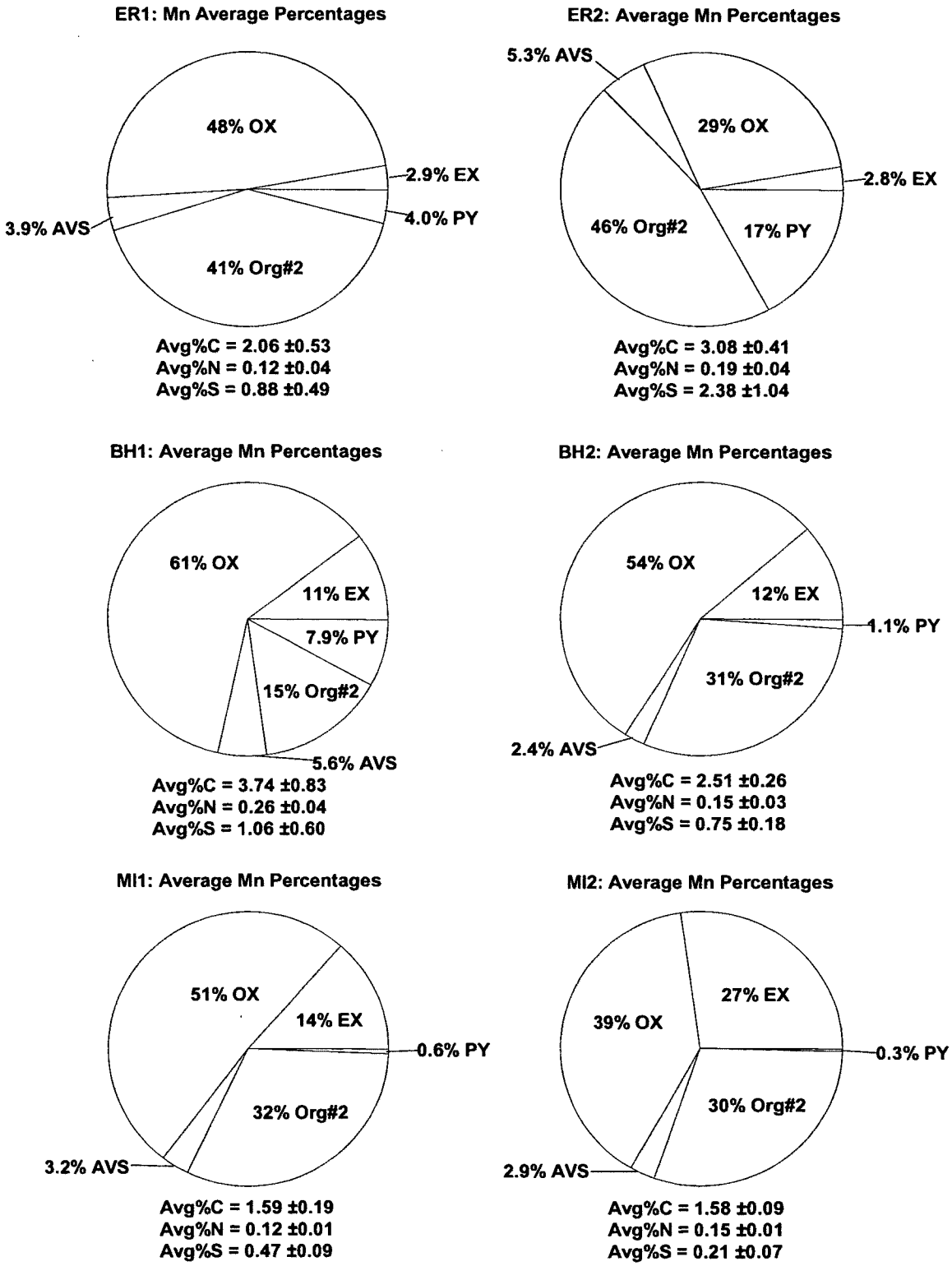

Fig. 11. Pie Graphs Showing the Average Percentages of the Sums of the Phases for Mn in Each Core. Average total carbon, nitrogen, and sulfur percentages for each core are noted below each graph.

Calcium Phase Speciation Profiles. The phase speciation distribution profiles for Ca in each sediment core (Fig. 12) are quite different from the Fe distribution profiles, but they do show some similarities to the Mn distribution profiles. The most obvious similarity between the Mn and Ca profiles is both of these elements have a significant percentage (> ~15%) in the readily exchangeable fraction. For Mn, this occurs throughout much of the Baltimore Harbor and Mare Island cores, and for Ca, this occurs in almost every section of all of the sediments cores. This similarity is likely due to the fact that these two metals are geochemically linked through the formation of carbonate minerals, and the fact that both of these elements can readily adsorb to mineral sediment surfaces (Morse, 1986). Finally, although large amounts of Ca were extracted in the AVS and organic #2 fractions throughout these cores, the significance of this result is questionable, as it likely reflects the dissolution of carbonate-rich shell material.

Average Calcium Phase Speciation. The average phase speciation pie graphs for Ca (Fig. 13) show few consistent trends. The varying amounts of Ca in the oxide, AVS, and organic #2 phases generally reflect the amount of shell hash present in these sediment cores. In cores with large amounts of shell material, such as those from Baltimore Harbor and Mare Island, significant amounts of Ca has likely been carried over into the organic #2 phase.

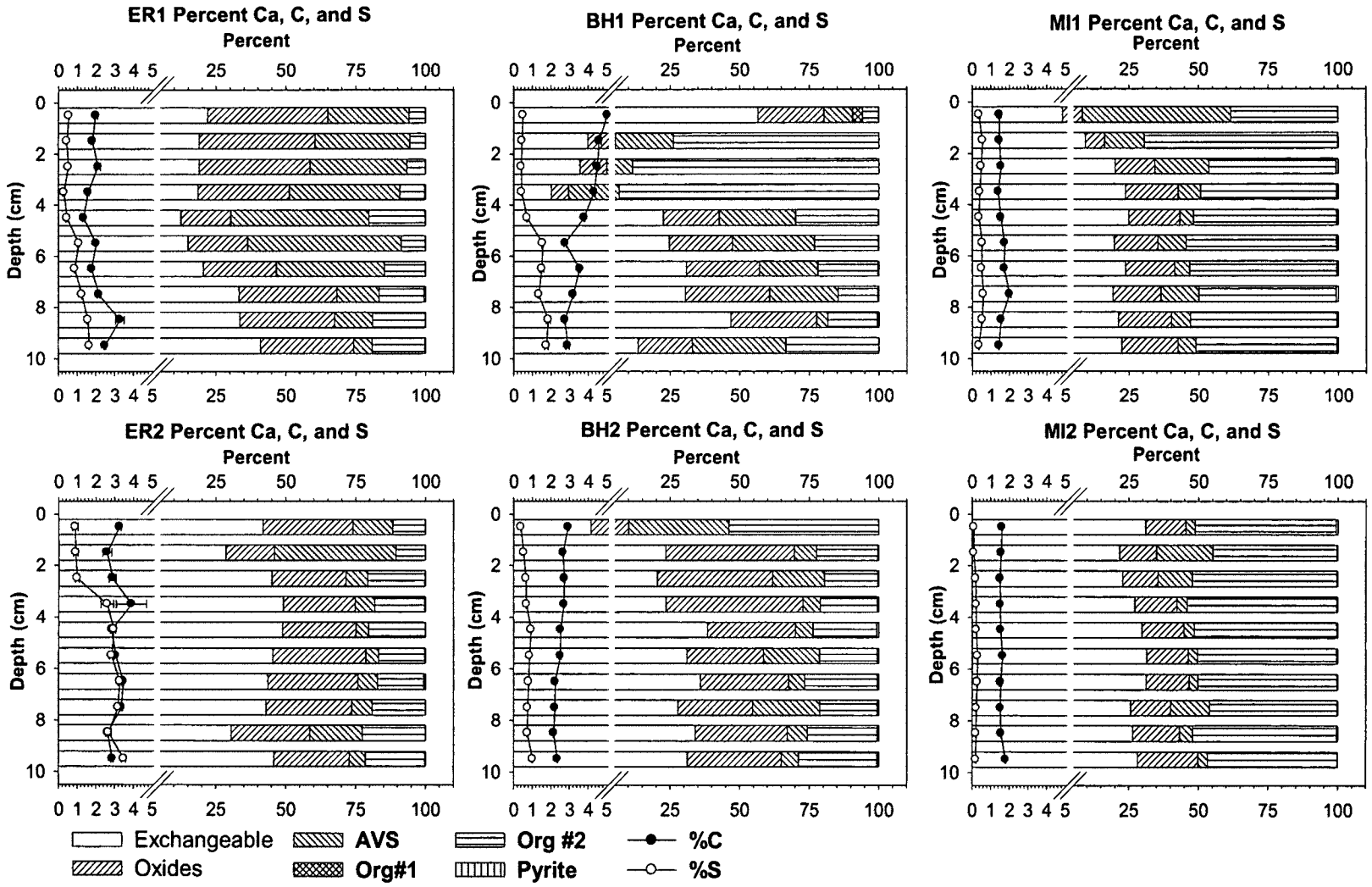

Fig.12. Sediment Profiles Showing the Total Percentage of Each Phase for Ca Out of the Sum of the Phases in Each of the Six Sediment Cores. Total C and S percents are by total weight of sediment.

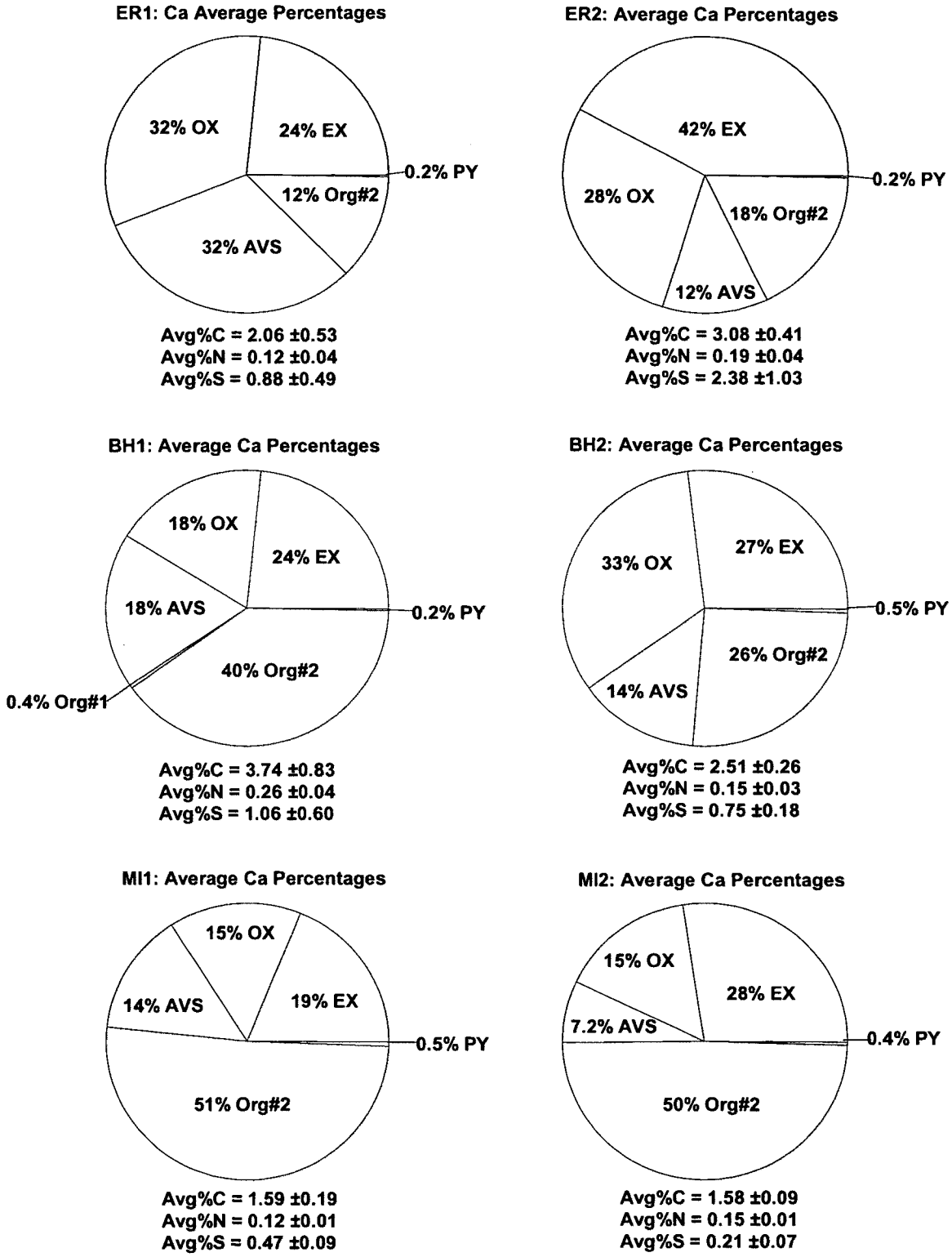

Fig. 13. Pie Graphs Showing the Average Percentages of the Sums of the Phases for Ca in Each Core. Average total carbon, nitrogen, and sulfur percentages for each core are noted below each graph.

Cadmium Phase Speciation Profiles. The phase speciation profiles for Cd (Fig. 14) show that, with the exceptions of ER2 and MI1, most of the core sections have a larger percentage of exchangeable Cd in the surface sediments than in the deeper sediments. Overall, the percentages of Cd associated with the oxide phase varies quite significantly throughout many of these cores, with apparent increases in the percentage of oxide-bound Cd occurring down core in four out of the six sediment cores (ER1, BH1, BH2, and MI2). The proportion of AVS associated Cd is low in all of these cores, with a slight increase occurring down core in most of the sediment profiles. These low Cd AVS phase percentages occur even in the anoxic material at the bases of these sediment cores. However, the AVS phase Cd concentrations in all of the sediment cores positively correlate (Pearson Correlation $r = 0.640$, $p < 0.001$) with the Cutter and Oatts (1987) sulfide AVS concentrations. Despite the apparent overall low percentage of AVS phase Cd in these sediment cores, AVS-bound Cd is important because it plays a major role in the bioavailability of this element in anoxic sediments (Di Toro et. al., 1992). Core BH1 shows a significant positive correlation between the percentage of organic bound Cd (organic #1 + organic #2) and total sediment C concentration (Pearson $r = 0.908$ and $p < 0.001$), whereas core MI2 shows a significant negative correlation between these two variables (Pearson $r = -0.801$ and $p = 0.005$). The significant positive correlation between total organic-bound Cd and total sediment C in BH1 suggests that Cd is being released from organic carbon down core, which is likely due to the remineralization of organic matter. The significant negative correlation between the total organic-bound Cd and total sediment C in MI2 might also be the result of organic C remineralization, as the

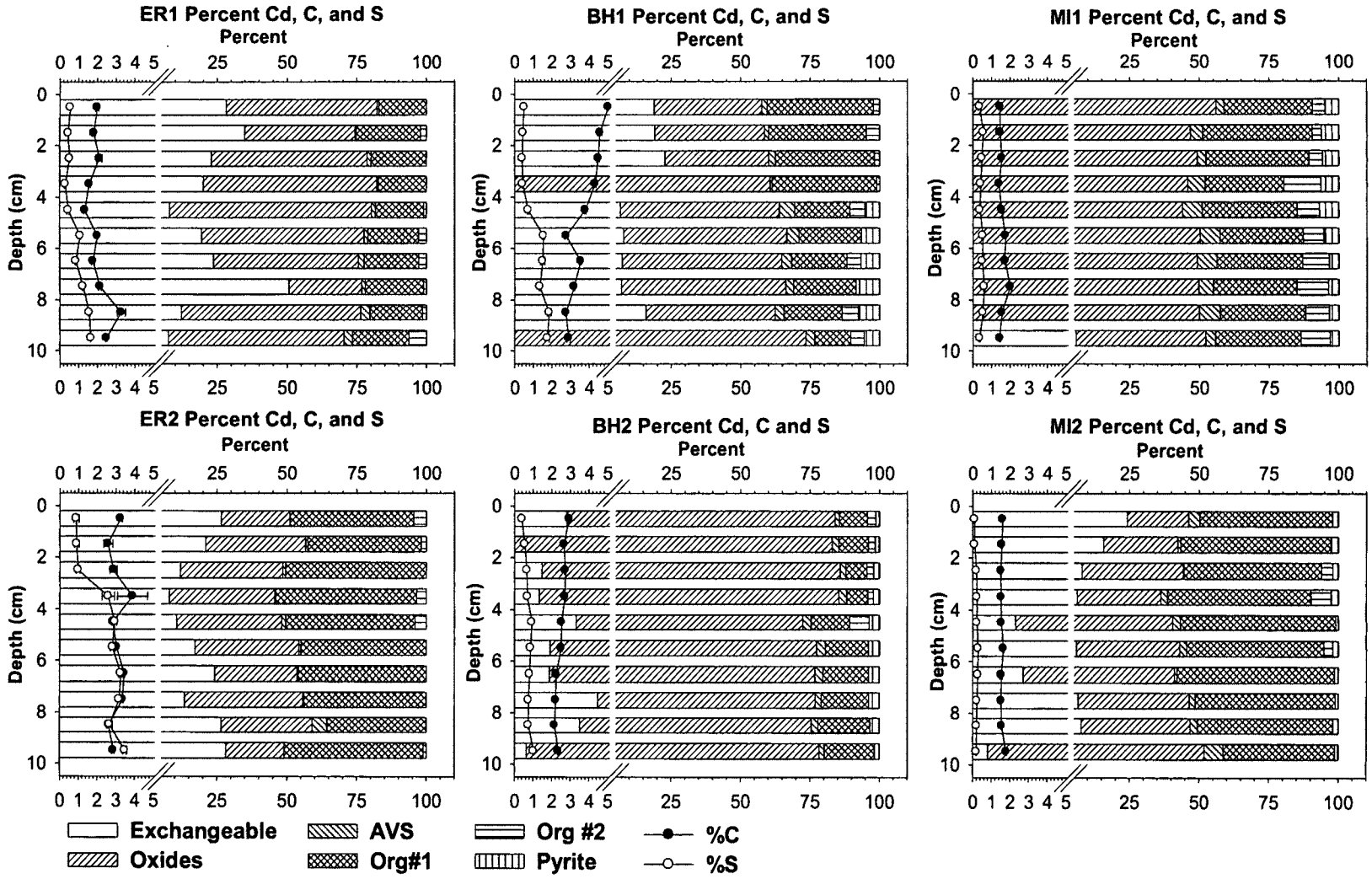

Fig. 14. Sediment Profiles Showing the Total Percentage of Each Phase for Cd Out of the Sum of the Phases in Each of the Six Sediment Cores. Total C and S percents are by total weight of sediment.

total organic-bound Cd percentage in this profile is decreasing down core. However, the type of organic carbon in core MI2 (greater concentration of carbon rich material such as black carbon deposits and/or protokerogen) could be changing down core in this profile, which could result in an overall increase in the total sediment C concentration (i.e., organic-bound Cd is being released from the remineralized labile organic C only). All of the core profiles show very little Cd incorporated into the pyrite phase. The profiles with the highest percentages of Cd in the pyrite phase (BH1 and MI1) show trends that are similar to the pyrite phase Fe distribution profiles (Fig. 8) for these sediment cores. However, the overall pyrite phase percentages of Cd in the profiles of BH1 and MI1 (Fig. 14) are low (~5%). This indicates that Cd is not readily associated with the pyrite phase of these sediments, which is similar to what has been reported by other authors for Cd in sediments taken from marine and estuarine environments (Huerta-Diaz and Morse, 1992; Kluckhohn, 1990).

Average Cadmium Phase Speciation. The average phase speciation distribution for Cd (Fig. 15) is different for each individual core, with no obvious similarities within the estuaries themselves. The reason for this might be due to relatively low concentrations of this element in all of these sediments, which led to significant analytical uncertainty (see discussion in Chapter 2). Overall, the sediment bound Cd in these three estuaries is mainly concentrated in the oxide and organic fractions, with a significant amount also being found in the exchangeable fraction of the Elizabeth River cores. This is similar to what has been observed by researchers in other estuaries (Riba et. al., 2002; Guo et. al., 1997; Abu-Hilal, 1993; Passo et. al., 2011; Amiard et. al., 2007). However, workers have also noted a significant amount of Cd in the carbonate phase of sediments

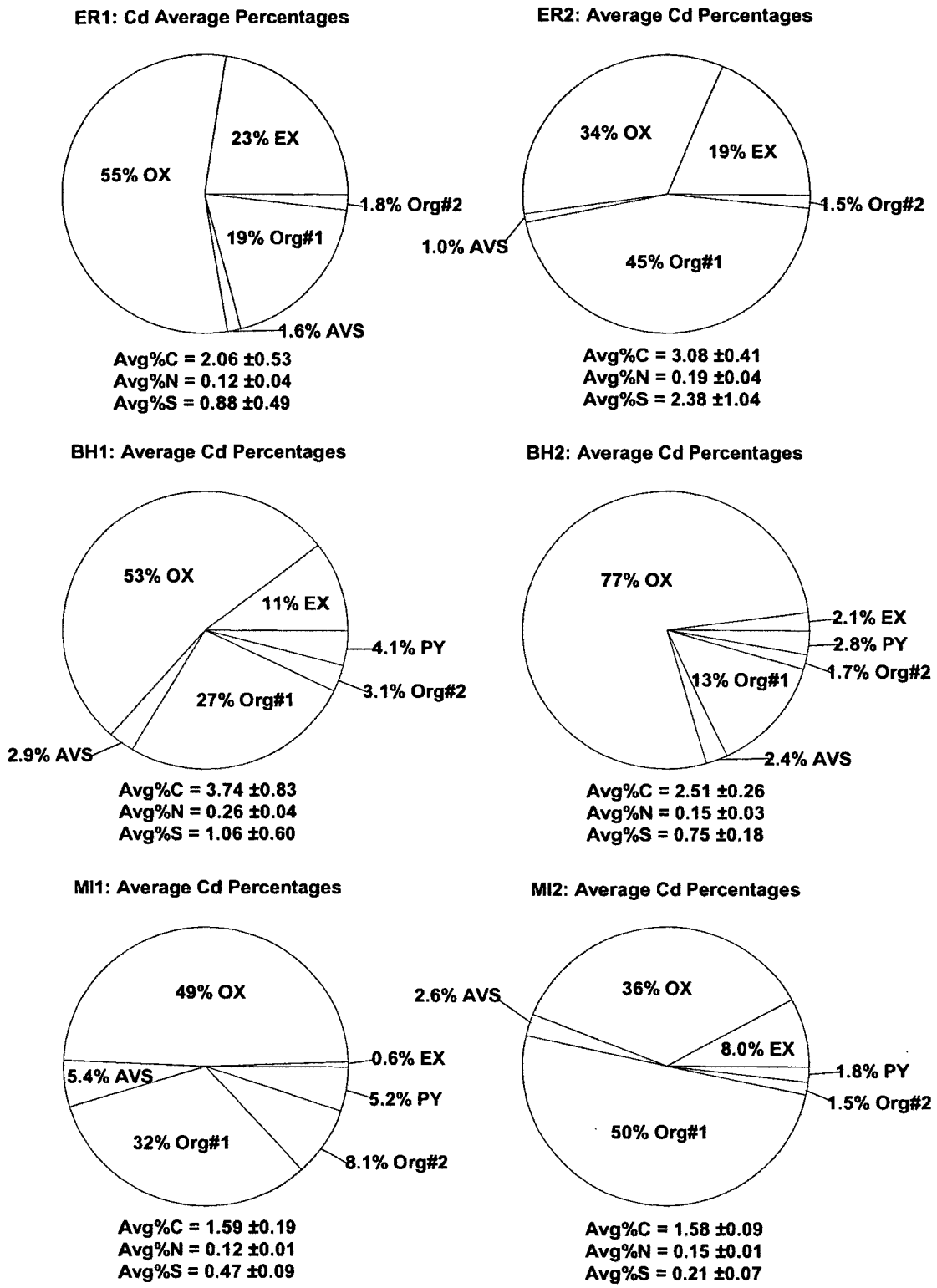

Fig. 15. Pie Graphs Showing the Average Percentages of the Sums of the Phases for Cd in Each Core. Average total carbon, nitrogen, and sulfur percentages for each core are noted below each graph.

(Rifatt et. al., 1992; Guo et. al., 1997; Abaychi and Douabul, 1986). Since the six step leaching method lacked a carbonate extraction step, any Cd associated with this phase would have been extracted in the AVS phase. However, since these sediments contained little carbonate (< 0.2%), the amount of carbonate-bound Cd extracted in the AVS phase should have been relatively small. The average percent AVS and pyrite phase Cd was rather small for all of the cores, with the highest being seen in cores BH1 and MI1. The reason why these cores contain the highest average percentages of sulfide-bound Cd is unclear, as these two cores represent the extremes when it comes to average total C sediment concentrations (BH1 total C >> MI1 total C), and neither core contains the highest average concentration of total S. In addition, neither of these cores contain the highest overall concentration of Cd (BH2 is the highest according to the sum of the phases and ER1 is the highest according to the total digests). Therefore, other factors such as the degree of bioturbation in these cores may be playing a major role in the phase distribution of Cd in these sediments. High levels of bioturbation can alter sediment redox conditions by increasing the amount of oxygen exposure to sediments below the sediment-water interface (Luoma and Rainbow, 2008).

Lead Phase Speciation Profiles. The phase speciation distribution for Pb (Fig. 16) for the sediment core profiles show that the oxide phase is by far the largest reservoir of Pb in these sediments over the entire lengths of all cores. This is similar to what other workers have reported for oxic estuarine sediments (Abaychi and Douabul, 1986; Riba et. al., 2002; Abu-Hilal, 1993). Others have also reported significant amounts of Pb present in the carbonate and organic phases (Scoullos, 1986; Passos et. al., 2011; Purchase and

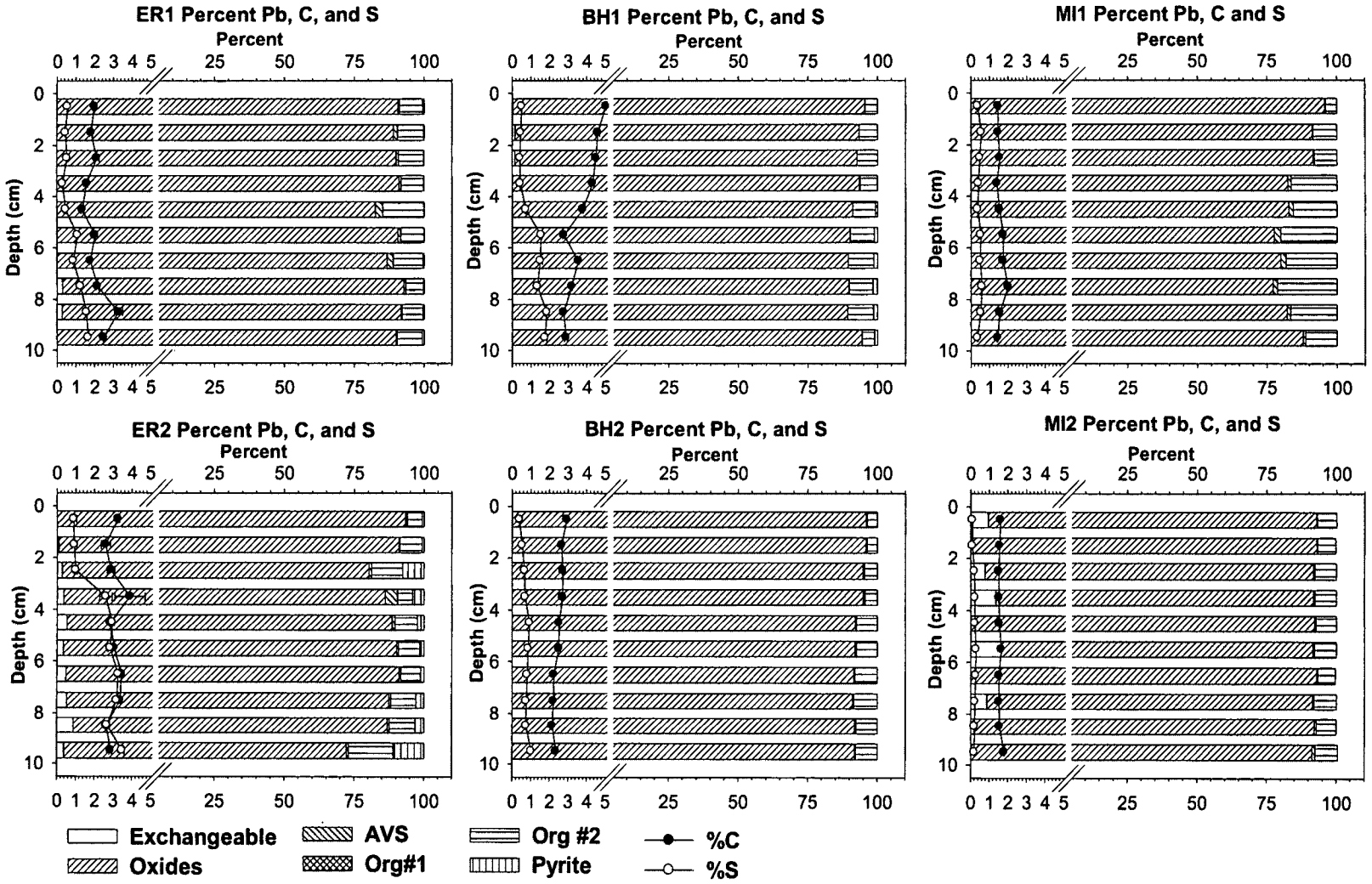

Fig. 16. Sediment Profiles Showing the Total Percentage of Each Phase for Pb Out of the Sum of the Phases in Each of the Six Sediment Cores. Total C and S percents are by total weight of sediment.

Fergusson, 1986; Abu-Hilal, 1993). However, any carbonate-bound Pb in these sediments (albeit likely small, given total sediment carbonate < 0.2% for all cores) would have been extracted in the AVS phase. The proportion of AVS phase Pb is small throughout all of the sediment cores. However, three of these cores (ER1, ER2, and MI1) show small increases in AVS associated Pb toward the middle of the profiles, then a general decrease down core, indicating possible diagenetic signatures for this element. Most of these sediments show a slight yet general increase in the percentage of organic-bound Pb (organic #2 phase only) down core (although this trend reverses toward the bases of cores BH1 and MI1). This may indicate that the oxide-bound Pb in these cores is slowly being incorporated into organic matter during burial. Only one of these core profiles (BH1 in Fig. 16) displays a significant positive correlation between the percent pyrite-bound Pb and total S percentage (Pearson $r = 0.911$ and $p < 0.001$). Overall, the percentage of pyrite-bound Pb in these profiles is low (< 4%), indicating that Pb has a low affinity for pyrite in these cores. This low affinity for pyrite by Pb is a diagenetic behavior seen by other authors studying similar sediments (Huerta-Diaz and Morse, 1992).

Average Lead Phase Speciation. The average phase speciation distribution for Pb in these cores (Fig. 17), again shows that the oxide phase overwhelmingly dominates the geochemistry of Pb in all of these sediments. Only the sediment core containing the highest average total C (BH1) shows a significant positive correlation (Pearson $r = 0.911$ and $p < 0.001$) between total S and pyrite associated Pb. However, no significant correlations (Pearson $p > 0.050$) were found between the total C and the percentages of Pb in the organic #2 phase for any of the sediment cores. With the exception of MI1 (which contains the same average percentage of total C as MI2), all of the sediment

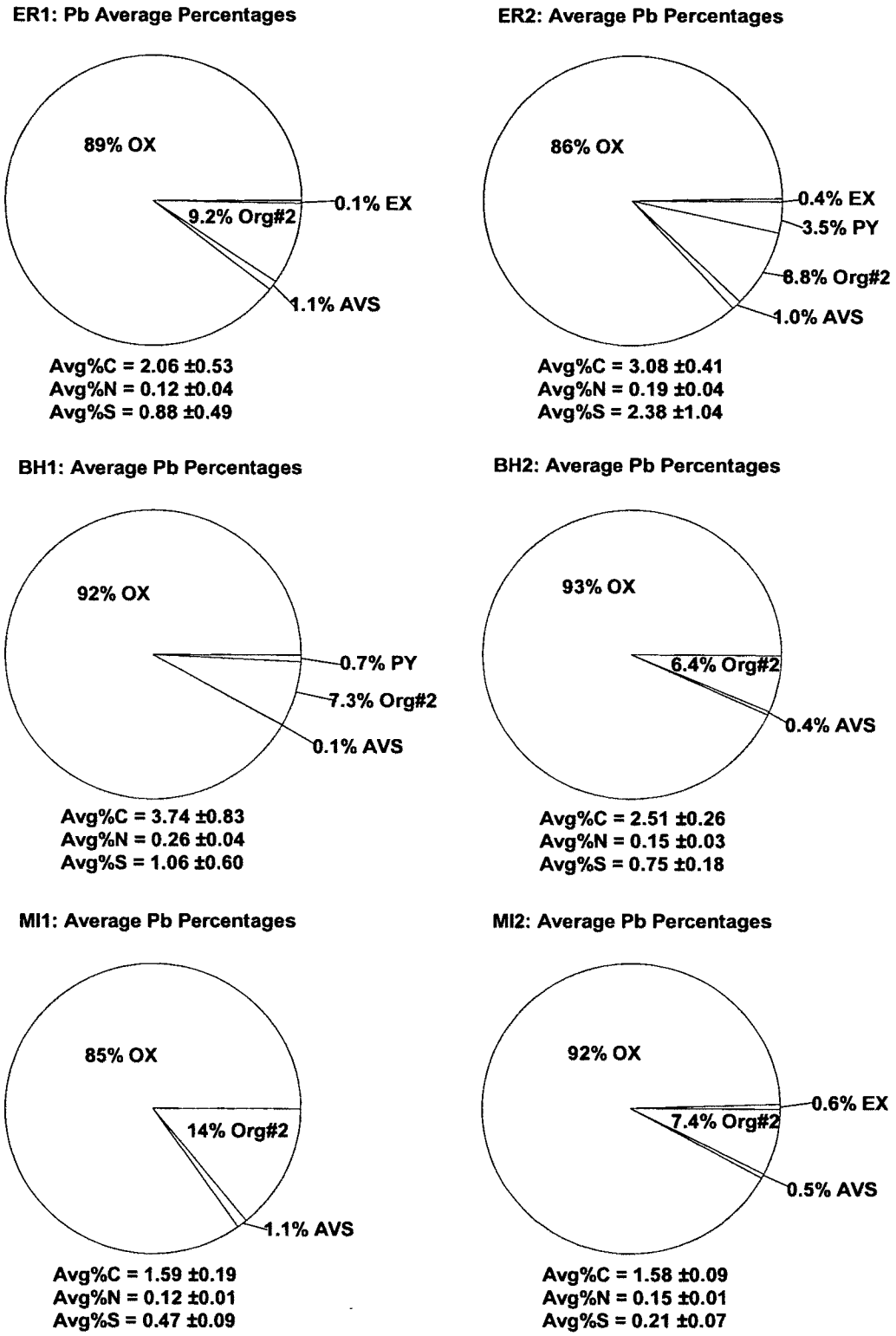

Fig. 17. Pie Graphs Showing the Average Percentages of the Sums of the Phases for Pb in Each Core. Average total carbon, nitrogen, and sulfur percentages for each core are noted below each graph.

cores contain about the same average percentage of Pb in the organic #2 phase. The average percentages of Pb in the AVS and pyrite phases are small for all of the sediment cores. Small amounts of pyrite-bound Pb are seen only in the cores with the highest average total S concentrations, with the largest percentage of pyrite-bound Pb being seen in the core with the highest total S concentration (ER2) (Fig. 17) and largest average percentage of pyrite-bound Fe (Fig. 9). This indicates that Pb may be demonstrating an apparent threshold pyritization behavior in these cores, like Mn (Fig. 10 and 11). Such threshold behavior for Pb pyritization also has been reported by other authors working with anoxic marine and estuarine sediments (Huerta-Diaz and Morse, 1992).

Chromium Phase Speciation Profiles. The phase speciation distribution of Cr in the six sediment cores (Fig. 18) shows that the geochemical distribution of this element is relatively uniform for almost all of the sediment profiles. The most obvious exception to this trend is seen in core BH2. The phase distribution in this core changes from about 75% of the total phase sum of Cr being in the oxide phase at the surface, to about 50% at the base of the core. This trend could be diagenetic, given that the Cr in this core is transitioning from an oxidized phase to a more reduced phase. On closer inspection, this same trend (although much less pronounced) can be seen in cores ER1, ER2, and MI2 (Fig. 18). An appreciable percentage (~5% or greater) of Cr is found in the AVS phase throughout all of the sediment cores. In cores ER2 and BH1, the percentage of AVS Cr generally increases until about mid-core, and then subsequently decreases down core. All profiles show little Cr (< 1%) is incorporated into the pyrite phase, even at the bases of

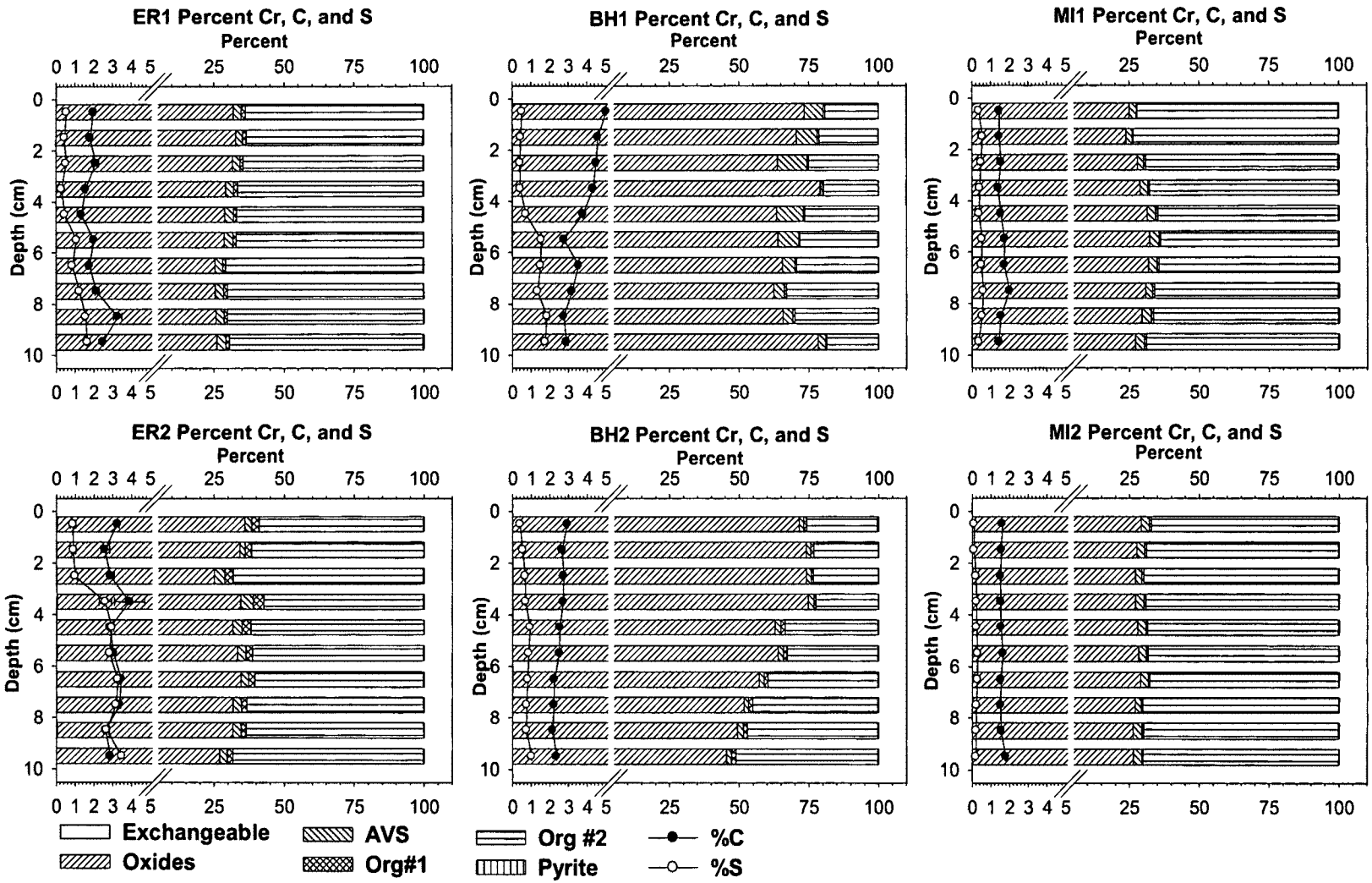

Fig. 18. Sediment Profiles Showing the Total Percentage of Each Phase for Cr Out of the Sum of the Phases in Each of the Six Sediment Cores. Total C and S percents are by total weight of sediment.

these sediment cores. This indicates a low affinity of Cr for the pyrite phase in these sediments, which has been observed in marine and estuarine environments by others (Huerta-Diaz and Morse, 1992).

Average Chromium Phase Speciation. The average percent phase speciation distribution for Cr (Fig. 19) shows striking similarities between the sediment cores taken from the same estuaries. In addition to this, the average phase distribution of this element in the cores taken from the Elizabeth River is similar to those taken near Mare Island. The reason for these similarities is unclear, as the cores from these two estuaries have very different total C and S concentrations, with the Elizabeth River cores containing almost twice as much average total C as the Mare Island cores. However, the Baltimore Harbor cores contain the highest average Cr concentrations of all the sediments analyzed (mainly within the first 5 cm of these cores). The phase distribution profiles (Fig. 18) for Cr within the first half of BH1 and BH2 show an overall higher percentage of oxide-associated Cr in these core sections. Given this observation, the phase speciation distribution of this element might be determined by its overall concentration in the sediment. The fact that most of the Cr within all of these sediments is essentially located in only two phases (the oxide and organic phases) is similar to what other researchers have observed in sediments taken from similar environments (Lam et. al., 1997; Elsokkary and Muller, 1990; Guo et. al., 1997; Abu-Hilal, 1993).

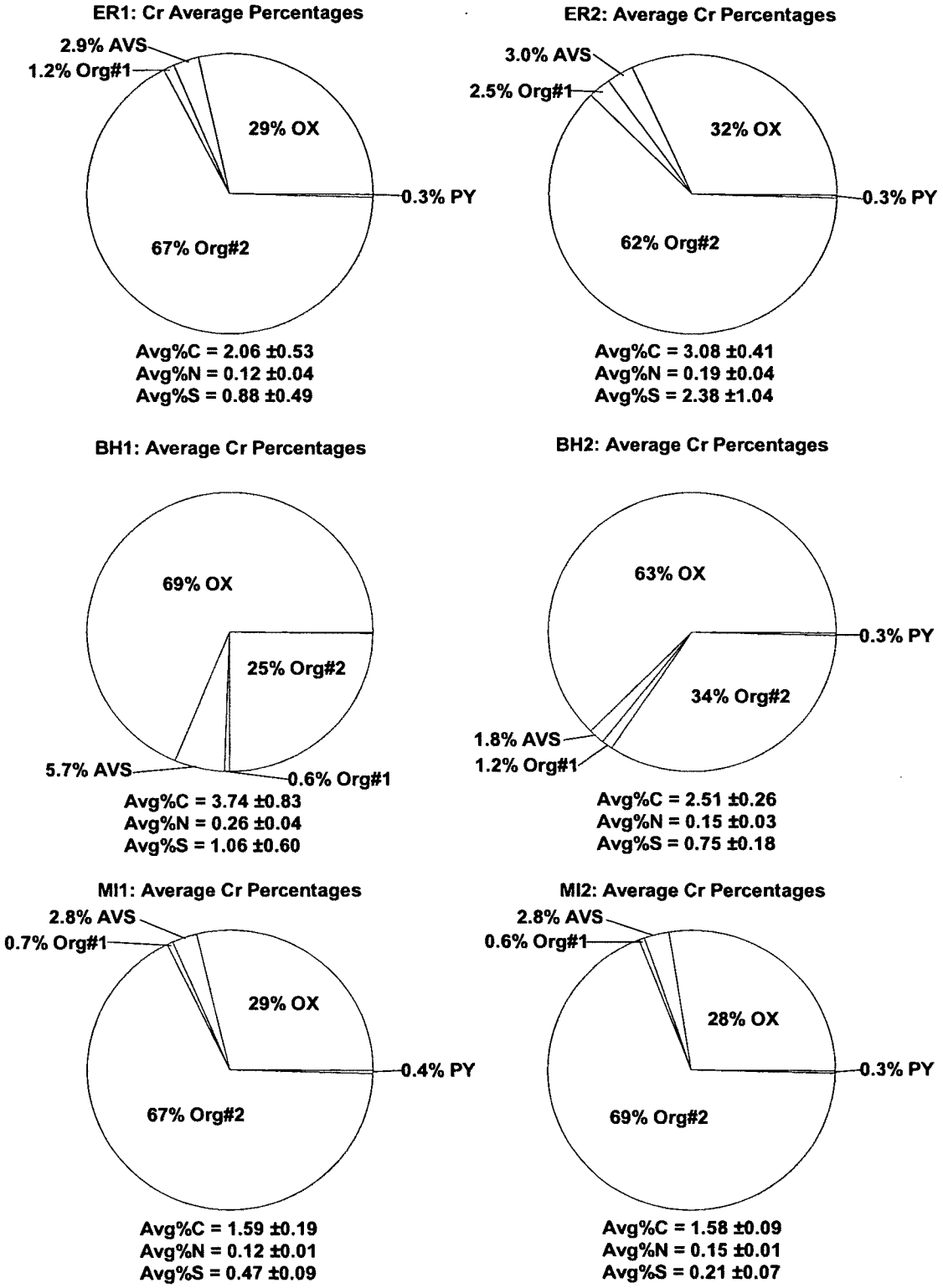

Fig. 19. Pie Graphs Showing the Average Percentages of the Sums of the Phases for Cr in Each Core. Average total carbon, nitrogen, and sulfur percentages for each core are noted below each graph.

Arsenic Phase Speciation Profiles. The phase speciation distribution of As in these sediment cores (Fig. 20) is somewhat similar to that of Fe (Fig. 8). With the exception of the Mare Island cores, the lowest overall percentage of pyrite bound As is near the sediment/water interface, and generally increases down core. Overall, the percentages of As in the oxide phase trends strongly in the opposite direction to As in the pyrite phase in cores ER2 and BH2,and trends less strongly so in cores ER1 and BH1. This suggests that the geochemistry of this element is tied to Fe redox cycling in these sediments. A significant correlation between Fe oxides and As in sediments has been noted by numerous workers, and reflects the tendency of As to adsorb onto Fe oxide minerals in oxic environments (Crecelius, 1975; Langston, 1986; Sullivan and Aller, 1996). Cores ER2, BH1, and BH2, show significant increases in the percentage of pyrite-bound As down core in these sediments, which indicates that As is being incorporated into the pyrite phase. This trend of apparent As pyritization seen in these sediment profiles (most obviously demonstrated in cores ER2, BH1 and BH2 in Fig. 20) has also been reported by other authors studying anoxic marine and estuarine sediments (Huerta-Diaz and Morse, 1992). With the exceptions of cores BH2 and MI1, the percentage of organic-bound As generally decreases down core. This likely indicates that organic-bound As is slowly being released during burial as the organic compounds that it is bound to are being remineralized. This trend is seen most obviously in BH1, where a significant positive correlation (Pearson $r = 0.835$ and $p = 0.003$) exists between total percent sediment C and the total percent organic-bound As (sum of organic #1 and #2 phases).

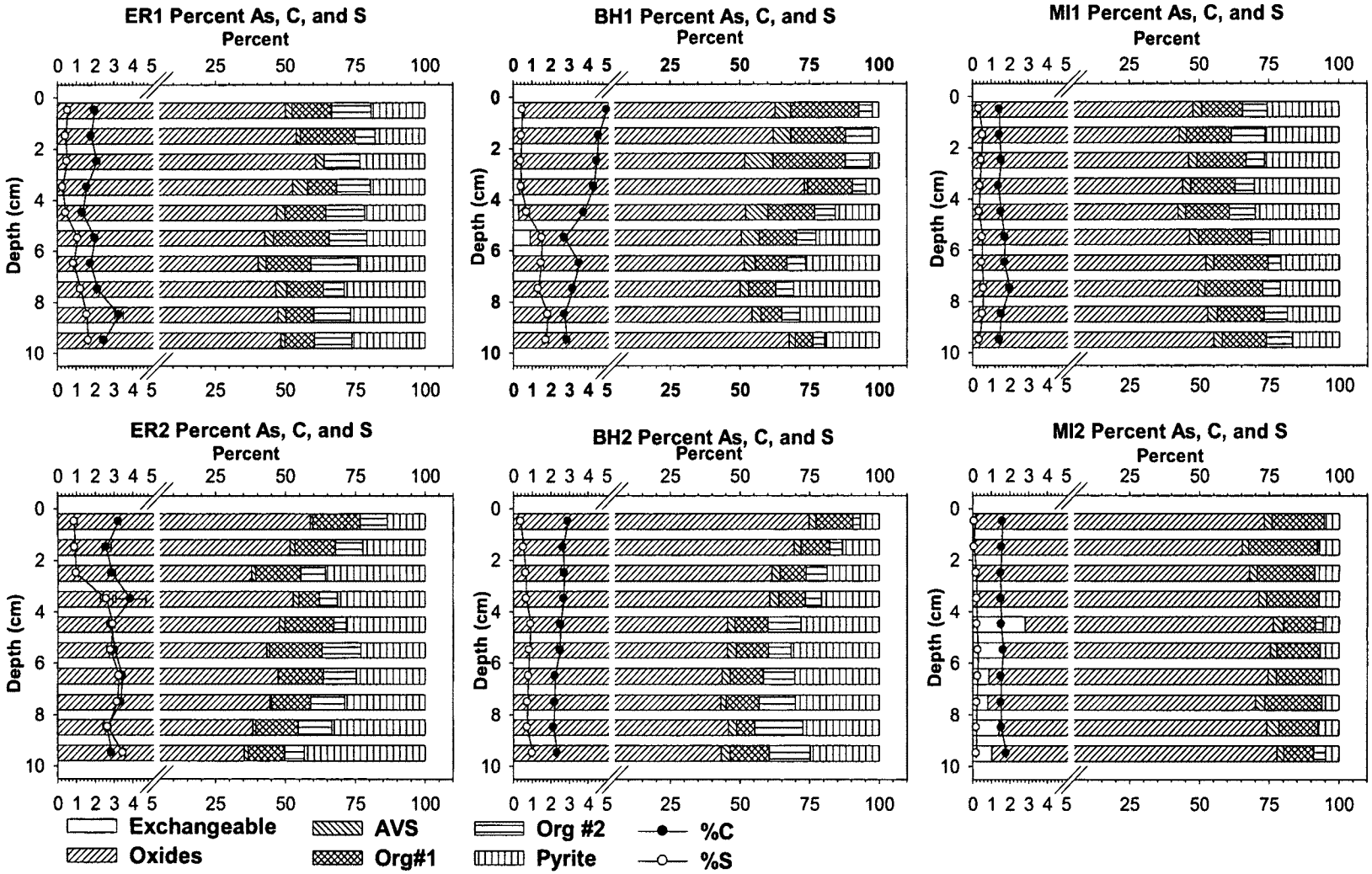

Fig. 20. Sediment Profiles Showing the Total Percentage of Each Phase for As Out of the Sum of the Phases in Each of the Six Sediment Cores. Total C and S percents are by total weight of sediment.

Average Arsenic Phase Speciation. The average phase speciation distribution for As (Fig. 21) shows overall similarities between cores taken in the Elizabeth River and Baltimore Harbor. However, the average phase distribution of As in core MI1 is very different from core MI2. In fact the As phase distribution in MI1 is quite similar to core ER1. This similarity might reflect the higher average total S concentration in core MI1, which is over twice that of MI2. Numerous workers have noted that the geochemistry of As in sediments is often closely tied to S, which is especially true in anoxic marine and estuarine environments, where As is often incorporated into arsenopyrite and other arsenic sulfide minerals (Sadiq, 1992; Neff, 1997; Huerta-Diaz and Morse, 1992). The average arsenic phase speciation pie graphs (Fig. 21) clearly illustrate that the majority of the As in all of these sediments is associated with oxide phase. This is similar to what other authors have noted for As in oxic estuarine sediments (Guo et. al, 1997; Angelidis and Grimanis, 1987; Larner et. al., 2008). A smaller but significant portion of As is found in the pyrite, organic #1, and organic #2 phases. The reason for the significant amount of As in the pyrite fraction is noted above, but the reason for the appreciable amounts of As in the organic phases is unclear. However, other authors have noted significant amounts of As in what they call the oxidizeable sediment fraction (extracted with H_2O_2), which includes both pyrite and organic phases (Angelidis and Grimanis, 1987). In addition, marine organisms often accumulate considerable amounts of organic As species, which in turn may be deposited into sediments (Neff, 1997; Kirby and Maher, 2002).

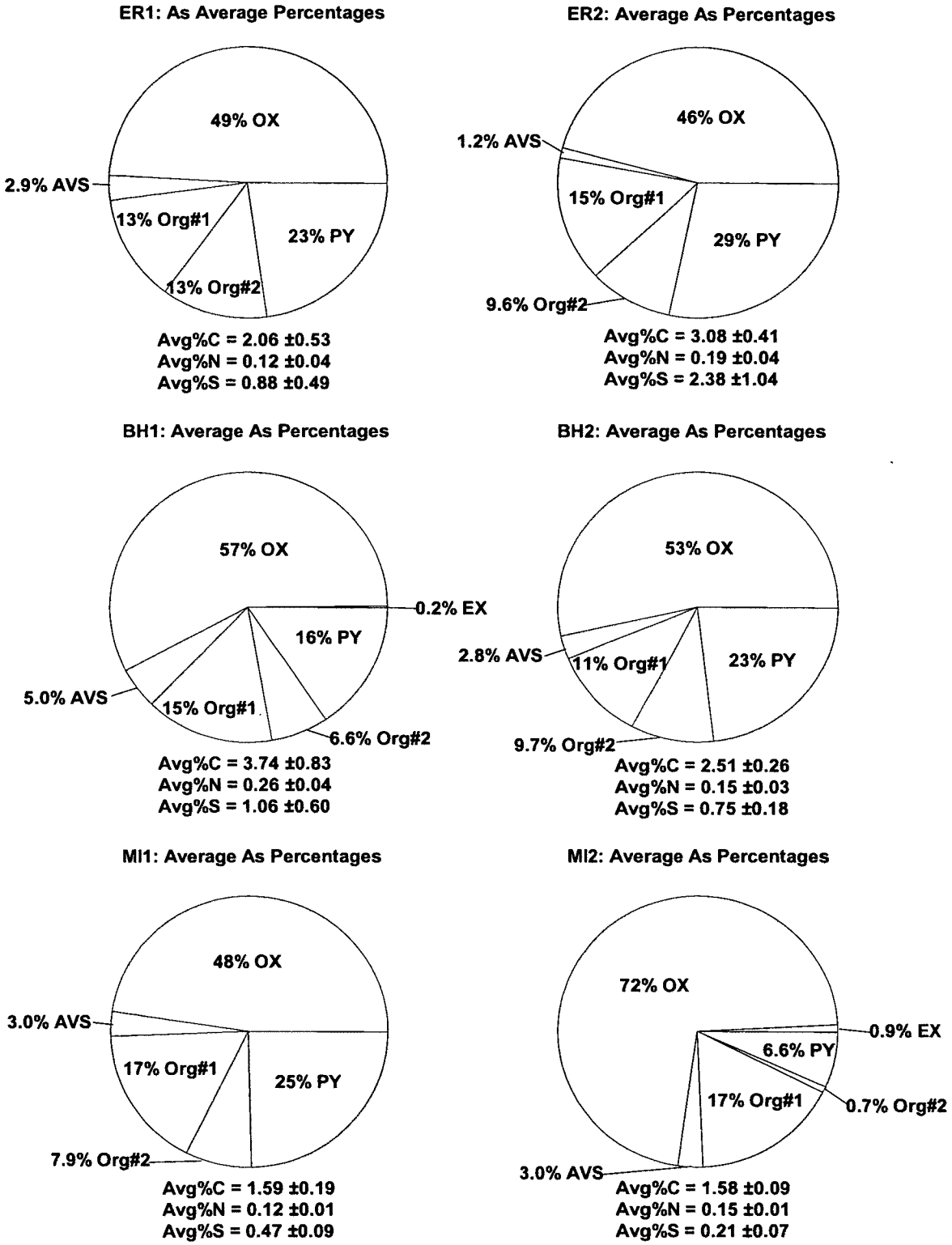

Fig. 21. Pie Graphs Showing the Average Percentages of the Sums of the Phases for As in Each Core. Average total carbon, nitrogen, and sulfur percentages for each core are noted below each graph.

3.3. Degree of Trace Metal Pyritization vs. Degree of Pyritization

In an effort to verify some of the findings discussed in Section 3.2. related to the degrees in which Mn, Cd, Pb, Cr, and As are incorporated into the pyrite phase of the sediments studied in this project, degree of trace metal pyritization vs. degree of pyritization (DTMP vs. DOP) plots were created using the metal phase speciation data obtained from the six step phase speciation leach. These plots were then compared to the DTMP vs. DOP plots published by Huerta-Diaz and Morse (1992) for anoxic marine and estuarine sediments.

The DTMP vs. DOP method for determining the degree to which trace metals are being incorporation into the pyrite phase of sediments in relation to the degree of Fe pyritization in sediments was first introduced by Huerta-Diaz and Morse (1990). In order to determine the DTMP vs. DOP in various marine and estuarine sediments, Huerta-Diaz and Morse (1990) utilized a three step leaching process to extract the Fe and trace metals from the reactive, silicate, and pyrite phases in sediment. In the method described by Huerta-Diaz and Morse (1990), two percentages are calculated and subsequently plotted against each other. The first percentage, the DOP, is calculated using the concentration of pyrite phase Fe ([Fe-pyrite]) and the concentration of the reactive phase Fe ([reactive-Fe]), as in Eq. [1].

$$\text{DOP (\%)} = [\text{pyrite-Fe}]/([\text{pyrite-Fe}] + [\text{reactive-Fe}]) * 100 \qquad [1]$$

The second percentage, the DTMP is calculated using the concentration of pyrite phase trace metal ([pyrite-metal]) and the concentration of the reactive phase trace metal ([reactive-metal]), as in Eq. [2].

$$\text{DTMP (\%)} = [\text{pyrite-metal}]/([\text{pyrite-metal}] + [\text{reactive-metal}]) * 100 \qquad [2]$$

In order to apply the Huerta-Diaz and Morse (1990) DTMP vs. DOP method to the data from the six step leach method, the Fe and trace metal (major metal Mn and trace elements Cd, Pb, Cr, and As) concentrations from the first five steps of my the leaching scheme are summed and defined as the reactive phase, while the Fe and trace metals extracted in the pyrite phase of this leach are assumed to be the same as the pyrite phase in Huerta-Diaz and Morse (1990). The DOP and DTMP percentages from this study were calculated using Eq. [1] and Eq. [2], then plotted and compared to the DTMP vs. DOP results published by Huerta-Diaz and Morse (1992) (Fig. 22 thru 26).

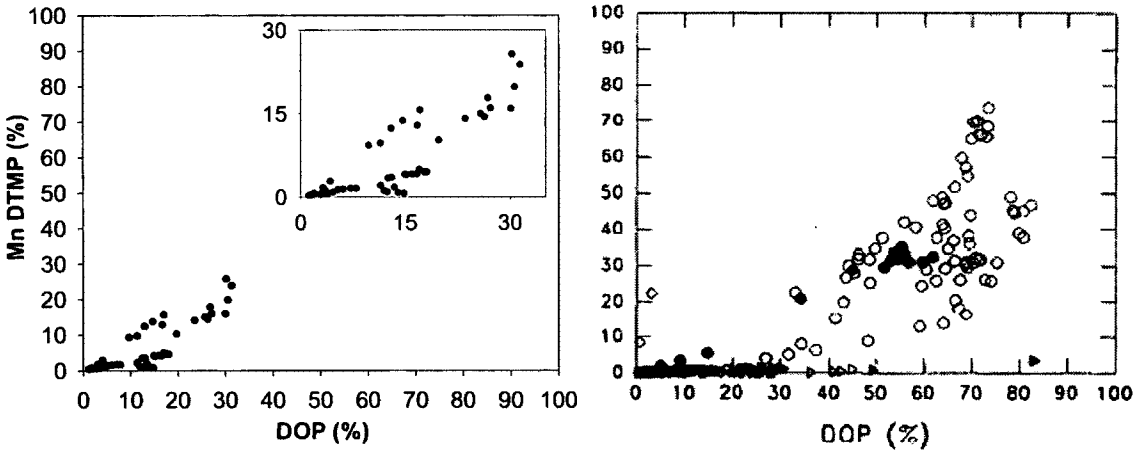

Fig. 22. Mn DTMP vs. DOP Plot for All of the Sediment Cores Studied in this Project (left) Compared to Huerta-Diaz and Morse (1992) for Mn DTMP (right).

Manganese DTMP vs. DOP. The Mn DTMP vs. DOP plot derived from this study (Fig. 22) somewhat resembles the plot published by Huerta-Diaz and Morse (1992). However, the apparent inflection points in these plots are not the same. The apparent inflection point for the graph with the data points from this study (left side of Fig. 22) occurs at about 15% DOP while the graph on the right is near 30% DOP. Nonetheless,

the general trends of these two plots are similar. This apparent inflection point is also indicated in the Fe and Mn speciation profiles (Fig. 8 and 10) and the Fe and Mn average phase speciation pie graphs (Fig. 9 and 11), where appreciable amounts of pyrite-bound Mn (≥ 4%) are only seen in the cores that also contain higher percentages (≥ 10%) of pyrite-bound Fe (ER1, ER2 and BH1).

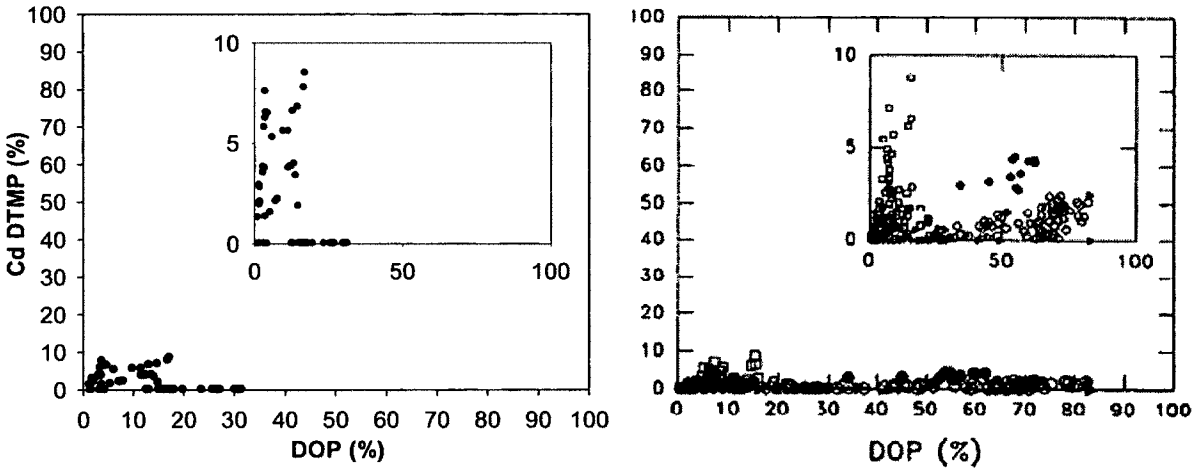

Fig. 23. Cd DTMP vs. DOP plot for All of the Sediment Cores Studied in this Project (left) Compared to Huerta-Diaz and Morse (1992) for Cd DTMP (right).

Cadmium DTMP vs. DOP. The percent DTMP of Cd for all of the sediment cores were calculated and plotted against the percent DOP in all of these sediment samples. The resulting plot (left side of Fig. 23) is similar to the Cd DTMP vs. DOP published by Huerta-Diaz and Morse (1992) (right side of Fig. 23). Both of these plots show Cd displaying an overall low (<10%) DTMP. This low DTMP is reflected in the relatively low percentage of pyrite-bound Cd seen in the Cd phase speciation profiles (Fig. 14) and average Cd phase speciation pie graphs (Fig. 15).

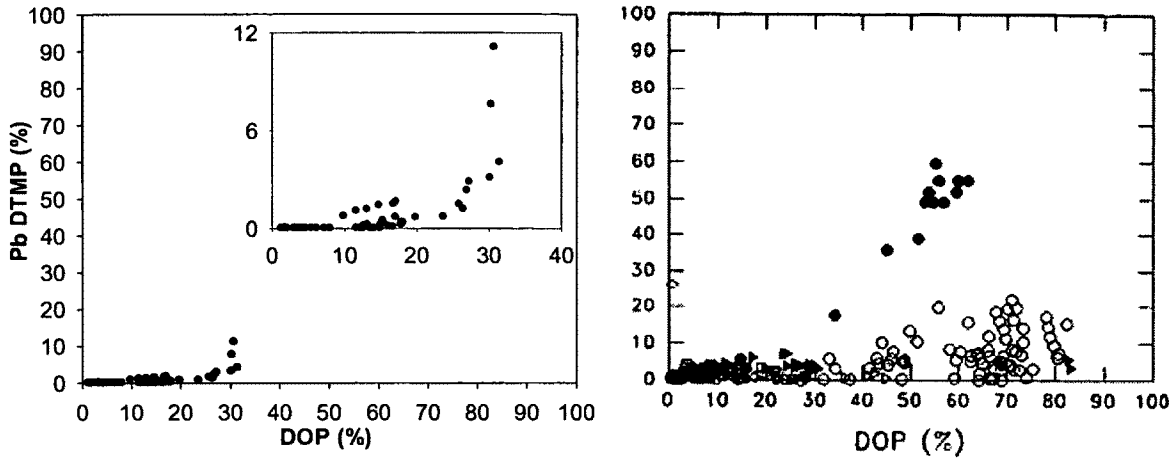

Fig. 24. Pb DTMP vs. DOP Plot for All of the Sediment Cores Studied in this Project (left) Compared to Huerta-Diaz and Morse (1992) for Pb DTMP (right).

Lead DTMP vs. DOP. A DTMP vs. DOP plot was created using the pyrite phase Pb concentrations from all six of the sediment cores and these results are compared to the Pb DTMP vs. DOP plot published by Huerta-Diaz and Morse (1992) (Fig. 24). The Pb DTMP vs. DOP plot for the sediment samples in this study (left side of Fig. 24) closely follows the trend seen by Huerta-Diaz and Morse (1992) (right side of Fig. 24). Both of these plots show a generally low DTMP for this element, which begins to significantly increase around 30% DOP. This threshold behavior for Pb pyritization is indicated by the Pb phase speciation profiles (Fig. 16) and average phase speciation pie graphs (Fig. 17) where significant amounts of pyrite-bound Pb are only seen in core ER2, which also has the highest percentage of pyrite phase Fe.

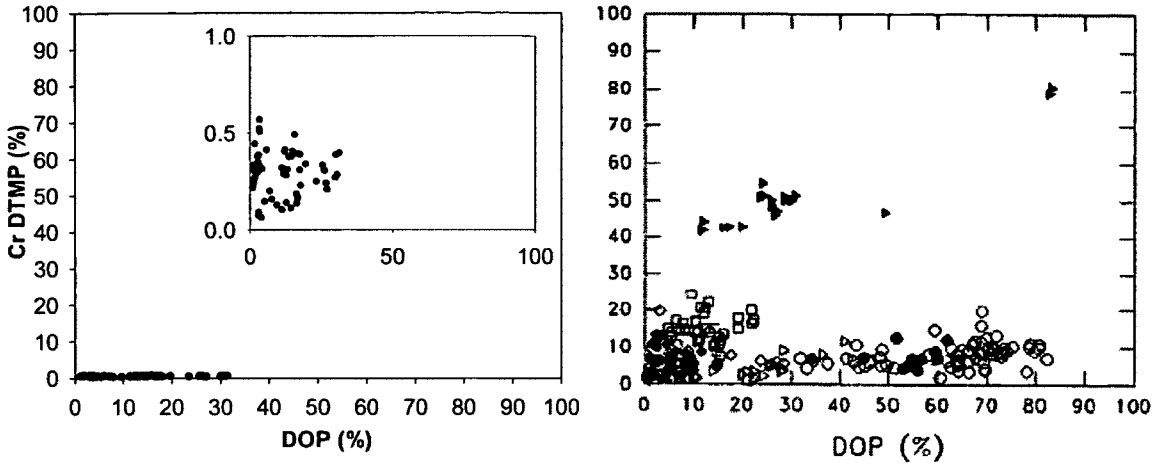

Fig. 25. Cr DTMP vs. DOP Plots for All of the Sediment Cores Studied in this Project (left) Compared to Huerta-Diaz and Morse (1992) for Cr DTMP (right).

Chromium DTMP vs. DOP. Cr DTMP vs. DOP percentages were plotted using the Cr concentrations from all six cores (left side of Fig. 25). The Cr DTMP vs. DOP plot derived from the this study (left side of Fig. 25) shows that Cr in these sediment cores demonstrates uniformly low (< 1%) DTMP. The Cr DTMP vs. DOP plot published by Huerta-Diaz and Morse (1992) (right side of Fig. 25) also shows Cr demonstrating a low (~10%) DTMP. However, the Cr DTMP percentages reported by Huerta-Diaz and Morse (1992) are higher than what is seen in this study. The reason for this difference is likely due to the addition of the organic leaching steps in this six step leaching process, which are not included in the three step leaching method utilized by Huerta-Diaz and Morse (1992). This low Cr DTMP (left side Fig. 25) is also observed in the Cr phase speciation profiles (Fig. 18) and average phase speciation pie graphs (Fig. 19).

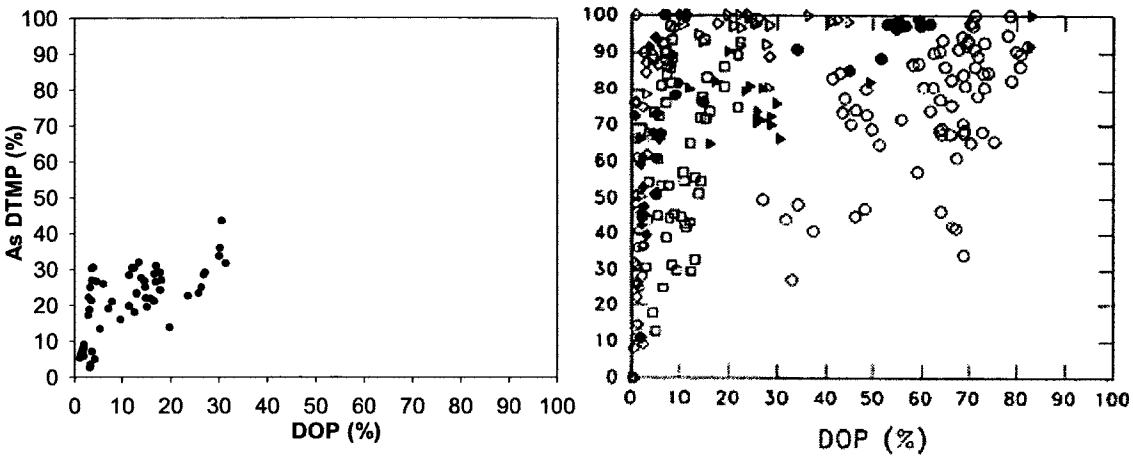

Fig. 26. As DTMP vs. DOP Plot for All of the Sediment Cores Studied in this Project (left) Compared to Huerta-Diaz and Morse (1992) for As DTMP (right).

Arsenic DTMP vs. DOP. An As DTMP vs. DOP plot was generated using the As data from all of the cores analyzed in this study (left side Fig. 26) This plot was then compared to the As DTMP vs. DOP published by Huerta-Diaz and Morse (1992) (right side Fig. 26). Both plots are similar and show As demonstrating a relatively high DTMP in sediments in comparison to the other trace metals studied in this project. This high As DTMP is exhibited in the As phase speciation profiles (Fig. 20) and average phase speciation pie graphs (Fig. 21) where appreciable percentages (> 5%) of pyrite-bound As are seen in all of the sediment cores.

3.4. Conclusions

Overall, the phase speciation leaching process developed in this study was fairly effective at separating the major and trace metals in sediment into operationally defined geochemical phases. This type of phase speciation separation is similar to what has been accomplished with other leaching methods (Filgueiras et. al., 2002 and references

therein). However, none of these previous methods attempted to use a single leaching scheme to separate trace metals in phases generally found in both oxic sediments (Fe and Mn oxide bound metals) and anoxic sediments (AVS and pyrite bound metals). Because the "phases" for all of these types of leaching methods are operationally defined, it can be difficult to make direct comparisons between the results obtained from different leaching methods (Sutherland and Tack, 2003). Nonetheless, this study appeared to be successful in showing that the modified Tovar-Sanchez (2003) oxide leaching method developed in this study was as effective at removing oxide-bound metals from sediment as the frequently used Tessier et. al. (1979) oxide leaching method. However, unlike the Tessier et. al. (1979) oxide leach, the modified pH 6 Tovar-Sanchez (2003) method does not appreciably attack AVS-bound metals in sediment. Using a phase speciation standard reference material (BCR-701), the results from the six step leaching method developed in this study were also compared to the recently developed optimized BCR phase speciation leaching method, and with the exception of Cr, the results from the two leaching methods were similar (both methods within 10% of mean recoveries). However, comparisons between the AVS leach Fe and the AVS sulfide calculated Fe generated using the Cutter and Oatts (1987) method indicated that the AVS leaching step attacked presumably leftover Fe and Mn oxides in the surface sediments. Nevertheless, besides the AVS leaching step, most of the other leaching steps were quite specific in separating major and trace elements in sediments from associated geochemical phases. Finally, with the exception of the organic phases, the overall efficiencies of each of the phase leaching steps that were tested in this study were good (within ~10% of expected values for the oxide and pyrite phases in dried sediment). Although the efficiency of the organic leaches

is only ~20% for total sediment C removal, these organic leaching steps were three times time more efficient at removing total sediment N, suggesting they were more efficient at removing metals associated with labile organic matter.

The results from the phase speciation analysis of elements in the core samples taken from the three estuaries are similar to what has been reported for sediments taken from similar geochemical environments using published leaching methods (Tessier et. al. (1979), optimized BCR or similar leaching methods). In addition, The DTMP vs. DOP plots generated from the metal phase distribution data are similar to what has been published by previous authors (Huerta-Diaz and Morse, 1992). However, a general lack of sediment homogeneity in the bulk sediment core samples and analytical errors associated with the use of ICP-OES to determine low concentration elements such as Cd were problematic issues. Unlike the errors associated with using ICP-OES, where ICP-MS or some other more sensitive analytical technique can be applied instead, the issue of bulk sediment heterogeneity is not an easy problem to solve. This is due to the fact that common methods used to homogenize sediments, such as drying, grinding, and sieving will change the oxidation states of the sediment bound metals, and hence change the overall phase distribution of these elements (Forstner and Salomons, 1991; Stephens et. al., 2001; Kersten and Forstner, 1986; Rapin et. al., 1986). Future work related to this topic should include the application of the leaching scheme developed in this study to sediments obtained from freshwater and hyper-saline environments, in order to assess the efficacy of this leaching method for sediments from these very different geochemical environments.

REFERENCES

Abaychi, J.K., and A.A. Douabul. 1986. Trace element geochemical associations in the Arabian Gulf. Marine Pollution Bulletin. 17:353-356.

Abu-Hilal, A. 1993. Observations on Heavy Metals Geochemical Association in Marine Sediments of the Jordan Gulf of Aqaba. Marine Pollution Bulletin. 26:85-90.

Amiard, J.C., C. Amiard-Triquet, B. Berthet, and C. Metayer. 1986. Comparative study of the patterns of bioaccumulation of essential (Cu, Zn) and non-essential (Cd, Pb) trace metals in various estuarine and coastal organisms. Journal of Experimental Marine Biology and Ecology. 106:73-89.

Amiard, J.C., A. Geffard, C. Amiard-Triquet, and C. Crouzet. 2007. Relationship between the lability of sediment-bound metals (Cd, Cu, Zn) and their bioaccumulation in benthic invertebrates. Estuarine, Coastal, and Shelf Science. 72:511-521.

Angelidis, M., and A.P. Grimanis. 1987. Arsenic geochemistry in sediments near the Athens sewage outfall. Marine Pollution Bulletin. 18:297-298.

Anju, M., and D.K. Banerjee. 2010. Comparison of two sequential extraction procedures for heavy metal partitioning in mine tailings. Chemosphere. 78:1393-1402.

Arain, M.B., T.G. Kazi, M.K. Jamali, H.I. Afaidi, N. Jalbani, R.A. Sarfraz, J.A. Baig, G.A. Kandho, and M.A. Memon. 2008. Time saving modified BCR sequential extraction procedure for the fraction of Cd, Cr, Ni, Pb, and Zn in sediment samples of polluted lake. Journal of Hazardous Materials. 160:235-239.

Arakaki, T., and J.W., Morse. 1993. Coprecipitation and adsorption of Mn (II) with makinawite (FeS) under conditions similar to those found in anoxic sediments. Geochimica et Cosmochimica Acta. 57:9-34.

Bacon, J.R. and C.M. Davidson. 2008. Is there a future for sequential chemical extraction? Analyst. 133:25-46.

Balistrieri, L.S., and J.W. Morse. 1982. The adsorption of Cu, Pb, Zn, and Cd on goethite from major ion seawater. Geochimica et. Cosmochimica Acta. 46:1253-1265

Balistrieri, L.S., and J.W. Morse. 1984. Marine scavenging: Trace metal adsorption by interfacial sediment from MANOP Site H. Geochimica et Cosmochimica Acta. 48:921-929.

Belzile, N., and J. Lebel. 1986. Capture of arsenic by pyrite in near-shore sediments. Chemical Geology. 54:279-281.

Berner, R.A. 1984. Sedimentary pyrite formation: An update. Geochimica et Cosmochimica Acta. 48:605-615.

Bryan G.W., and W.J. Langston. 1992. Bioavailability, accumulation and effects of heavy metals in sediments with special reference to United Kingdom estuaries: a review. Environmental Pollution. 76:89-131.

Bull, K.R., W.J. Every, P. Freestone, J.R. Hall, D. Osborn, A.S. Cooke, and T. Stowe. 1983. Alkyl lead pollution and bird mortalities on the Mersey Estuary, UK, 1979-1981. Environmental Pollution (Series A). 31:239-259.

Burdige, D.J. 1993. The biogeochemistry of manganese and iron reduction in marine sediments. Earth Science Reviews. 35:249-284.

Burdige, D.J. 2006. Geochemistry of Marine Sediments. Princeton University Press, Princeton, NJ.

Casado-Martinez, M.C., B.D. Smith, S.N. Luoma, and P.S. Rainbow. 2010. Bioaccumulation of arsenic from water and sediment by a deposit-feeding polycheate (*Arenicola marina*): A biodynamic modelling approach. Aquatic Toxicology. 98:34-43.

Chada, V.G.R., D.B. Hausner, D.R. Strongin, A.A. Rouff and A.A. Reeder. 2005. Divalent Cd and Pb uptake on calcite {1014} cleavage faces: An XPS and AFM study. Journal of Colloid and Interface Science. 288:350-360.

Chen, L., L. Ye-Qing, and D. Bao-Lin. 2007. Catalysis of Manganese (II) on chromium (VI) reduction by citrate. Pedosphere. 17:318-323.

Chao, T.T. 1984. Use of partial dissolution techniques in geochemical exploration. Journal of Geochemical Exploration. 20:101-135.

Chao, T.T., and L. Zhou. 1983. Extraction techniques for selective dissolution of amorphous iron oxides from soils and sediments. Soil Science Society of America Journal. 47:225-232.

Cooper, D.C., and J.W. Morse. 1998. Extractability of metal sulfide minerals in acidic solutions: application to environmental studies of trace metal contamination with anoxic sediments. Environmental Science and Technology. 32:1076-1078.

Crecelius, E.A., M.H., Bothner, and R., and Carpenter. 1975. Geochemistry of arsenic, antimony, mercury and related elements in sediments of Puget Sound. Current Research. 9:325-333.

Cutter, G. and T.J. Oatts. 1987. Determination of dissolved sulfide and sedimentary sulfur speciation using gas chromatography-photoionization detection. Analytical Chemistry. 59:717-721.

Cutter, G. and J. Radford-Knoery. 1991. Determination of carbon, nitrogen, and sulfur and inorganic sulfur species in marine particles. p. 57-63. *In* Hurd, D., D. Spencer (ed.) Marine Particles: Analysis and Characterization. American Geophysical Union, Washington D.C.

Davis, A., C. Sellstone, S. Clough, R. Barrick, and B. Yare. 1996. Bioaccumulation of arsenic, chromium, and lead in fish: constraints imposed by sediment geochemistry. Applied Geochemistry. 11:409-423.

Davis, J.A., C.C. Fuller, and A.D. Cook. 1987. A model for trace metal sorption processes at the calcite surface: Adsorption of Cd^{2+} and subsequent solid solution formation. Geochimica et. Cosmochimica Acta. 51:1477-1490.

Di Toro, D.M., J.D. Mahony, D.J. Hansen, K.J. Scott, A.R. Carlson, and G.T. Ankley. 1992. Acid volatile sulfide predicts the acute toxicity of cadmium and nickel in sediments. Environmental Science and Technology. 26:96-101.

Dossing, L.N., K. Dideriksen, S.L.S. Stipp, and R. Frei. 2011. Reduction of hexavalent chromium by ferrous iron: A process of chromium isotope fractionation and its relevance to the natural environment. Chemical Geology. 285:157-166.

Douglas, G.S., G.L. Mills, and J.G. Quinn. 1986. Organic copper and chromium complexes in the interstitial waters of Narragansett Bay sediments. Marine Chemistry. 19:161-174.

Elsokkary, I.H., and G. Muller. 1990. Assessment and speciation of chromium, nickel, lead, and cadmium in the sediments of The River Nile, Egypt. The Science of the Total Environment. 97/98:455-463.

Eray, L.E. and D. Rai. 1987. Kinetics of chromium (III) oxidation to chromium (VI) by reaction with manganese dioxide. Environmental Science and Technology. 21:1187-1193.

Fan, W. and X-W. Wang. 2001. Sediment Geochemical Controls on Cd, Cr, and Zn Assimilation by the Clam *Ruditapes philippinarum*. Environmental Toxicology and Chemistry. 20:2309-2317.

Filgueiras, A.V., I. Lavilla, and C. Bendicho. 2002. Chemical sequential extraction for metal partitioning in environmental solid samples. Journal of Environmental Monitoring. 4:823-857.

Forstner, U., and W. Salomons. 1991. Mobilization of Metals from Sediments. p. 379-398. *In* Merian, E. (ed.) Metals and Their Compounds in the Environment. VCH Publishers, Weinheim, Federal Republic of Germany.

Fulghum, J.E., S.R. Bryan, and R.W. Linton. 1988. Discrimination between adsorption and coprecipitation in aquatic particle standards by surface analysis techniques: Lead distributions in calcium carbonates. Environmental Science and Technology. 22:463-467.

Gauglhofer, J. and V. Bianchi. 1991. Chromium. p. 853-878. *In* Merian, E. (ed.) Metals and Their Compounds in the Environment. VCH Publishers, Weinheim, Federal Republic of Germany.

Gambrell, R.P., A.K., Khalid, and W.H., Patrick. 1980. Chemical Availability of Mercury, Lead, and Zinc in Mobile Bay Sediment Suspensions as Affected by pH Oxidation-Reduction Conditions. American Chemical Society. 14:431-435.

Gleyzes, C., S. Tellier, and M. Astruc. 2002. Fractionation studies of trace elements in contaminated soils and sediments: a review of extraction procedures. Trends in analytical chemistry. 21:451-467.

Goldberg, E.D. and G.O.S. Arrhenius. 1958. Chemistry of Pacific pelagic sediments. Geochemica et Cosmochimica Acta. 13:153-212.

Griscom, S.B., N.S., Fisher and S.N., Luoma. 2000. Geochemical Influences on Assimilation of Sediment-Bound Metals in Clams and Mussels. Environmental Science and Technology. 34:91-99.

Griscom, S.B., N.S. Fisher, R.C. Aller, and B. Lee. 2002. Effects of gut chemistry in marine bivalves on the assimilation of metals from ingested sediment particles. Journal of Marine Research. 60:101-120.

Griscom, S. B. and N.S. Fisher. 2004. Bioavailability of Sediment-bound Metals to Marine Bivalve Mollusks: An Overview. Estuaries. 27:826-838.

Guo, T., R.D., DeLaune, and W.H. Patrick. 1997. The Influence of Sediment Redox Chemistry on Chemistry on Chemically Active Forms of Arsenic, Cadmium, Chromium, and Zinc in Estuarine Sediment. Environment International. 23:305-316.

Harvey, R.W., and S.N. Luoma. 1985. Effect of adherent bacteria and bacterial extracellular polymers upon assimilation by *Macoma baltica* of sediment-bound Cd, Zn, and Ag. Marine Ecology Progress Series. 22:281-289.

Huerta-Diaz, M.A., and J. W. Morse. 1990. A quantitative method for determination of trace metal concentrations in sedimentary pyrite. Marine Chemistry. 29:119-144.

Huerta-Diaz, and M.A., J. W. Morse. 1992. Pyritization of trace metals in anoxic marine sediments. Geochemica et Cosmochimica Acta. 56:2681-2702.

Izquierdo, C., J. Usero, and I. Gracia. 1997. Speciation of heavy metals in sediments from salt marshes on the southern Atlantic coast of Spain. Marine Pollution Bulletin. 34:123-128.

Johnson, A.C., and A.G. Xyla. 1991. The oxidation of chromium (III) to chromium (VI) on the surface of manganite (γ-MnOOH). Geochimica et. Cosmochimica. 55:2861-2866.

Jones, K.D. and W-H. Huang. 2003. Evaluation of toxicity of pesticides, chlopyrifos, and arsenic in the presence of compost humic substances in aqueous systems. Journal of Hazardous Materials. B103:93-105.

Ke, Caihuan and W. Wang. 2001. Bioaccumulation of Cd, Se, and Zn in an estuarine oyster (*Crassostrea rivularis*) and a coastal oyster (*Saccostrea glomerata*). Aquatic Toxicology 56:33-51.

Kersten, M. and U. Forstner. 1986. Chemical fractionation of heavy metals in anoxic estuarine and coastal sediments. Water Science and Technology. 18:121-130.

Kirby, J., and W. Maher. 2002. Tissue accumulation and distribution of arsenic compounds in three marine fish species: relationship to trophic position. Applied Organometallic Chemistry. 16:108-115.

Krishnamurti, G.S.R., P.M. Huang, K.C.J. Van Rees, L.M. Kozak, and H.P.W. Rostad. 1995. Speciation of particulate-bound cadmium in soils and its bioavailability. Analyst. 120:659-665

Kyziol, J., I. Twardowska, and Ph. Schmitt-Kopplin. 2006. The role of humic substances in chromium sorption onto natural organic matter (peat). Chemosphere. 63:1974-1982.

Kluckohn, R.S. 1990. Trace Metals and Pyrite in Sediments of Chesapeake Bay. Master's Thesis Unpublished.

Lam, M. H-W., A.Y-W. Tjia, C-C. Chan, W-P. Chan, and W-S. Lee. 1997. Speciation study of chromium, copper, and nickel in coastal estuarine sediments polluted by domestic and industrial effluents. Marine Pollution Bulletin. 11:949-959.

Lane, T.W., and F.M.M. Morel. 2000. A biological function for cadmium in marine diatoms. Proceedings of the National Academy of Sciences. 97:4627-4631.

Langston, W.J. 1986. Metals in sediments and benthic organisms in the Mersey estuary. Estuarine, Coastal and Shelf Science. 23:239-261.

Larner, B.L., A.S. Palmer, A.J. Seen, and A.T. Townsend. 2008. A comparison of an optimized sequential extraction procedure and dilute acid leaching of elements in anoxic sediments, including the effects of oxidation on sediment metal partitioning. Analytica Chimica Acta. 608:147-157.

Lee, B-G., S.B. Griscom, J-S. Lee, H.J. Choi, C-H. Koh, S.N. Luoma, and N.S. Fisher. 2000. Influences of dietary uptake and reactive sulfides on metal bioavailability from aquatic environments. Science. 287:282-284.

Lopez-Gonzalez, J., J. Borrego, J.A. Morales, B. Carro, and O. Lozano-Soria. 2006. Metal fractionation in oxic sediments of an estuary affected by acid mine drainage (south-western Spain). Estuarine, Coastal, and Shelf Science. 68:297-304.

Lord, C.J., III. 1982. A Selective and Precise Method for Pyrite Determination in Sedimentary Materials. Journal of Sediment Petrology. 52:664-666.

Lin, J-G, and S-Y. Chen. 1998. The relationship between adsorption of heavy metal and organic matter in river sediments. Environment International. 24:345-352.

Lu, X.Q., I. Werner, and T.M. Young. 2005. Geochemistry and bioavailability of metals in sediments from northern San Francisco Bay. Environment International. 31:593-602.

Lui, C., C. Liang, K. Lin, C. Jang, S. Wang, Y. Huang, and Y. Hsueh. 2007. Bioaccumulation of arsenic compounds in aquacultural clams (*Mertrix lusoria*) and assessment of potential carcinogenic risk to human health by ingestion. Chemosphere. 69:128-134.

Luoma, S.N. 1986. Biological Availability of Sediment-Bound Trace Metals. Actes de Colloques. 4:347-362.

Luoma, S.N., and G.W. Bryan. 1978. Factors controlling the availability of sediment-bound lead to the estuarine bivalve *Scrobicularia plana*. Journal of Marine Biology Association. 58:793-802.

Luoma, S.N., and P.S. Rainbow. 2008. Metal Contamination in Aquatic Environments: Science and Lateral Management. Cambridge University Press, Cambridge, UK.

Mahaffey, K.R. 1977. Quantities of lead producing health effects in humans: Sources and bioavailability. Environmental Health Perspectives. 19:285-295.

Martin, J.M., P. Nirel, and A.J. Thomas. 1987. Sequential Extraction Techniques: Promises and Problems, Marine Chemistry. 22:313-341.

Morse, J.W. 1986. The surface chemistry of calcium carbonate minerals in natural waters: An overview. Marine Chemistry. 20:91-112.

Morse, J.W., and T. Arakaki. 1993. Adsorption and coprecipitation of divalent metals with mackinawite (FeS). Geochimica et. Cosmochimica Acta. 57:3635-3640.

Morse, J.W. 1994. Interactions of trace metals with authigenic sulfide minerals: implications for their bioavailability. Marine Chemistry. 46:1-6.

Morse, J.W., and G.W. Luther III. 1999. Chemical influences on trace metal-sulfide interaction in anoxic sediments. Geochimica et. Cosmochimica Acta. 63:3373-3378.

Murray, R.W. and M. Leinen. 1996. Scavenged aluminum and its relationship to bulk titanium in biogenic sediment from the central equatorial Pacific Ocean. Geochimica et. Cosmochimica Acta. 60:3869-3878.

Nakayama, E., T., Kuwamoto, S, Tsurubo, and T., Fuinaga. 1981a. Chemical speciation of chromium in seawater. 1. Effect of naturally occuring organic materials on the complex formation of chromium (III). Analytica Chimica Acta. 130:289-294.

Nakayama, E., T., Kuwamoto, S, Tsurubo, and T., Fuinaga. 1981b. Chemical speciation of chromium in seawater. 2. Effects of manganese oxides and reducible organic materials on the redox processes of chromium. Analytica Chimica Acta. 130:401-404.

Nakayama, E, H. Tokoro, T. Kuwamoto, and T. Fujinaga. 1981c. Dissolved state of chromium in seawater. Nature. 290:768-769.

Neff, J.M. 1997. Ecotoxicology of arsenic in the marine environment. Environmental Toxicology and Chemistry. 16:917-927.

Nogawa, K. and A., Ishizaki. 1979. A Comparison between Cadmium in Rice and Renal Effects among Inhabitants of the Jinzu River Basin. Environmental Research. 18:410-420.

Nriagu, J.O. 1980. Cadmium in the Environment. I. Ecological Cycling. John Wiley and Sons, New York, NY.

Oshida, P.S., and L.S. Word. 1982. Bioaccumulation of chromium and its effects on reproduction in *Neanthes arenaceodentata* (polycheata). Marine Environmental Research. 7:167-174.

Park, H., B. Song, and F.M.M. Morel. 2007. Diversity of cadmium-containing carbonic anhydrase in marine diatoms in natural waters. Environmental Microbiology. 9:403-413.

Passos, E.A., J.P.H. Alves, C.A.B. Garcia, and A.C.S. Costa. 2011. Metal fractionation in sediments of the Sergipe River, Northeast, Brazil. Journal of the Brazilian Chemical Society. 22:828-836.

Patterson, R.R., S. Fendorf, and M. Fendorf. 1997. Reduction of hexavalent chromium by amorphous iron sulfide. Environmental Science and Technology. 31:2039-2044.

Peijnenburg, W.J.G.M. and T. Jager. 2003. Monitoring approaches to assess bioaccessibility and bioavailability of metals: Matrix issues. Ecotoxicology and Environmental Safety. 56:63-77.

Pempkowjak, J., A. Sikora, and E. Biernacka. 1999. Speciation of Heavy Metals in Marine Sediments vs. their Bioaccumulation by Mussels. Chemosphere. 39:313-321.

Pickering, W.F. 1986. Metal ion speciation - Soils and sediments (A Review). Ore Geology Reviews. 1:83-146.

Pierce, M., and C.B. Moore. 1982. Adsorption of arsenite and arsenate on amorphous iron hydroxide. Water Research. 16:1247-1253.

Purchase, N.G. and J.E. Fergusson. 1986. The Distribution and Geochemistry of Lead in River Sediments, Christchurch, New Zealand. Environmental Pollution. 12:203-216.

Rai, D., L.E. Eary, and J.M. Zachara. 1989. Environmental chemistry of chromium. The Science of the Total Environment. 86:15-23.

Rapin, F., A. Tessier, P.G.C. Cambell, and R. Carignan. 1986. Potential artifacts in the determination of metal partitioning in sediments by a sequential extraction procedure. Environmental Science and Technology. 20:836-840.

Riba, I., T.A. DelValls, J.M. Forja, and A. Gomez-Parra. 2002. Influence of the Aznalcollar mining spill on the vertical distribution of heavy metals in sediments from the Guadalquivir estuary (SW Spain). Marine Pollution Bulletin. 44:39-47.

Richard, F.C., and A.C.M. Bourg. 1991. Aqueous Geochemistry of Chromium: A Review. Water Research. 25:807-816.

Rifaat, A.E., M.K. El-Sayed, A. Beltagy, M.A. Morsy, and A. Nawar. 1992. Geochemical predictive models of manganese, zinc, nickel, copper, and cadmium in Nile shelf sediments. Marine Geology. 108:59-71.

Rule, J.H. 1986. Assessment of trace element geochemistry of Hampton Roads Harbor and Lower Chesapeake Bay area sediments. Environmental Geology and Water Science. 8:209-219.

Sadiq. M. 1990. Arsenic chemistry in marine environments: A comparison between theoretical and field observations. Marine Chemistry. 31:285-297.

Sadiq, M. 1992. Toxic Metal Chemistry in Marine Environments. Mercel Dekker Inc., New York, NY.

Sahuquillo, A., J.F. Lopez-Sanchez, R. Rubio, G. Rauret, R.P. Thomas, C.M. Davidson, and A.M. Ure. 1999. Use of a certified reference material for extractable trace metals to assess sources of uncertainty in the BCR three-stage sequential extraction procedure. Analytica Chimica Acta. 382:317-327.

Salomons, W., and U. Fortsner. 1984. Metals in the Hydrocycle. Springer-Verlag, Berlin, Federal Republic of Germany.

Schultz, D.M., and R.E. Miller. 1986. Humic substances isolated from surface sediments: Analytical characteristics. Technical Report OCS/MMS-86/0118. USDI-MMS, Vienna, VA.

Scoullos, M.J. 1986. Lead in coastal sediments: The case of the Elefis Gulf, Greece. The Science of the Total Environment. 49:199-219.

Sharma, V.K., and M. Sohn. 2009. Aquatic arsenic: Toxicity, speciation, transformations, and remediation. Environmental International. 35:743-759.

Stephens, S.R., B.J., Alloway, A., Parker, J.E., Carter, and M.E., Hodson. 2001. Changes in the leachability of metals from dredged canal sediments during drying and oxidation. Environmental Pollution. 114:407-413.

Sullivan, K.A., and R.C. Aller. 1996. Diagenetic cycling of arsenic in Amazon Shelf sediments. Geochimica et Cosmochimica Acta. 60:1465-1477.

Sundary, S.K., B.B. Nayak, S. Lin, and D. Bhatta. 2011. Geochemical speciation and risk assessment of heavy metals in the river estuarine sediments - A case study: Mahanadi basin, India. Journal of Hazardous Materials. 186:1837-1846.

Sundelin, B., and A-K, Eriksson. 2001. Mobility and Bioavailability of Trace Metals in Sulfidic Coastal Sediments. Environmental Toxicology and Chemistry. 20:748-756.

Sutherland, R.A., and F.M.G. Tack. 2003. Fractionation of Cu, Pb, and Zn in certified reference soils SRM 2710 and SRM 2711 using the optimized BCR sequential extraction procedure. Advances in Environmental Research. 8:27-50.

Sutherland, R.A. 2010. A review of 10-years of sequential extraction analyses. Analytica Chimica Acta. 680:10-20.

Tsai, C-F., J. Welch, K-Y. Chang, and J. Shaeffer. 1979. Bioassay of Baltimore Harbor sediments. Estuaries. 2:141-153.

Tessier, A., P.G. C. Cambell, and M. Bisson 1979. Sequential Extraction Procedure for the Speciation of Particulate Trace Metals. Analytical Chemistry. 51:844-851.

Tovar-Sanchez, A., S.A. Sanudo-Wilhelmy, M. Garcia-Vargas, R.S. Weaver, L.C. Popels, and D.A. Hutchins. 2003. A trace metal clean reagent to remove surface-bound iron from marine phytoplankton. Marine Chemistry. 82:91-99.

Ulrich, E. and H-W. Schlipkoter. 1991. Lead. p. 971-1014. *In* Merian, E. (ed.) Metals and Their Compounds in the Environment. VCH Publishers, Weinheim, Federal Republic of Germany.

Usero, J., M. Gamero, J. Morillo, and I. Gracia. 1998. Comparative study of three sequential extraction procedures for metals in marine sediments. Environmental International. 24:487-496.

Von Burg, R., and M.R. Greenwood. 1991. Mercury. p. 1045-1088. *In* Merian, E. (ed.) Metals and Their Compounds in the Environment. VCH Publishers, Weinheim, Federal Republic of Germany.

Wang, Q., and J.W., Morse. 1996. Pyrite formation under conditions approximating those in anoxic sediments I. Pathway and Morphology. Marine Chemistry. 52:99-121.

Wang, S., Y. Jia, S. Wang, X. Wang, H. Wang, Z. Zhao, and B. Liu. 2010. Fractionation of heavy metals in shallow marine sediments from Jinzhou Bay, China. Journal of Environmental Sciences. 22:23-31.

Warren, L.A., and A.P., Zimmerman. 1994. The importance of surface area in metal oxides and organic matter in a heterogeneous natural sediment. Applied Geochemistry. 9:245-254.

Warren, L.A., A. Tessier, and L. Hare. 1998. Modeling cadmium accumulation by benthic invertebrates in situ: The relative contributions of sediment and overlying water reservoirs to organism cadmium concentrations. Limnology and Oceanography. 43:1442-1454.

Wiese, S.B. O'Reilly, R.H.C. Emmerson, C.L. MacLeod, and J.N. Lester. 1997. Trends in the solid phase partitioning of metals in the Thames Estuary sediments during recent decades. Estuaries. 20:494-503.

Westrich, J.T., and R.A. Berner. 1984. The role of sedimentary organic matter in bacterial sulfate reduction: The G model tested. Limnology and Oceanography. 29:236-249.

Whiteley, J.D., and N.J.G. Pearce. 2003. Metal distribution during diagenesis in the contaminated sediments of Dulas Bay, Anglesey, N. Wales, UK. Applied Geochemistry. 18:901-913.

Wilkie, J.A., and J.G. Hering. 1996. Adsorption of arsenic onto hydrous ferric oxide: effects of adsorbate/adsorbent ratios and co-occurring solutes. Colloids Surfaces A: Physicochemical and Engineering Aspects. 107:97-110.

Wu, X., Y. Jia, and H. Zhu. 2012. Bioaccumulation of cadmium bound to ferric hydroxide and particulate organic matter by the bivalve M. meretrix. Environmental Pollution. 165:133-139.

APPENDIX A

PROCEDURES FOR PHASE SPECIATION OF METALS

Exchangeable Fraction pH ~7.0
Step 1) weigh ~2 g wet sediment (should equal ~1g dried) into 50 mL TFE centrifuge tubes
Step 2) add 8 mL 1M $MgCl_2$
Step 3) vortex and agitate for 1 hour in sonic bath
Step 4) centrifuge for 10 min. at 2000 rpm
Step 5) without disturbing pellet, pour supernatant into pre-weighed 30 mL LDPE bottle
Rinse pellet w/8mL of $MgCl_2$, centrifuge for 10 min. at 2000 rpm, add to collected supernatant,(add to 30mL bottle), **repeat; record combined solution and bottle weight.** Filter collected supernatant using acid-cleaned syringes, filter holders, and 1.0μm 25mm polycarbonate filters into labeled 30mL LDPE bottles

Fe/Mn Oxide Fraction
Step 10) add 20 mL of Oxalate reagent at pH 6
Step 11) place in heating block at 96±3 °C 9 hours
Step 12) centrifuge for 10 min. at 2000 rpm
Step 13) without disturbing pellet, pour supernatant into pre-weighed 60 mL LDPE bottle
Rinse pellet w/10mL of 0.1 M KCl solution, centrifuge for 10 min. at 2000 rpm, add to collected supernatant(add to 60mL bottle), **rinse 3 more times; record combined solution and bottle weight**. Filter collected supernatant using acid-cleaned syringes, filter holders, and 1.0μm 25mm polycarbonate filters into labeled 30mL LDPE bottles

AVS Fraction
Step 10) add 10 mL 0.5 M Baker Instra-analyzed HCl
Step 11) vortex and agitate for ½ hour in sonic bath
Step 12) centrifuge for 10 min. at 2000 rpm
Step 13) without disturbing pellet, pour supernatant into pre-weighed 30 mL LDPE bottle
Rinse pellet w/8mL of 18 MΩ H_20, centrifuge for 10 min. at 2000 rpm, add to collected supernatant(add to 30mL bottle), **repeat; record combined solution and bottle weight.** Filter collected supernatant using acid-cleaned syringes, filter holders, and 1.0μm 25mm polycarbonate filters into labeled 30mL LDPE bottles

Organic Fraction #1: 1M NaOH

Step 18) add 20mL 1M NaOH

Step 19) vortex, place in heating block (80°C) with occasional agitation for 8 hours

Step 20) centrifuge for 10 min. at 2000 rpm

Step 21) without disturbing pellet transfer supernatant into pre-weighed 30 mL LDPE bottle

Rinse pellet once 10mL of 18 MΩ H_20, centrifuge for 10 min. at 2000 rpm, add to collected supernatant(add to 30mL bottle); **record combined solution and bottle weight**. Filter collected supernatant using acid-cleaned syringes, filter holders, and 1.0μm 25mm polycarbonate filters into labeled 30mL LDPE bottles

Organic Fraction #2: 6M HCl

Step 22) add 20mL 6M HCl Instra Analyzed

Step 23) heat at 85° C for 8 hours in hot blocks

Step 24) centrifuge for 10 min. at 2000 rpm

Step 25) without disturbing pellet, carefully pour supernatant into pre-weighed 60 mL LDPE bottle

Rinse pellet w/10mL of 18 MΩ H_20, centrifuge for 10 min. at 2000 rpm, add to collected supernatant (add to 60mL bottle), **repeat 3 more times; record combined solution and bottle weight**. Filter collected supernatant using acid-cleaned syringes, filter holders, and 1.0μm 25mm polycarbonate filters into labeled 30mL LDPE bottles

Pyrite Fraction

Step 26) add 3mL conc Instra Analyzed HNO_3

Step 27) vortex and agitate for 2 hours in sonic bath

Step 28) add 7mL 18 MΩ H_20

Step 29) centrifuge for 10 min. at 2000 rpm

Step 30) without disturbing pellet, pour supernatant into pre-weighed 30 mL LDPE bottle

Rinse pellet w/8mL of 18 MΩ H_20, centrifuge for 10 min. at 2000 rpm, add to collected supernatant(add to 30mL bottle), **repeat; record combined solution and bottle weight**. Filter collected supernatant using acid-cleaned syringes, filter holders, and 1.0μm 25mm polycarbonate filters into labeled 30mL LDPE bottles

Reagents

1 M $MgCl_2$- Omni Pure 203.3g $MCl_2 \cdot 4H_2O$ to 1L 18 MΩ H_20

For 1L Oxalate Reagent:
(Based on Tovar-Sanchez et al., 2003)
Step 1
Add
18.58g Omni-Pur EDTA
14.67g Instra-Analyzed Na Citrate
7.45g KCl USP grade
To 750mL 18 MΩ H_20, adjust pH ~8 till dissolution with Intra-Analyzed 30% NH_4OH solution
Step 2
Add 12.58g Insta Analyzed Oxalic Acid
Dilute to 1L with 18 MΩ H_20
Adjust pH again with 30% NH_4OH sol'n till dissolution and a pH of 6.0 (No extraction step needed)

0.1 M KCl wash solution- 7.45g KCl USP to 1L with 18 MΩ H_20

0.5 M HCl-48mL of Ultrex HCl diluted to 1L with 18 MΩ H_20

1 M NaOH-137 mL of Suprapur 30% NaOH diluted to 1L with 18 MΩ H_20

6M HCl- Half-and-half Instra Analyzed concentrated HCl to 18 MΩ H_20

HNO_3- 16M Instra Analyzed nitric acid

Cleaning Procedure
All lab ware used for trace element analysis should be used only for trace analysis and kept in sealed containers after cleaning.

Clean off all visible residue and labels
Soak in Micro overnight- use a 10% Micro detergent solution and dilute 50 mL of this solution to 1 L with reagent grade water
Rinse 3x with reagent grade water

Soak sample bottles for several days with 0.5 M HCl -use HCl bath
Rinse 5x with 18 MΩ H_20
Place in kimwipe lined container, cover with kimwipes, and place in drying oven
(Not for nylon labware-rinse only)
Rinse 3x with 18 MΩ H_20

APPENDIX B

PROCEDURES FOR TOTAL SEDIMENT DIGESTS

Method for ~ 100 mg sediment

Digestion # 1

- Weigh out sediment in each vessel.
- Add 3mL 16M HNO_3 to each vessel and allow to effervesce.
- Add 12mL 49% HF to each vessel. Swirl vessels gently.
- Microwave Settings:
    - Ramp Time = 5:00 mins
    - Hold Time = 60:00 mins
    - Hold Temperature = 175° C
    - Power = 100%
    - Wattage =
        - 400W for 1-3 vessels
        - 800W for 4-7 vessels
        - 1600W for 7-12 vessels

Evaporation #1

- Switch the digestion caps for the evaporation caps. It is best to keep the digestion caps in order on a tray because you will need to use them again for the 2nd digestion.
- Complete a series of 2 evaporations:
    - 1st Evaporation Microwave Setting
        - Ramp Time = 5:00 mins
        - Hold Time = 30:00 mins
        - Wattage =
            - 400W for 1-3 vessels
            - 800W for 4-12 vessels
        - Hold Temperature = 120°C
    - 2nd Evaporation: Add 18 MΩ H_20 until all volumes in vessels are approximately equal.
        - Microwave setting same as 1st evaporation

All vessels completely dry before moving on to digestion # 2

Digestion # 2

- Each vessel receives 16mL of aqua regia. In order to do this, first add 4 mL Instra Analyzed 16M HNO_3 then 12mL Instra Analyzed 12M HCl, using repipet dispensers, to a plastic graduated cylinder, then add the mix to the reaction vessel.
    - Aqua Regia = 1:3 ratio of 16M HNO_3: 12M HCl
- Microwave Settings
    - Ramp Time = 5:00 mins
    - Hold Time = 60:00 mins
    - Hold Temperature = 175° C
    - Power = 100%
    - Wattage =
        - 400W for 1-3 vessels
        - 800W for 4-7 vessels
        - 1600W for 7-12 vessels

Evaporation # 2

- Remove the digestion caps and replace with the evaporation caps used previously.
- Turn the "pressure sensor" off
- Complete another series of 2 evaporations. Use the same exact method and settings used in Evaporation #1.

Dissolution of Dried Samples

- Label and weigh trace metal clean 30 mL wide mouth LDPE bottles
- Add 10 mL 1M HNO_3 Instra-Analyzed to each reaction vessel with evaporated samples.
- Place tops back on reaction vessels and place back into microwave run with the following settings:
    - Ramp Time = 5:00 mins
    - Hold Time = 2:00 mins
    - Wattage = 800W for 4-12 vessels
    - Hold Temperature = 100°C
- Pour dissolved samples into corresponding labeled and tared bottles.
- Rinse each reaction vessel 3 times with 7mL 1M HNO_3 using repipet dispenser. Pour each rinse into appropriate wide mouth LDPE 30mL bottle. Total volume in each bottle should be about 31 mL. Do not exceed 34 mL.

APPENDIX C

METAL PHASE SPECIATION PROFILES

Elizabeth River Core ER 1: Major Metals

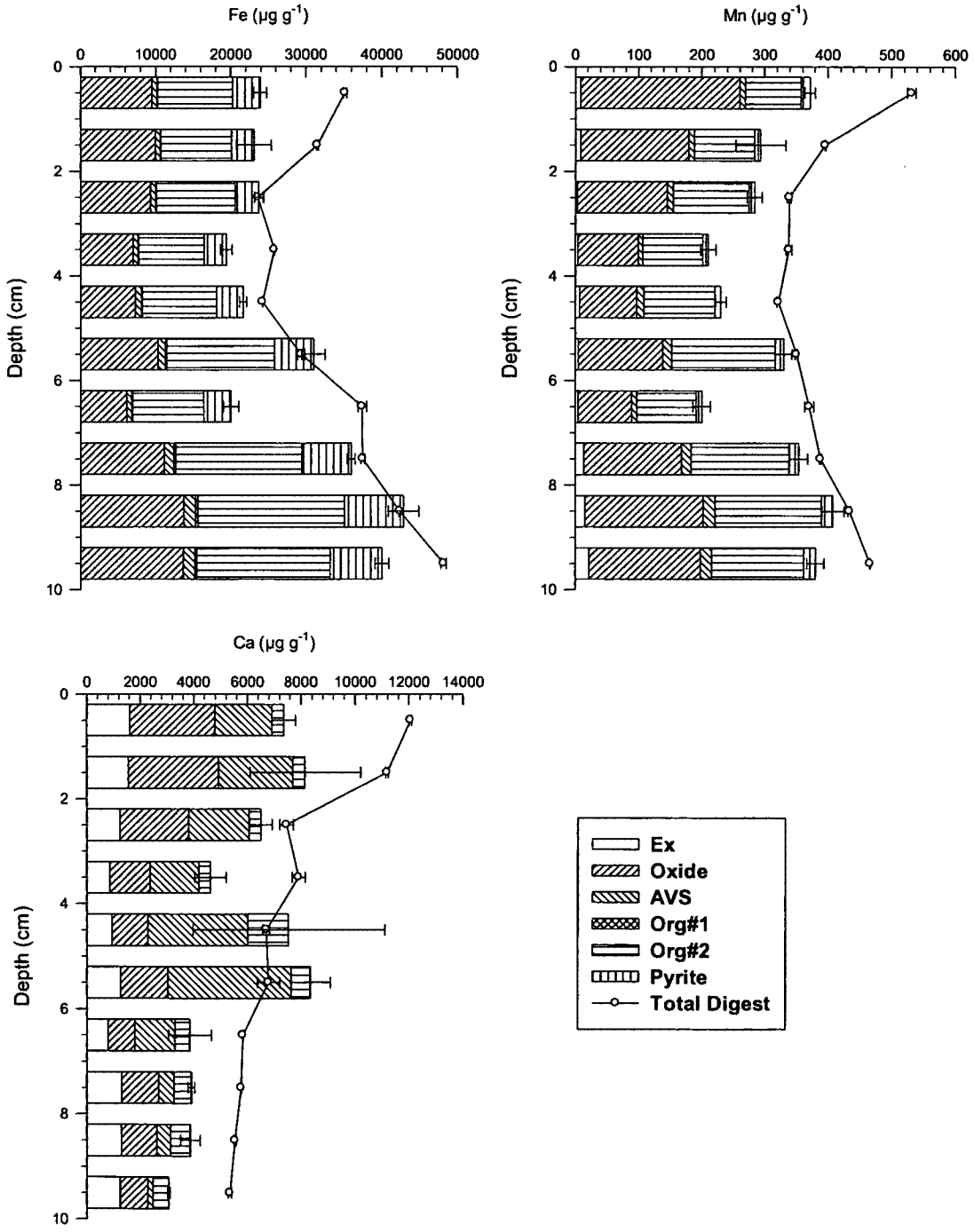

Elizabeth River Core ER 1: Trace Metals

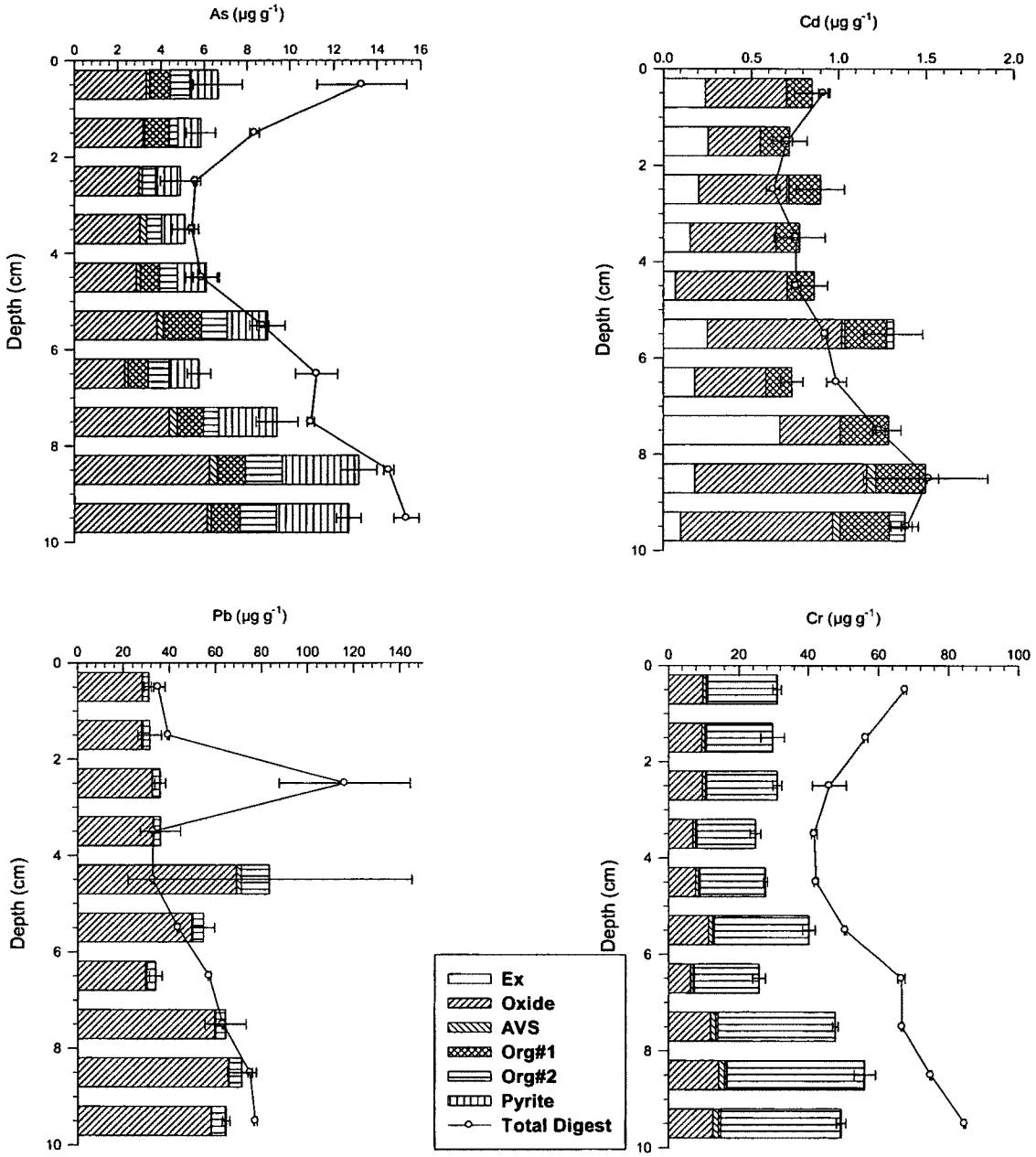

Elizabeth River Core ER 2: Major Metals

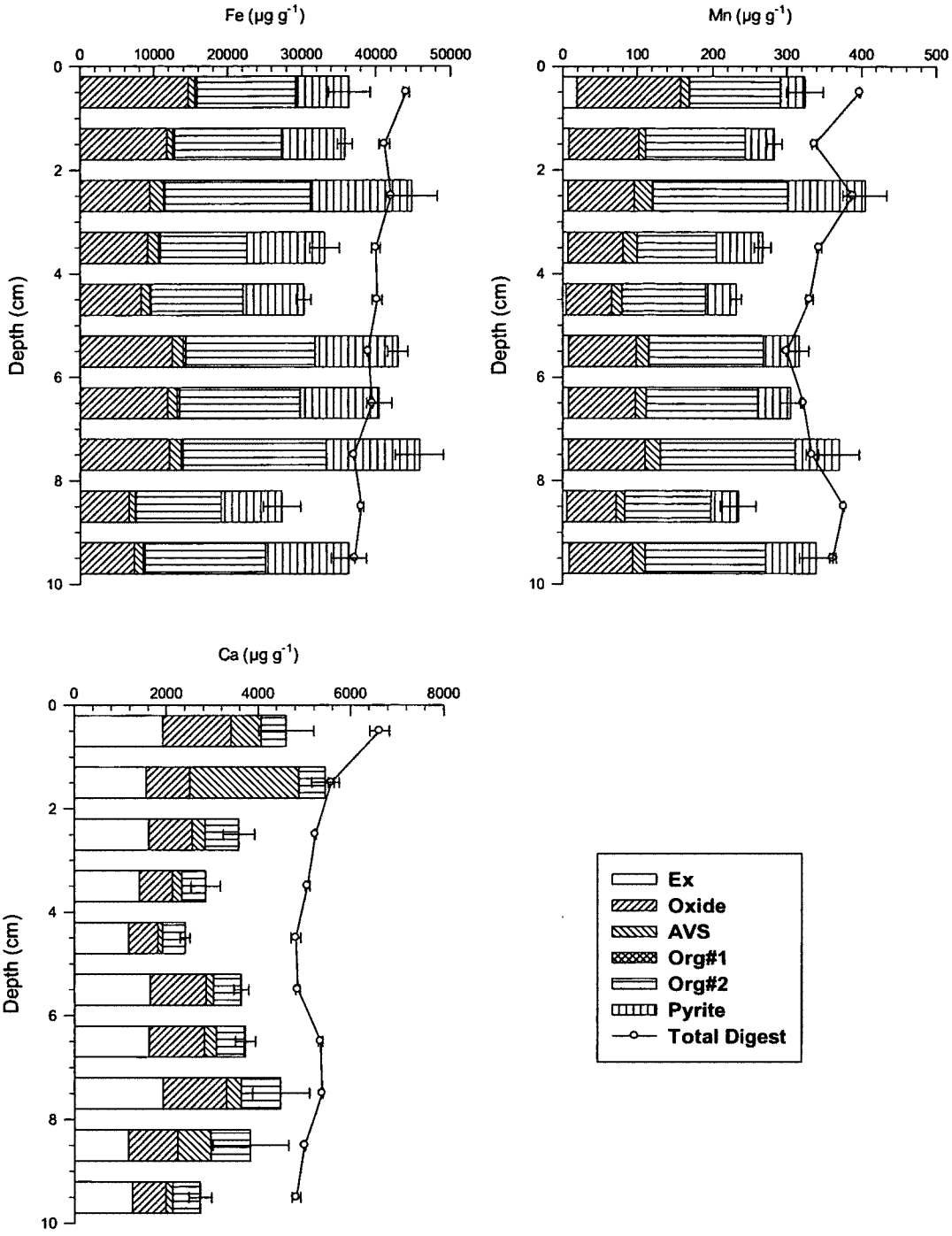

Elizabeth River Core ER 2: Trace Metals

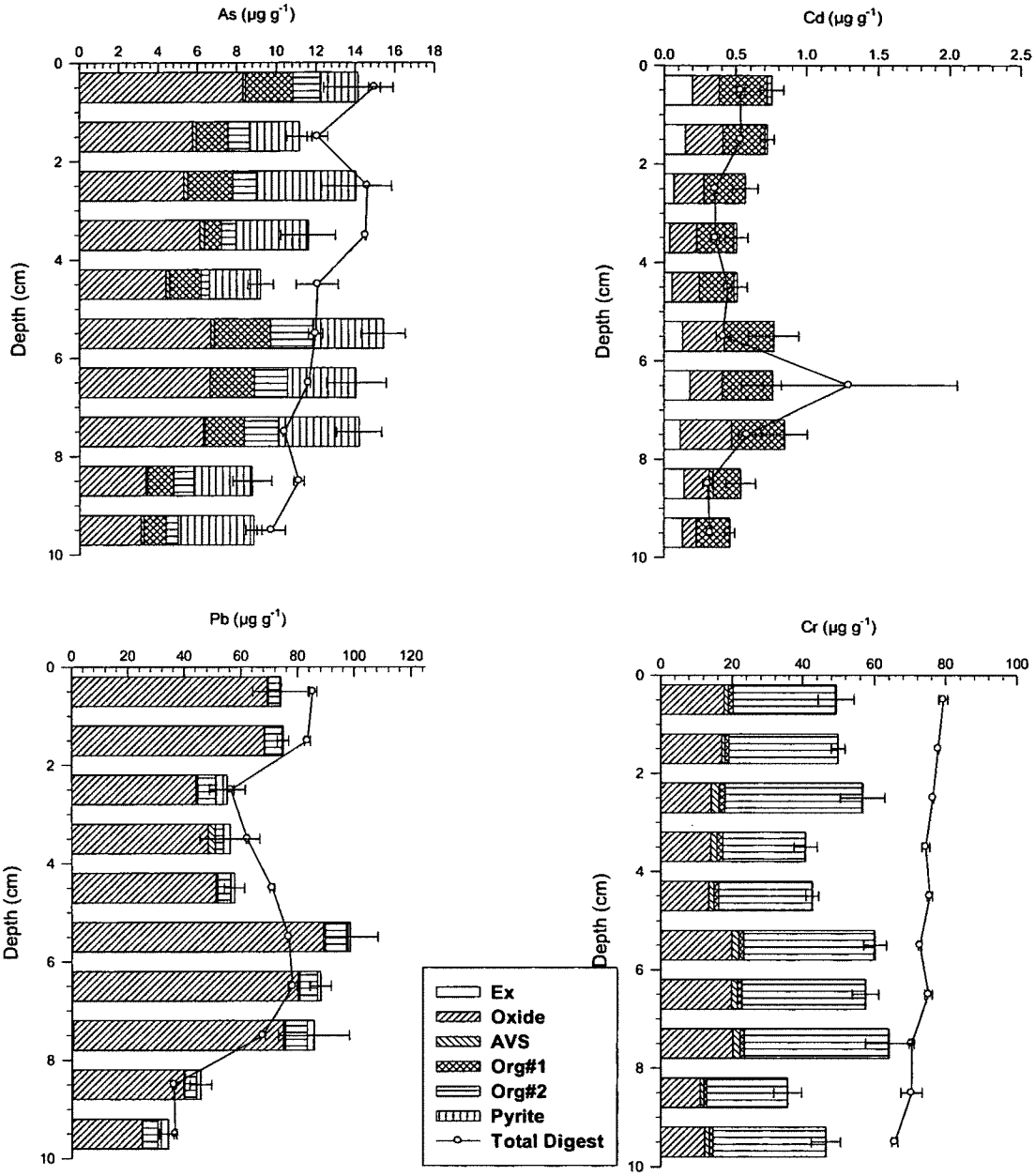

Baltimore Harbor Core BH 1: Major Metals

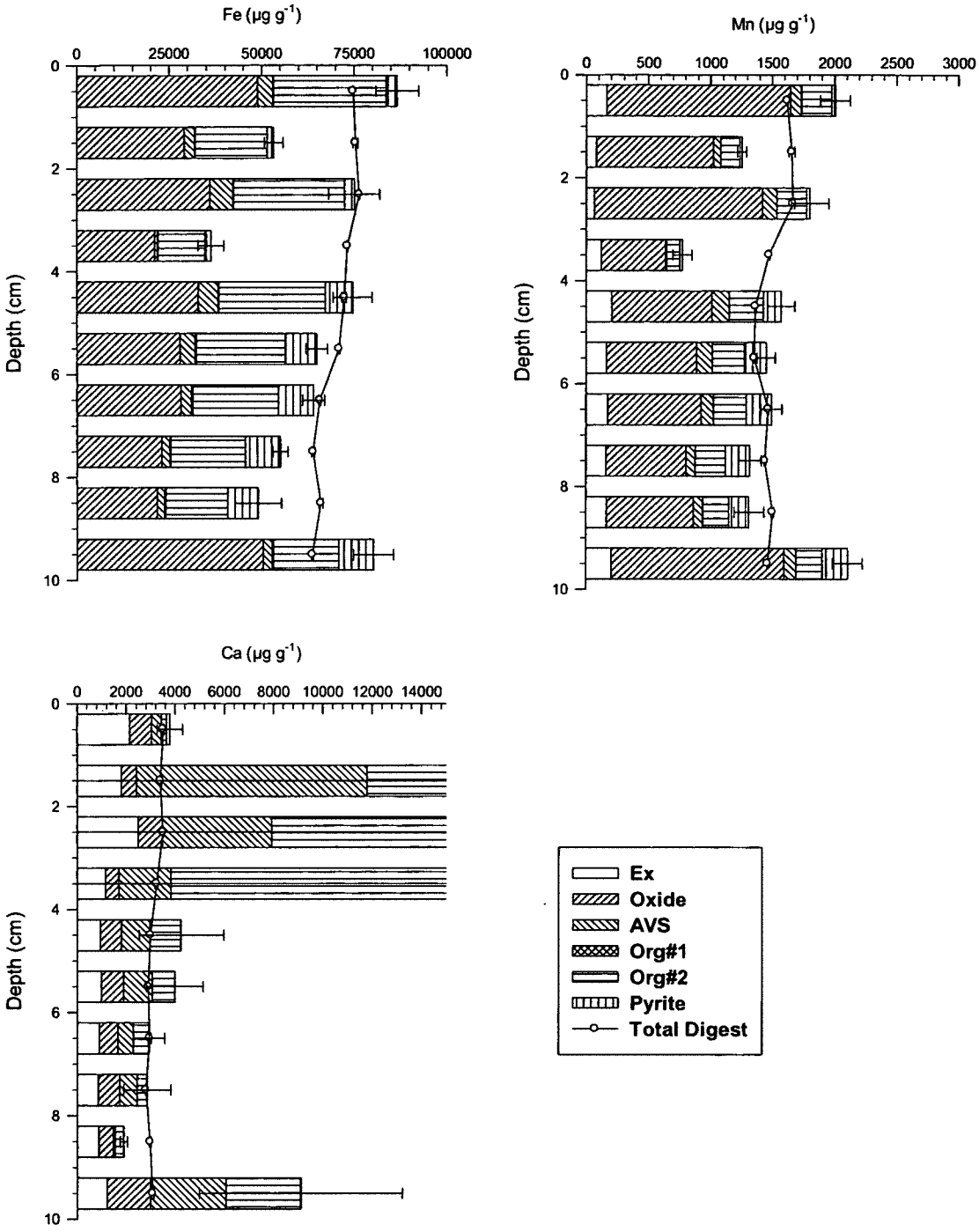

Baltimore Harbor Core BH 1: Trace Metals

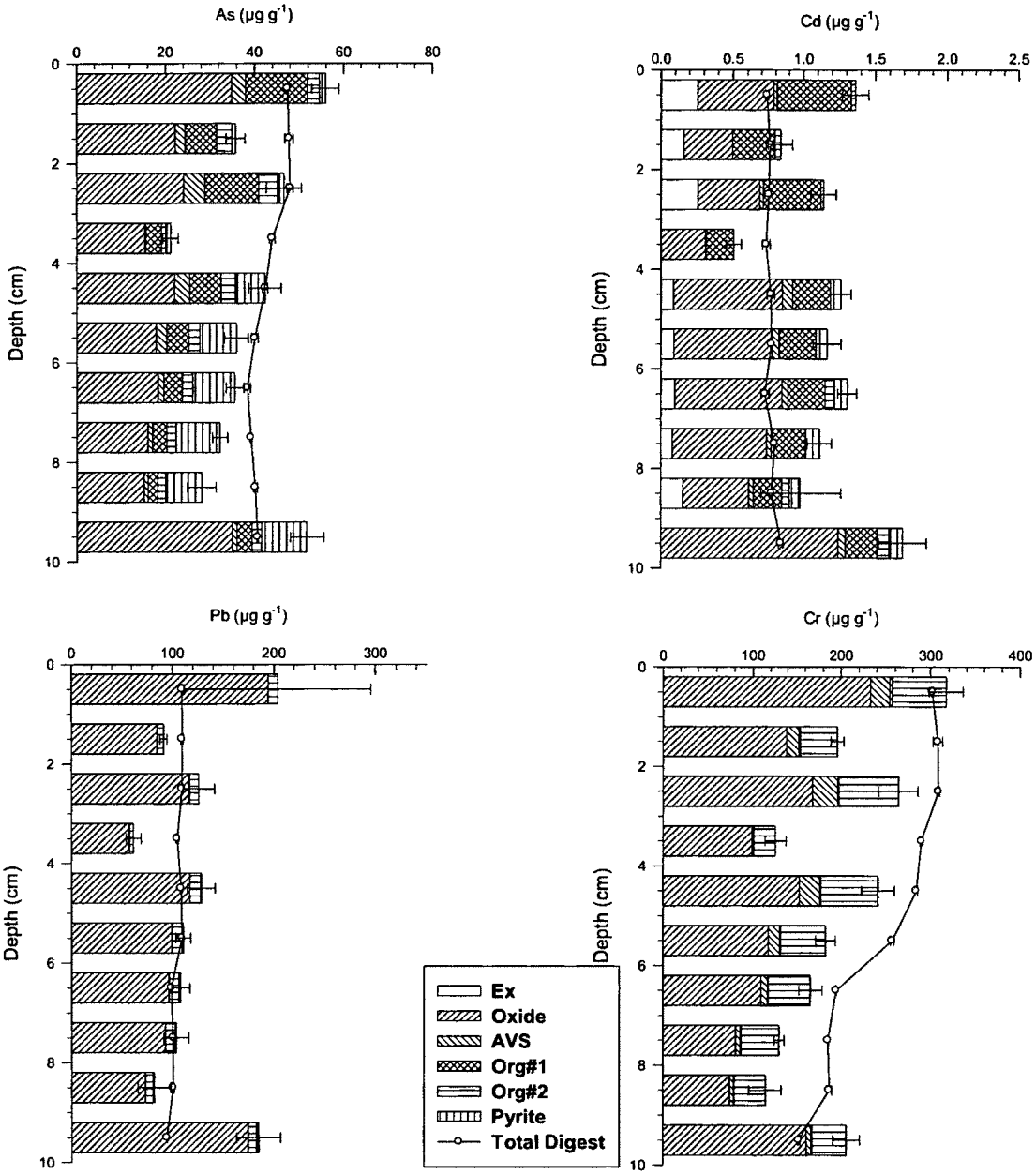

Baltimore Harbor Core BH 2: Major Metals

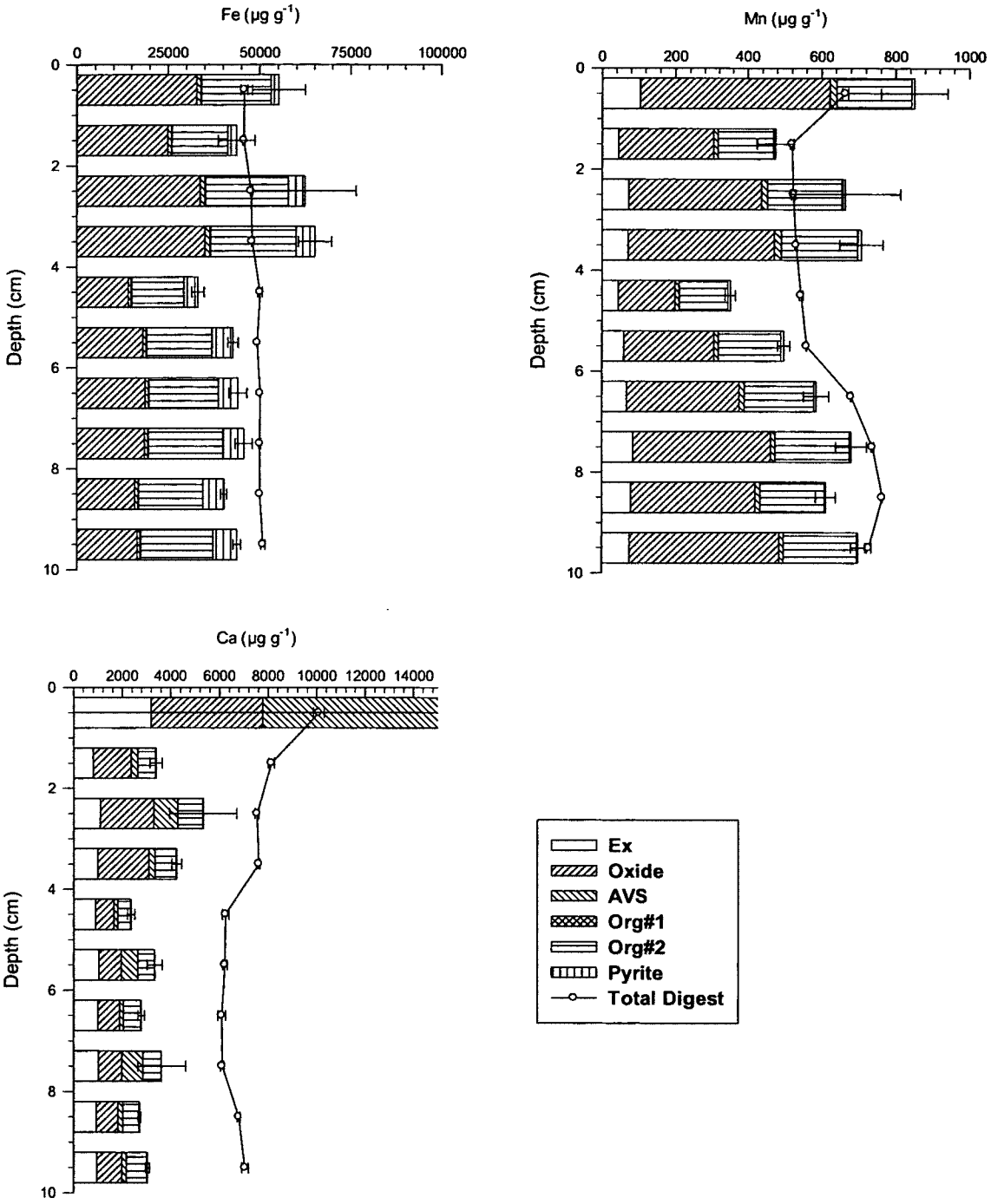

Baltimore Harbor Core BH 2: Trace Metals

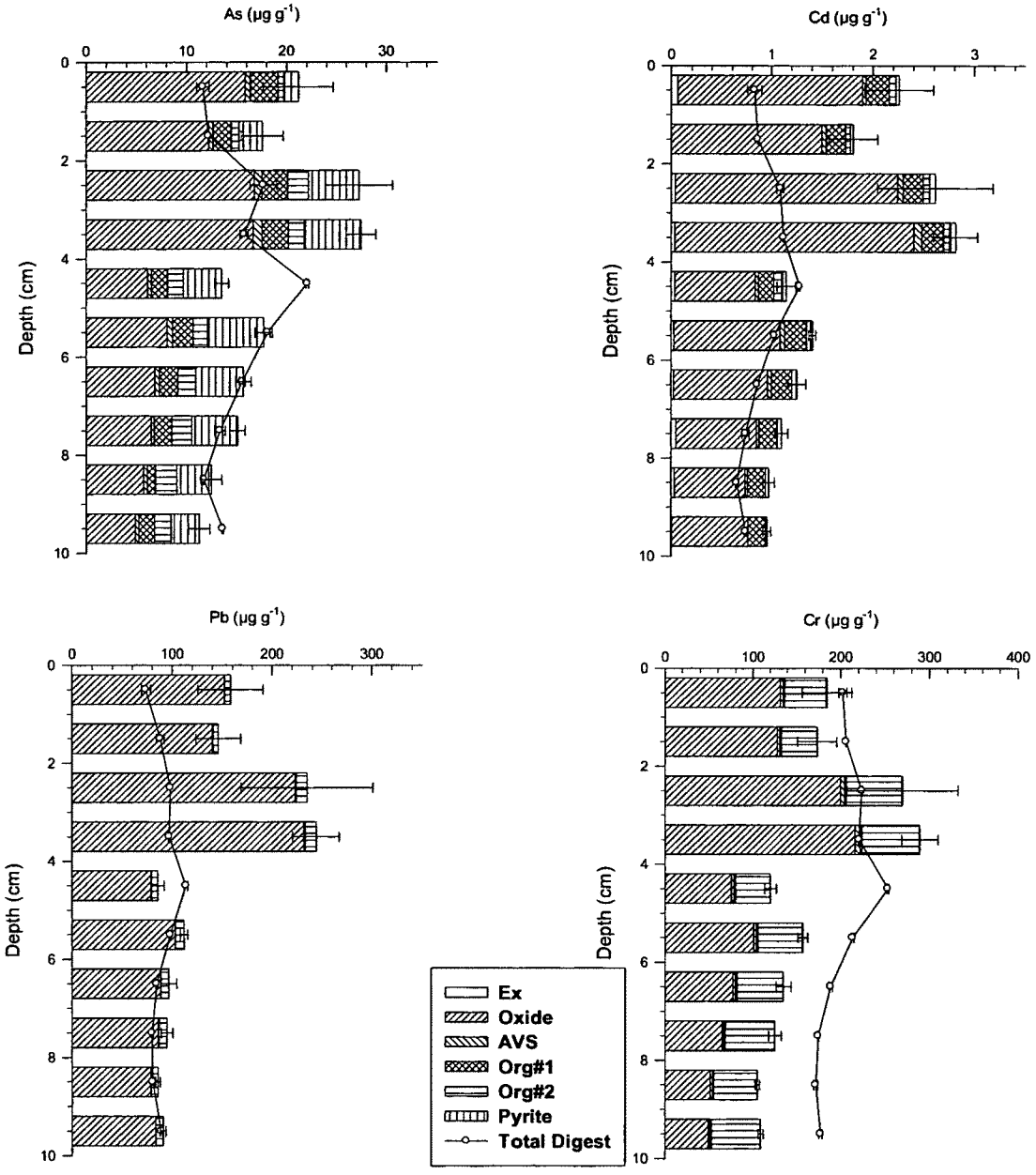

Mare Island Core MI 1: Major Metals

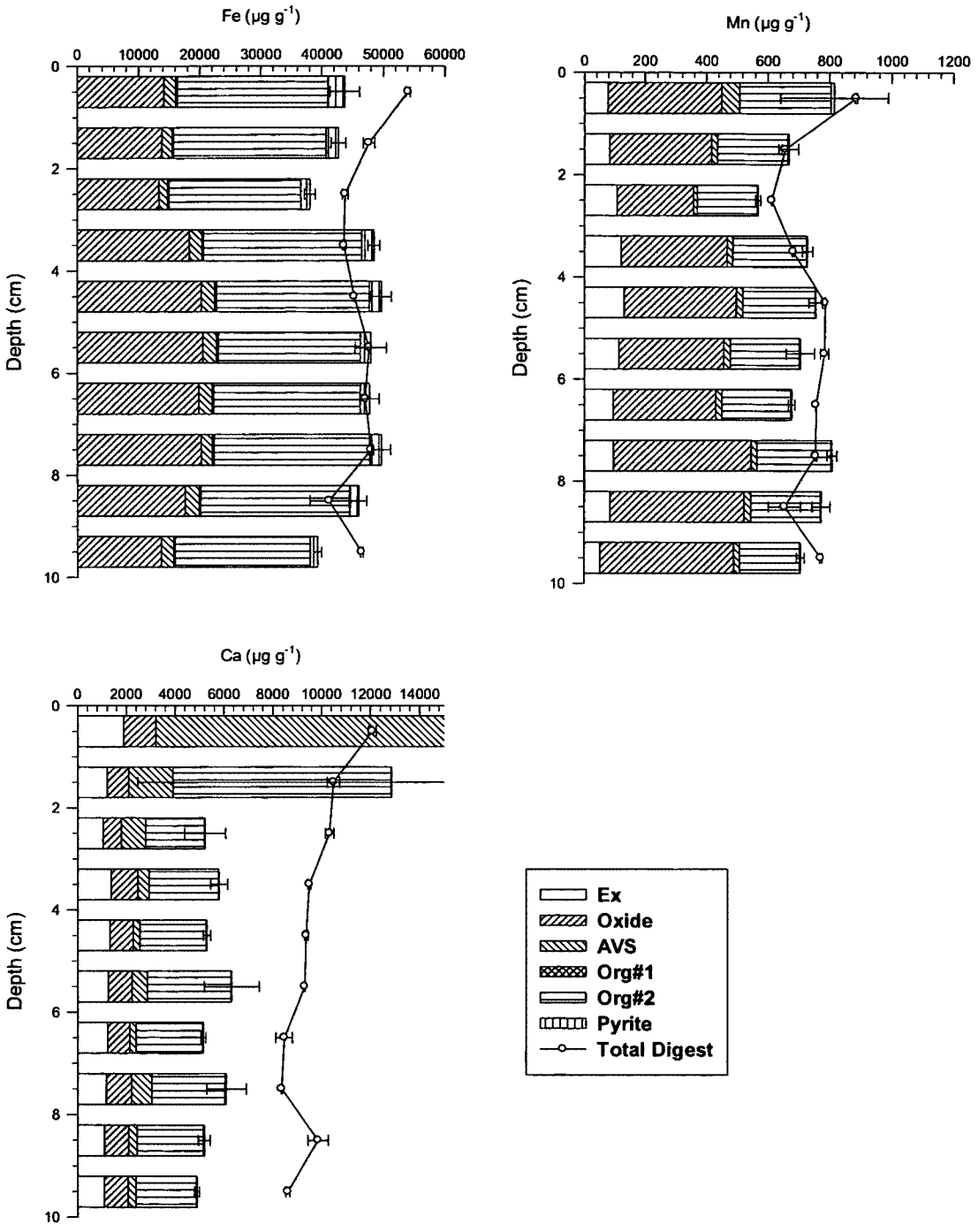

Mare Island Core MI 1: Trace Metals

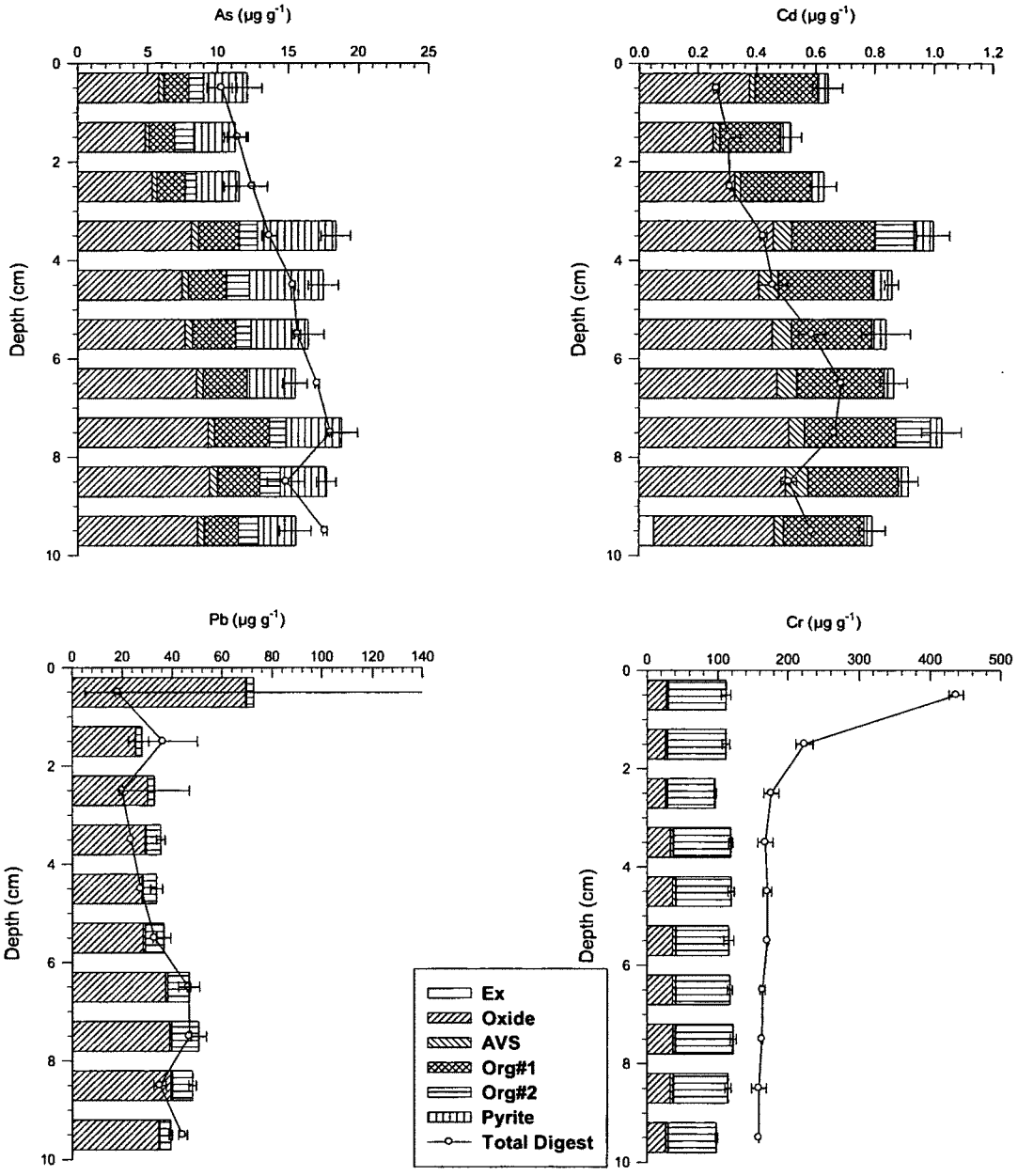

Mare Island Core MI 2: Major Metals

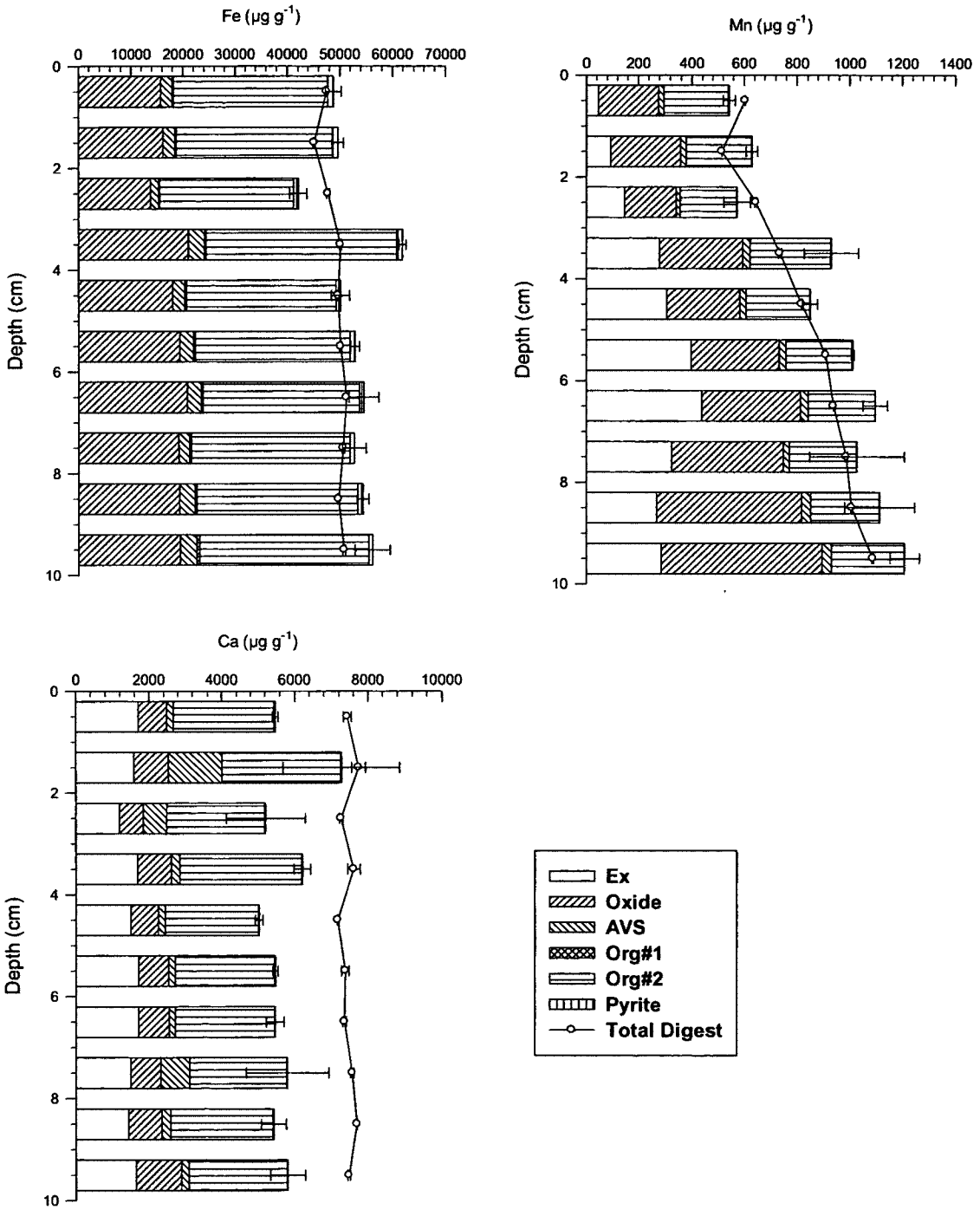

Mare Island Core MI 2: Trace Metals

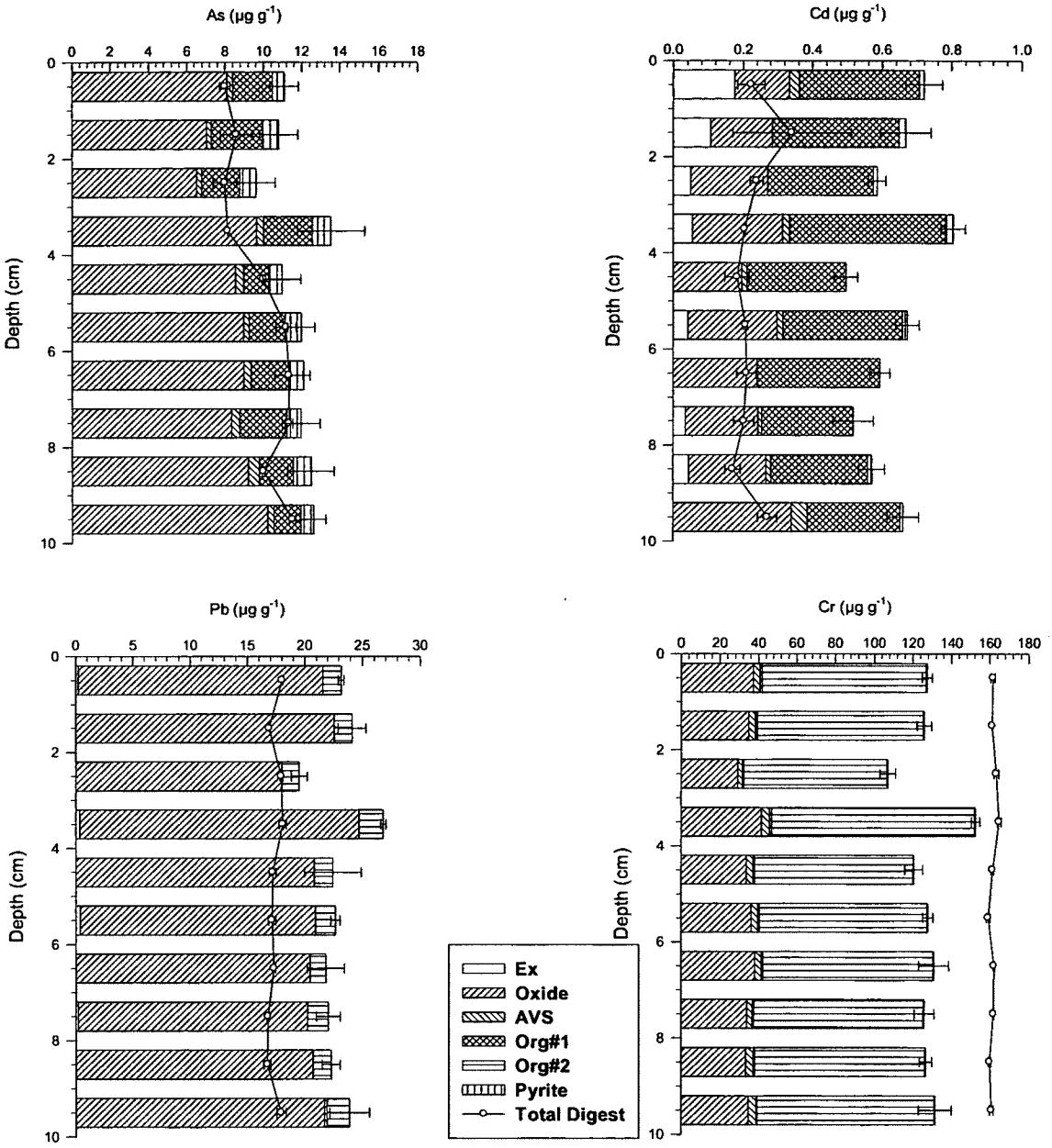

APPENDIX D

METAL PHASE SPECIATION DATA ALL CORES

ER1: Exchangeable Phase

	Fe 238.863 nm		Ca 315.887 nm		Mn 293.305 nm	
	Det. Limit (ppm)		Det. Limit (ppm)		Det. Limit (ppm)	
	0.32		**0.17**		**0.37**	
Depth (cm)	Fe (ppm)	SD	Ca (ppm)	SD	Mn (ppm)	SD
0.5	0.00	0.00	1621.79	92.93	8.79	3.56
1.5	0.00	0.00	1556.45	116.08	8.50	5.92
2.5	0.57	0.46	1238.43	58.91	3.16	0.71
3.5	2.29	1.15	866.43	61.55	4.17	2.79
4.5	0.41	0.38	942.38	67.11	6.71	3.40
5.5	2.54	1.67	1261.22	131.68	5.10	2.28
6.5	0.00	0.00	791.70	29.10	4.54	2.38
7.5	0.00	0.00	1306.39	54.85	14.10	6.39
8.5	0.00	0.00	1305.10	77.34	15.80	3.54
9.5	0.00	0.00	1261.09	18.48	22.21	4.59

	As 188.979 nm		Cd 228.802 nm		Pb 220.353 nm		Cr 205.560 nm	
	Det. Limit (ppm)		Det. Limit (ppm)		Det. Limit (ppm)		Det. Limit (ppm)	
	0.44		**0.03**		**0.14**		**0.02**	
Depth (cm)	As (ppm)	SD	Cd (ppm)	SD	Pb (ppm)	SD	Cr (ppm)	SD
0.5	0.00	0.00	0.24	0.05	0.00	0.00	0.00	0.00
1.5	0.00	0.00	0.26	0.01	0.00	0.00	0.00	0.00
2.5	0.00	0.00	0.21	0.03	0.00	0.00	0.00	0.00
3.5	0.00	0.00	0.16	0.05	0.00	0.00	0.00	0.00
4.5	0.00	0.00	0.07	0.02	0.00	0.00	0.00	0.00
5.5	0.00	0.00	0.26	0.07	0.00	0.00	0.00	0.00
6.5	0.00	0.00	0.18	0.02	0.00	0.00	0.00	0.00
7.5	0.00	0.00	0.67	0.03	0.19	0.22	0.00	0.00
8.5	0.00	0.00	0.19	0.19	0.20	0.13	0.00	0.00
9.5	0.00	0.00	0.10	0.04	0.00	0.00	0.00	0.00

ER1: Oxide Phase

	Fe 253.681 nm		Ca 315.887 nm		Mn 293.305 nm	
	Det. Limit (ppm)		Det. Limit (ppm)		Det. Limit (ppm)	
	0.69		**0.28**		**0.01**	
Depth (cm)	Fe (ppm)	SD	Ca (ppm)	SD	Mn (ppm)	SD
0.5	9492.57	272.18	3159.95	30.02	251.17	4.06
1.5	9962.78	995.35	3368.39	209.14	171.38	24.96
2.5	9308.23	328.01	2575.70	267.48	143.45	8.49
3.5	7078.26	134.94	1504.57	49.57	95.24	4.70
4.5	7353.05	157.72	1347.23	136.29	90.50	2.98
5.5	10311.99	514.59	1782.26	142.15	134.52	5.58
6.5	6185.63	419.27	1009.65	36.77	84.68	5.64
7.5	11156.07	150.65	1371.83	33.34	154.67	7.13
8.5	13792.57	481.22	1315.44	8.11	187.42	9.33
9.5	13695.18	349.25	1025.14	25.89	176.53	7.11

	As 188.979 nm		Cd 228.802 nm		Pb 220.353 nm		Cr 205.560 nm	
	Det. Limit (ppm)		Det. Limit (ppm)		Det. Limit (ppm)		Det. Limit (ppm)	
	0.22		**0.01**		**0.05**		**0.03**	
Depth (cm)	As (ppm)	SD	Cd (ppm)	SD	Pb (ppm)	SD	Cr (ppm)	SD
0.5	3.32	0.21	0.46	0.04	28.06	1.43	9.94	0.26
1.5	3.16	0.32	0.29	0.07	27.87	3.26	9.74	0.80
2.5	2.99	0.58	0.50	0.09	32.29	1.57	9.84	0.85
3.5	3.02	0.36	0.49	0.09	32.80	6.10	7.22	0.46
4.5	2.87	0.19	0.64	0.05	68.96	42.76	7.98	0.17
5.5	3.82	0.22	0.77	0.09	49.66	3.39	11.58	0.40
6.5	2.33	0.30	0.40	0.04	29.40	1.37	6.54	0.47
7.5	4.37	0.63	0.34	0.03	59.43	6.33	12.22	0.21
8.5	6.24	0.49	0.98	0.16	65.35	4.45	14.51	0.61
9.5	6.15	0.16	0.87	0.04	58.03	1.11	12.94	0.52

ER1: AVS Phase

	Fe 238.863 nm		Ca 315.887 nm		Mn 293.305 nm	
	Det. Limit (ppm)		Det. Limit (ppm)		Det. Limit (ppm)	
	0.63		**0.19**		**0.09**	
Depth (cm)	Fe (ppm)	SD	Ca (ppm)	SD	Mn (ppm)	SD
0.5	715.64	99.54	2138.96	293.31	8.87	1.22
1.5	642.29	117.95	2775.45	1425.76	8.87	2.69
2.5	695.67	100.60	2254.97	114.48	8.66	1.30
3.5	606.30	15.76	1830.21	393.04	7.40	0.07
4.5	812.52	43.07	3719.76	2174.99	11.24	2.61
5.5	1034.74	64.42	4595.72	471.55	13.76	0.80
6.5	677.85	76.73	1493.00	497.77	8.48	0.90
7.5	1280.11	103.22	590.01	62.20	15.24	1.01
8.5	1586.85	228.33	526.68	247.50	18.68	2.30
9.5	1563.06	158.44	201.81	14.92	18.00	1.81

	As 188.979 nm		Cd 228.802 nm		Pb 220.353 nm		Cr 205.560 nm	
	Det. Limit (ppm)		Det. Limit (ppm)		Det. Limit (ppm)		Det. Limit (ppm)	
	0.05		**0.02**		**0.02**		**0.02**	
Depth (cm)	As (ppm)	SD	Cd (ppm)	SD	Pb (ppm)	SD	Cr (ppm)	SD
0.5	0.16	0.04	0.00	0.00	0.15	0.09	0.86	0.12
1.5	0.08	0.07	0.00	0.00	0.47	0.57	0.75	0.08
2.5	0.14	0.09	0.01	0.01	0.29	0.14	0.83	0.11
3.5	0.31	0.03	0.00	0.00	0.25	0.15	0.70	0.03
4.5	0.19	0.03	0.00	0.00	2.20	1.31	0.87	0.01
5.5	0.28	0.13	0.02	0.00	0.53	0.27	1.24	0.04
6.5	0.16	0.03	0.00	0.00	0.73	0.49	0.71	0.10
7.5	0.37	0.12	0.00	0.00	0.46	0.11	1.45	0.27
8.5	0.37	0.05	0.05	0.01	0.28	0.06	1.64	0.21
9.5	0.19	0.06	0.04	0.01	0.24	0.03	1.55	0.17

ER1: Org#1 Phase

	Fe 238.863 nm		Ca 315.887 nm		Mn 293.305 nm	
	Det. Limit (ppm)		Det. Limit (ppm)		Det. Limit (ppm)	
	0.81		**0.15**		**0.09**	
Depth (cm)	Fe (ppm)	SD	Ca (ppm)	SD	Mn (ppm)	SD
0.5	76.34	4.67	0.00	0.00	0.00	0.00
1.5	79.50	15.67	0.00	0.00	0.00	0.00
2.5	74.94	1.32	0.00	0.00	0.00	0.00
3.5	67.96	13.91	0.00	0.00	0.00	0.00
4.5	83.49	17.52	0.00	0.00	0.00	0.00
5.5	126.16	6.06	0.00	0.00	0.00	0.00
6.5	124.15	29.62	0.00	0.00	0.00	0.00
7.5	260.68	30.66	0.00	0.00	0.00	0.00
8.5	300.66	34.40	0.00	0.00	0.00	0.00
9.5	237.13	25.64	0.00	0.00	0.00	0.00

	As 197.197 nm		Cd 228.802 nm		Pb 220.353 nm		Cr 267.716 nm	
	Det. Limit (ppm)		Det. Limit (ppm)		Det. Limit (ppm)		Det. Limit (ppm)	
	0.70		**0.01**		**0.20**		**0.02**	
Depth (cm)	As (ppm)	SD	Cd (ppm)	SD	Pb (ppm)	SD	Cr (ppm)	SD
0.5	0.94	0.59	0.15	0.02	0.00	0.00	0.44	0.02
1.5	1.14	0.17	0.17	0.02	0.00	0.00	0.40	0.00
2.5	0.00	0.00	0.18	0.00	0.00	0.00	0.35	0.01
3.5	0.00	0.00	0.14	0.01	0.00	0.00	0.36	0.06
4.5	0.88	0.17	0.15	0.01	0.00	0.00	0.29	0.07
5.5	1.78	0.30	0.24	0.02	0.00	0.00	0.44	0.05
6.5	0.92	0.22	0.15	0.01	0.00	0.00	0.27	0.09
7.5	1.23	0.13	0.28	0.02	0.00	0.00	0.61	0.00
8.5	1.31	0.09	0.29	0.02	0.00	0.00	0.64	0.06
9.5	1.33	0.20	0.28	0.01	0.00	0.00	0.66	0.04

ER1: Org#2 Phase

	Fe 253.681 nm		Ca 315.887 nm		Mn 293.305 nm	
	Det. Limit (ppm)		Det. Limit (ppm)		Det. Limit (ppm)	
	6.79		**3.38**		**0.12**	
Depth (cm)	Fe (ppm)	SD	Ca (ppm)	SD	Mn (ppm)	SD
0.5	9968.55	522.46	433.51	30.62	88.92	1.59
1.5	9474.71	1281.27	446.27	111.94	95.31	11.30
2.5	10516.19	179.10	430.33	5.18	119.49	1.64
3.5	8754.17	533.98	417.35	84.01	95.66	6.25
4.5	9915.33	292.33	1514.07	1255.64	112.53	2.95
5.5	14333.66	914.90	713.06	57.82	164.25	7.05
6.5	9460.44	582.47	562.84	264.99	94.41	7.41
7.5	16861.62	317.93	635.72	3.75	155.82	3.04
8.5	19442.82	1314.81	733.21	27.05	169.41	6.81
9.5	17693.40	515.41	583.21	16.09	146.72	4.05

	As 188.979 nm		Cd 228.802 nm		Pb 220.353 nm		Cr 205.560 nm	
	Det. Limit (ppm)		Det. Limit (ppm)		Det. Limit (ppm)		Det. Limit (ppm)	
	0.51		**0.04**		**0.04**		**0.13**	
Depth (cm)	As (ppm)	SD	Cd (ppm)	SD	Pb (ppm)	SD	Cr (ppm)	SD
0.5	0.94	0.51	0.00	0.00	2.61	0.37	19.70	0.86
1.5	0.42	0.31	0.00	0.00	2.95	1.32	18.71	2.35
2.5	0.63	0.31	0.00	0.00	3.23	0.41	19.98	0.40
3.5	0.69	0.25	0.00	0.00	2.90	0.48	16.36	0.99
4.5	0.85	0.34	0.00	0.00	12.32	8.19	18.35	0.35
5.5	1.19	0.43	0.04	0.01	4.53	0.36	27.02	1.20
6.5	0.97	0.05	0.00	0.00	3.66	1.30	18.17	1.19
7.5	0.71	0.22	0.00	0.00	4.12	0.11	33.52	0.40
8.5	1.73	0.31	0.00	0.00	5.38	0.14	39.38	2.01
9.5	1.70	0.29	0.09	0.01	5.84	0.31	34.30	0.78

ER1: Pyrite Phase

	Fe 238.863 nm		Ca 315.887 nm		Mn 293.305 nm	
	Det. Limit (ppm)		Det. Limit (ppm)		Det. Limit (ppm)	
	1.06		**0.87**		**0.06**	
Depth (cm)	Fe (ppm)	SD	Ca (ppm)	SD	Mn (ppm)	SD
0.5	3671.93	234.89	3.20	1.42	14.21	0.97
1.5	2939.59	414.51	8.88	3.95	9.40	1.24
2.5	3131.19	156.13	4.83	2.17	9.43	0.44
3.5	2936.93	175.77	10.59	1.59	8.14	0.49
4.5	3485.61	121.79	12.36	4.65	9.01	0.33
5.5	5195.95	335.35	10.83	0.52	12.96	0.91
6.5	3609.35	266.09	7.93	2.12	8.82	0.66
7.5	6439.15	82.53	21.26	12.33	14.94	0.19
8.5	7814.31	405.33	5.92	1.42	17.60	0.86
9.5	6859.75	108.59	7.02	2.07	18.12	0.40

	As 188.979 nm		Cd 228.802 nm		Pb 220.353 nm		Cr 205.560 nm	
	Det. Limit (ppm)		Det. Limit (ppm)		Det. Limit (ppm)		Det. Limit (ppm)	
	0.31		**0.01**		**0.00**		**0.01**	
Depth (cm)	As (ppm)	SD	Cd (ppm)	SD	Pb (ppm)	SD	Cr (ppm)	SD
0.5	1.28	0.12	0.00	0.00	0.14	0.05	0.12	0.03
1.5	1.04	0.24	0.00	0.00	0.05	0.07	0.12	0.03
2.5	1.14	0.04	0.00	0.00	0.08	0.11	0.09	0.00
3.5	1.12	0.09	0.00	0.00	0.08	0.02	0.09	0.03
4.5	1.32	0.07	0.00	0.00	0.10	0.05	0.13	0.09
5.5	1.87	0.14	0.00	0.00	0.04	0.02	0.07	0.01
6.5	1.38	0.16	0.00	0.00	0.12	0.09	0.10	0.02
7.5	2.71	0.17	0.00	0.00	0.13	0.08	0.15	0.06
8.5	3.52	0.19	0.00	0.00	0.24	0.06	0.13	0.02
9.5	3.33	0.06	0.00	0.00	0.43	0.07	0.19	0.03

ER2: Exchangeable Phase

	Fe 238.863 nm		Ca 315.887 nm		Mn 293.305 nm	
	Det. Limit (ppm)		Det. Limit (ppm)		Det. Limit (ppm)	
	0.32		**0.17**		**0.37**	
Depth (cm)	Fe (ppm)	SD	Ca (ppm)	SD	Mn (ppm)	SD
0.5	1.77	0.47	1925.52	162.42	18.88	2.71
1.5	0.80	1.03	1552.38	38.11	8.37	2.51
2.5	0.00	0.00	1611.96	146.75	7.44	0.69
3.5	0.39	0.49	1401.42	147.30	7.47	2.01
4.5	0.85	0.16	1173.70	57.28	4.69	0.32
5.5	0.51	0.53	1643.90	12.14	8.48	1.30
6.5	0.00	0.00	1619.92	72.09	8.21	1.25
7.5	1.35	0.54	1924.81	163.80	7.97	1.29
8.5	3.69	1.04	1164.23	146.67	5.71	1.33
9.5	19.52	22.28	1245.97	132.28	8.69	1.33

	As 188.979 nm		Cd 228.802 nm		Pb 220.353 nm		Cr 205.560 nm	
	Det. Limit (ppm)		Det. Limit (ppm)		Det. Limit (ppm)		Det. Limit (ppm)	
	0.44		**0.03**		**0.14**		**0.02**	
Depth (cm)	As (ppm)	SD	Cd (ppm)	SD	Pb (ppm)	SD	Cr (ppm)	SD
0.5	0.00	0.00	0.20	0.05	0.00	0.00	0.02	0.02
1.5	0.00	0.00	0.15	0.02	0.00	0.00	0.00	0.00
2.5	0.00	0.00	0.07	0.01	0.14	0.08	0.00	0.00
3.5	0.00	0.00	0.04	0.01	0.19	0.03	0.02	0.01
4.5	0.00	0.00	0.05	0.03	0.31	0.10	0.00	0.00
5.5	0.00	0.00	0.13	0.07	0.34	0.11	0.02	0.02
6.5	0.00	0.00	0.18	0.02	0.42	0.21	0.00	0.00
7.5	0.00	0.00	0.11	0.08	0.45	0.26	0.03	0.01
8.5	0.00	0.00	0.14	0.02	0.40	0.02	0.00	0.00
9.5	0.00	0.00	0.13	0.01	0.00	0.00	0.00	0.00

ER2: Oxide Phase

	Fe 253.681 nm		Ca 315.887 nm		Mn 293.305 nm	
	Det. Limit (ppm)		Det. Limit (ppm)		Det. Limit (ppm)	
	0.69		**0.28**		**0.01**	
Depth (cm)	Fe (ppm)	SD	Ca (ppm)	SD	Mn (ppm)	SD
0.5	14638.96	1465.50	1479.60	369.30	139.11	12.06
1.5	11784.20	163.02	950.11	8.90	93.77	1.06
2.5	9448.47	883.70	945.18	133.95	88.22	7.82
3.5	9136.07	1040.88	730.27	112.78	73.12	5.85
4.5	8270.42	212.90	633.39	25.43	60.77	2.35
5.5	12528.20	585.02	1209.77	101.19	90.22	6.40
6.5	11897.00	486.58	1198.97	38.82	89.19	3.66
7.5	12099.30	929.12	1375.77	292.28	103.40	4.03
8.5	6556.13	408.49	1079.60	262.25	65.82	5.97
9.5	7255.20	388.69	737.14	73.91	85.37	6.82

	As 188.979 nm		Cd 228.802 nm		Pb 220.353 nm		Cr 205.560 nm	
	Det. Limit (ppm)		Det. Limit (ppm)		Det. Limit (ppm)		Det. Limit (ppm)	
	0.22		**0.01**		**0.05**		**0.03**	
Depth (cm)	As (ppm)	SD	Cd (ppm)	SD	Pb (ppm)	SD	Cr (ppm)	SD
0.5	8.33	0.97	0.19	0.03	69.29	7.00	17.69	1.96
1.5	5.77	0.11	0.26	0.03	68.17	1.37	17.03	0.25
2.5	5.33	1.03	0.21	0.06	44.08	4.45	14.22	1.50
3.5	6.13	0.87	0.19	0.05	48.12	7.04	14.06	1.71
4.5	4.41	0.08	0.19	0.04	50.79	2.35	13.54	0.25
5.5	6.68	0.60	0.29	0.10	88.68	6.63	20.01	1.52
6.5	6.66	1.01	0.22	0.03	79.77	2.57	19.93	1.00
7.5	6.33	0.41	0.36	0.08	74.59	8.73	20.37	1.58
8.5	3.38	0.36	0.17	0.06	39.36	2.61	11.31	0.61
9.5	3.13	0.18	0.10	0.02	24.66	2.15	12.54	0.57

ER2: AVS Phase

	Fe 238.863 nm		Ca 315.887 nm		Mn 293.305 nm	
	Det. Limit (ppm)		Det. Limit (ppm)		Det. Limit (ppm)	
	0.63		**0.19**		**0.09**	
Depth (cm)	Fe (ppm)	SD	Ca (ppm)	SD	Mn (ppm)	SD
0.5	921.46	88.77	659.44	83.51	11.20	1.18
1.5	793.88	75.17	2370.59	207.00	9.83	0.92
2.5	1930.87	308.41	279.07	97.22	25.93	4.22
3.5	1543.48	218.89	201.36	124.46	19.46	2.53
4.5	1153.54	50.08	107.65	25.05	13.91	0.58
5.5	1451.45	131.28	165.34	31.38	17.74	1.40
6.5	1261.04	188.64	260.25	127.14	15.46	2.28
7.5	1616.05	274.47	326.79	169.92	20.63	3.38
8.5	870.21	181.22	720.35	281.56	11.75	2.70
9.5	1263.13	126.82	157.80	46.82	17.48	1.66

	As 188.979 nm		Cd 228.802 nm		Pb 220.353 nm		Cr 205.560 nm	
	Det. Limit (ppm)		Det. Limit (ppm)		Det. Limit (ppm)		Det. Limit (ppm)	
	0.05		**0.02**		**0.02**		**0.02**	
Depth (cm)	As (ppm)	SD	Cd (ppm)	SD	Pb (ppm)	SD	Cr (ppm)	SD
0.5	0.12	0.04	0.00	0.00	0.40	0.10	1.21	0.13
1.5	0.20	0.04	0.00	0.00	0.19	0.11	0.95	0.09
2.5	0.20	0.11	0.00	0.00	0.48	0.07	2.09	0.32
3.5	0.24	0.06	0.00	0.00	2.49	2.53	1.80	0.23
4.5	0.19	0.07	0.00	0.00	0.57	0.08	1.43	0.05
5.5	0.17	0.18	0.00	0.00	0.67	0.18	1.85	0.12
6.5	0.00	0.00	0.00	0.00	0.57	0.14	1.58	0.24
7.5	0.07	0.02	0.00	0.00	0.58	0.15	1.89	0.28
8.5	0.09	0.02	0.03	0.03	0.31	0.09	1.02	0.19
9.5	0.13	0.06	0.00	0.00	0.21	0.10	1.26	0.10

ER2: Org#1 Phase

	Fe 238.863 nm		Ca 315.887 nm		Mn 293.305 nm	
	Det. Limit (ppm)		Det. Limit (ppm)		Det. Limit (ppm)	
	0.41		**0.08**		**0.04**	
Depth (cm)	Fe (ppm)	SD	Ca (ppm)	SD	Mn (ppm)	SD
0.5	269.07	36.27	0.00	0.00	0.22	0.02
1.5	230.74	39.58	0.00	0.00	0.06	0.02
2.5	190.27	30.32	0.00	0.00	0.17	0.06
3.5	197.70	17.56	0.00	0.00	0.13	0.03
4.5	188.12	18.85	0.00	0.00	0.15	0.02
5.5	309.79	17.63	0.00	0.00	0.23	0.03
6.5	308.78	32.86	0.00	0.00	0.18	0.04
7.5	242.92	16.39	0.00	0.00	0.24	0.02
8.5	125.10	8.53	0.00	0.00	0.11	0.02
9.5	195.62	25.83	0.00	0.00	0.13	0.04

	As 197.197 nm		Cd 228.802 nm		Pb 220.353 nm		Cr 267.716 nm	
	Det. Limit (ppm)		Det. Limit (ppm)		Det. Limit (ppm)		Det. Limit (ppm)	
	0.35		**0**		**0.1**		**0.01**	
Depth (cm)	As (ppm)	SD	Cd (ppm)	SD	Pb (ppm)	SD	Cr (ppm)	SD
0.5	2.40	0.15	0.33	0.02	0.00	0.00	1.29	0.07
1.5	1.61	0.41	0.29	0.01	0.00	0.00	1.15	0.02
2.5	2.27	0.62	0.29	0.02	0.00	0.00	1.73	0.18
3.5	0.86	0.11	0.26	0.01	0.00	0.00	1.54	0.15
4.5	1.61	0.29	0.24	0.00	0.00	0.00	1.30	0.06
5.5	2.88	0.14	0.35	0.00	0.00	0.00	1.41	0.04
6.5	2.27	0.33	0.35	0.03	0.00	0.00	1.26	0.07
7.5	1.99	0.14	0.37	0.03	0.00	0.00	1.26	0.08
8.5	1.33	0.22	0.19	0.02	0.00	0.00	0.68	0.08
9.5	1.15	0.08	0.23	0.00	0.00	0.00	0.96	0.10

ER2: Org#2 Phase

	Fe 253.681 nm		Ca 315.887 nm		Mn 293.305 nm	
	Det. Limit (ppm)		Det. Limit (ppm)		Det. Limit (ppm)	
	1.41		**0.70**		**0.03**	
Depth (cm)	Fe (ppm)	SD	Ca (ppm)	SD	Mn (ppm)	SD
0.5	13366.41	1362.01	536.43	71.98	122.28	11.56
1.5	14553.51	683.99	568.34	31.60	132.56	6.55
2.5	19614.91	2217.83	733.30	100.41	179.79	18.62
3.5	11776.95	920.65	509.89	24.38	104.90	3.96
4.5	12490.47	641.08	487.88	31.26	111.61	4.76
5.5	17529.77	710.55	599.54	46.53	153.16	6.88
6.5	16306.43	1035.60	617.48	40.99	149.45	8.18
7.5	19388.16	2050.04	860.65	212.65	179.74	18.17
8.5	11542.30	1635.69	861.35	419.69	115.12	15.83
9.5	16500.76	1611.73	580.08	72.10	161.88	13.94

	As 188.979 nm		Cd 228.802 nm		Pb 220.353 nm		Cr 205.560 nm	
	Det. Limit (ppm)		Det. Limit (ppm)		Det. Limit (ppm)		Det. Limit (ppm)	
	0.11		**0.01**		**0.01**		**0.03**	
Depth (cm)	As (ppm)	SD	Cd (ppm)	SD	Pb (ppm)	SD	Cr (ppm)	SD
0.5	1.37	0.77	0.03	0.02	4.00	0.52	28.92	2.94
1.5	1.09	0.15	0.01	0.01	5.99	0.43	30.67	1.39
2.5	1.23	0.31	0.00	0.00	6.23	0.69	38.51	4.11
3.5	0.74	0.42	0.02	0.02	3.04	0.47	23.25	1.56
4.5	0.40	0.32	0.02	0.02	4.70	0.83	26.40	1.24
5.5	2.14	0.44	0.00	0.00	7.57	1.84	36.80	1.68
6.5	1.65	0.17	0.00	0.00	6.27	0.65	34.72	2.40
7.5	1.71	0.67	0.00	0.00	7.79	1.48	40.52	4.30
8.5	1.05	0.54	0.00	0.00	4.28	0.76	22.64	2.76
9.5	0.62	0.14	0.00	0.00	5.50	0.38	31.76	2.84

ER2: Pyrite Phase

	Fe 238.863 nm		Ca 315.887 nm		Mn 293.305 nm	
	Det. Limit (ppm)		Det. Limit (ppm)		Det. Limit (ppm)	
	1.06		**0.87**		**0.06**	
Depth (cm)	Fe (ppm)	SD	Ca (ppm)	SD	Mn (ppm)	SD
0.5	7255.53	578.72	4.90	1.81	32.53	2.45
1.5	8504.72	212.88	5.87	1.88	39.59	0.69
2.5	13611.07	1433.32	7.63	0.52	103.26	12.43
3.5	10442.48	1022.96	8.08	4.73	63.38	5.64
4.5	8161.15	362.54	2.94	0.49	40.91	3.64
5.5	11120.07	523.19	10.72	15.88	46.85	2.36
6.5	10725.67	533.12	20.96	22.87	43.49	2.45
7.5	12532.68	1268.94	1.09	1.43	58.61	7.09
8.5	8272.34	1244.80	4.04	0.82	36.98	6.82
9.5	11210.32	1043.02	7.82	3.65	66.60	7.75

	As 188.979 nm		Cd 228.802 nm		Pb 220.353 nm		Cr 205.560 nm	
	Det. Limit (ppm)		Det. Limit (ppm)		Det. Limit (ppm)		Det. Limit (ppm)	
	0.31		**0.01**		**0.00**		**0.01**	
Depth (cm)	As (ppm)	SD	Cd (ppm)	SD	Pb (ppm)	SD	Cr (ppm)	SD
0.5	1.93	0.18	0.00	0.00	0.49	0.04	0.16	0.03
1.5	2.50	0.09	0.00	0.00	0.52	0.32	0.12	0.02
2.5	5.02	0.62	0.00	0.00	4.17	0.59	0.22	0.06
3.5	3.66	0.35	0.00	0.00	2.27	0.25	0.16	0.07
4.5	2.61	0.21	0.00	0.00	1.33	0.48	0.10	0.01
5.5	3.56	0.37	0.00	0.00	1.44	0.40	0.20	0.04
6.5	3.48	0.20	0.00	0.00	1.02	0.14	0.17	0.04
7.5	4.10	0.58	0.00	0.00	2.43	0.37	0.13	0.02
8.5	2.94	0.40	0.00	0.00	1.41	0.46	0.09	0.03
9.5	3.84	0.47	0.00	0.00	3.78	0.63	0.13	0.05

BH1: Exchangeable Phase

	Fe 238.863 nm		Ca 315.887 nm		Mn 293.305 nm	
	Det. Limit (ppm)		Det. Limit (ppm)		Det. Limit (ppm)	
	0.32		**0.17**		**0.37**	
Depth (cm)	Fe (ppm)	SD	Ca (ppm)	SD	Mn (ppm)	SD
0.5	0.00	0.00	2138.55	123.03	163.40	26.29
1.5	0.00	0.00	1797.53	570.63	80.92	16.81
2.5	0.00	0.00	2476.89	240.92	65.98	41.61
3.5	0.00	0.00	1166.14	254.11	122.60	35.95
4.5	0.00	0.00	955.03	78.75	205.66	22.41
5.5	0.00	0.00	981.66	34.28	163.31	11.58
6.5	0.00	0.00	904.91	111.73	176.82	16.97
7.5	0.00	0.00	869.59	140.67	162.12	48.55
8.5	0.00	0.00	889.09	58.39	162.94	40.91
9.5	0.00	0.00	1219.05	56.25	203.95	5.16

	As 188.979 nm		Cd 228.802 nm		Pb 220.353 nm		Cr 205.560 nm	
	Det. Limit (ppm)		Det. Limit (ppm)		Det. Limit (ppm)		Det. Limit (ppm)	
	0.44		**0.03**		**0.14**		**0.02**	
Depth (cm)	As (ppm)	SD	Cd (ppm)	SD	Pb (ppm)	SD	Cr (ppm)	SD
0.5	0.00	0.00	0.26	0.02	0.00	0.00	0.00	0.00
1.5	0.00	0.00	0.16	0.05	0.00	0.00	0.00	0.00
2.5	0.00	0.00	0.26	0.04	0.00	0.00	0.00	0.00
3.5	0.00	0.00	0.00	0.00	0.00	0.00	0.00	0.00
4.5	0.00	0.00	0.09	0.03	0.00	0.00	0.00	0.00
5.5	0.00	0.00	0.09	0.02	0.00	0.00	0.00	0.00
6.5	0.00	0.00	0.10	0.03	0.00	0.00	0.00	0.00
7.5	0.00	0.00	0.08	0.03	0.00	0.00	0.00	0.00
8.5	0.00	0.00	0.16	0.11	0.00	0.00	0.00	0.00
9.5	0.00	0.00	0.00	0.00	0.00	0.00	0.00	0.00

BH1: Oxide Phase

	Fe 253.681 nm		Ca 315.887 nm		Mn 293.305 nm	
	Det. Limit (ppm)		Det. Limit (ppm)		Det. Limit (ppm)	
	0.69		**0.28**		**0.01**	
Depth (cm)	Fe (ppm)	SD	Ca (ppm)	SD	Mn (ppm)	SD
0.5	48808.33	1077.20	900.25	132.47	1483.98	73.57
1.5	29197.99	230.92	604.14	296.05	939.90	14.38
2.5	35979.83	2862.26	999.46	305.09	1355.18	90.32
3.5	21120.33	1629.76	540.58	191.36	514.52	38.38
4.5	32911.00	1700.53	852.42	96.92	806.44	64.34
5.5	28076.93	1626.82	904.98	108.26	724.84	47.62
6.5	28355.02	1008.10	770.06	140.64	745.83	53.85
7.5	23064.47	689.25	866.54	72.52	643.58	12.04
8.5	21776.48	2778.83	587.37	55.07	700.40	63.96
9.5	50491.89	3209.57	1784.39	282.10	1394.38	80.98

	As 188.979 nm		Cd 228.802 nm		Pb 220.353 nm		Cr 205.560 nm	
	Det. Limit (ppm)		Det. Limit (ppm)		Det. Limit (ppm)		Det. Limit (ppm)	
	0.22		**0.01**		**0.05**		**0.03**	
Depth (cm)	As (ppm)	SD	Cd (ppm)	SD	Pb (ppm)	SD	Cr (ppm)	SD
0.5	34.93	1.09	0.53	0.04	194.40	65.07	232.77	6.72
1.5	22.21	0.34	0.33	0.01	85.20	2.34	138.27	1.73
2.5	24.13	2.03	0.43	0.02	116.49	10.92	168.28	12.82
3.5	15.48	0.78	0.31	0.03	57.68	5.22	99.21	7.87
4.5	22.03	1.68	0.76	0.04	116.88	9.47	153.17	8.16
5.5	18.01	1.69	0.68	0.04	99.73	5.01	116.93	7.05
6.5	18.39	0.94	0.75	0.02	96.59	6.36	108.78	8.35
7.5	16.17	0.74	0.66	0.05	93.22	8.64	81.04	1.20
8.5	15.30	1.83	0.45	0.16	73.52	11.25	75.03	9.90
9.5	35.03	2.30	1.24	0.12	174.39	15.22	161.57	9.35

BH1: AVS Phase

	Fe 238.863 nm		Ca 315.887 nm		Mn 293.305 nm	
	Det. Limit (ppm)		Det. Limit (ppm)		Det. Limit (ppm)	
	0.63		**0.19**		**0.09**	
Depth (cm)	Fe (ppm)	SD	Ca (ppm)	SD	Mn (ppm)	SD
0.5	4265.99	1131.36	387.64	272.42	86.94	16.50
1.5	2764.75	381.70	9390.75	11427.67	57.19	5.17
2.5	6305.54	1394.77	4445.27	3827.30	116.88	23.14
3.5	710.12	120.76	2120.83	358.54	8.79	1.49
4.5	5250.40	1159.16	1164.87	826.62	136.41	24.59
5.5	4091.51	497.76	1171.82	669.18	126.17	11.04
6.5	2820.38	478.65	610.57	354.13	101.38	13.56
7.5	2183.85	1158.42	703.67	663.06	71.94	43.87
8.5	2095.62	590.39	73.92	14.48	74.82	21.83
9.5	2498.16	410.56	3057.95	2000.57	96.48	15.40

	As 188.979 nm		Cd 228.802 nm		Pb 220.353 nm		Cr 205.560 nm	
	Det. Limit (ppm)		Det. Limit (ppm)		Det. Limit (ppm)		Det. Limit (ppm)	
	0.05		**0.02**		**0.02**		**0.02**	
Depth (cm)	As (ppm)	SD	Cd (ppm)	SD	Pb (ppm)	SD	Cr (ppm)	SD
0.5	3.16	1.26	0.03	0.01	0.00	0.00	21.51	5.95
1.5	2.21	0.38	0.00	0.00	0.00	0.00	14.54	2.52
2.5	4.76	0.75	0.03	0.00	0.00	0.00	28.10	3.90
3.5	0.24	0.05	0.00	0.00	0.16	0.08	0.85	0.14
4.5	3.43	1.02	0.07	0.01	0.00	0.00	23.31	6.53
5.5	2.31	0.45	0.05	0.01	0.00	0.00	13.71	2.15
6.5	1.35	0.20	0.05	0.01	0.00	0.00	7.36	1.56
7.5	1.01	0.68	0.03	0.02	0.14	0.12	4.86	3.31
8.5	0.89	0.24	0.03	0.02	0.00	0.00	3.95	1.24
9.5	1.13	0.24	0.05	0.01	0.20	0.12	5.54	1.37

BH1: Org#1 Phase

	Fe 238.863 nm		Ca 315.887 nm		Mn 293.305 nm	
	Det. Limit (ppm)		Det. Limit (ppm)		Det. Limit (ppm)	
	0.41		**0.08**		**0.04**	
Depth (cm)	Fe (ppm)	SD	Ca (ppm)	SD	Mn (ppm)	SD
0.5	166.47	7.00	137.39	168.91	0.92	0.13
1.5	116.68	1.18	18.91	17.62	0.65	0.15
2.5	133.15	9.95	20.50	20.80	0.51	0.09
3.5	86.97	13.42	0.00	0.00	0.39	0.12
4.5	246.66	30.01	2.91	2.41	0.61	0.02
5.5	286.23	40.85	5.28	2.32	0.35	0.08
6.5	357.12	14.47	2.76	1.64	0.36	0.04
7.5	279.19	27.26	1.44	1.24	0.36	0.02
8.5	258.31	87.45	0.00	0.00	0.39	0.15
9.5	321.33	27.36	9.72	6.00	0.43	0.10

	As 197.197 nm		Cd 228.802 nm		Pb 220.353 nm		Cr 267.716 nm	
	Det. Limit (ppm)		Det. Limit (ppm)		Det. Limit (ppm)		Det. Limit (ppm)	
	0.35		**0.00**		**0.10**		**0.01**	
Depth (cm)	As (ppm)	SD	Cd (ppm)	SD	Pb (ppm)	SD	Cr (ppm)	SD
0.5	13.73	1.15	0.52	0.04	0.00	0.00	2.38	0.11
1.5	7.08	1.41	0.30	0.02	0.00	0.00	1.30	0.34
2.5	12.07	1.57	0.41	0.03	0.00	0.00	1.20	0.31
3.5	3.42	0.55	0.19	0.02	0.00	0.00	0.72	0.16
4.5	7.11	1.64	0.26	0.02	0.00	0.00	1.04	0.29
5.5	4.89	0.71	0.26	0.05	0.00	0.00	0.76	0.17
6.5	4.09	0.81	0.26	0.02	0.00	0.00	1.02	0.06
7.5	3.12	0.54	0.25	0.01	0.00	0.00	1.04	0.00
8.5	2.13	1.01	0.20	0.05	0.00	0.00	0.88	0.29
9.5	3.28	0.97	0.22	0.00	0.00	0.00	0.79	0.39

BH1: Org#2 Phase

	Fe 253.681 nm		Ca 315.887 nm		Mn 293.305 nm	
	Det. Limit (ppm)		Det. Limit (ppm)		Det. Limit (ppm)	
	1.41		**0.70**		**0.03**	
Depth (cm)	Fe (ppm)	SD	Ca (ppm)	SD	Mn (ppm)	SD
0.5	30484.76	3771.39	216.88	58.22	241.27	25.79
1.5	19443.24	1745.40	33320.70	40527.10	157.92	13.17
2.5	30068.59	3726.71	61520.80	74549.34	239.41	21.29
3.5	12783.27	1808.61	53836.82	64560.14	106.70	11.03
4.5	28863.14	3096.11	1258.05	884.21	281.08	30.25
5.5	23966.66	1174.00	911.50	470.62	261.91	10.25
6.5	23127.55	1770.62	633.89	206.11	269.60	15.51
7.5	20142.11	516.36	410.01	15.31	238.79	4.57
8.5	16716.17	3453.45	340.25	54.99	208.09	35.20
9.5	17697.12	2072.75	3043.79	2100.78	210.55	22.41

	As 188.979 nm		Cd 228.802 nm		Pb 220.353 nm		Cr 205.560 nm	
	Det. Limit (ppm)		Det. Limit (ppm)		Det. Limit (ppm)		Det. Limit (ppm)	
	0.11		**0.01**		**0.01**		**0.03**	
Depth (cm)	As (ppm)	SD	Cd (ppm)	SD	Pb (ppm)	SD	Cr (ppm)	SD
0.5	2.73	0.75	0.03	0.03	9.17	0.94	60.42	9.73
1.5	3.43	0.22	0.04	0.03	6.09	0.33	41.70	4.09
2.5	4.18	0.75	0.02	0.02	9.32	0.88	66.26	8.07
3.5	1.03	0.74	0.00	0.00	3.86	0.54	24.70	3.40
4.5	3.15	0.08	0.00	0.00	10.53	1.15	63.57	7.70
5.5	2.53	0.19	0.00	0.00	9.69	0.27	51.30	2.63
6.5	2.36	0.63	0.07	0.01	9.83	0.73	48.68	3.63
7.5	2.09	0.44	0.00	0.00	8.88	0.46	42.68	1.76
8.5	1.82	0.71	0.06	0.01	7.59	1.74	34.12	8.04
9.5	2.19	0.66	0.08	0.01	8.31	1.37	38.16	4.74

BH1: Pyrite Phase

	Fe 238.863 nm		Ca 315.887 nm		Mn 293.305 nm	
	Det. Limit (ppm)		Det. Limit (ppm)		Det. Limit (ppm)	
	1.06		**0.87**		**0.06**	
Depth (cm)	Fe (ppm)	SD	Ca (ppm)	SD	Mn (ppm)	SD
0.5	2976.18	315.98	6.09	2.06	29.17	4.01
1.5	1800.54	83.06	5.71	7.94	18.62	0.89
2.5	2599.10	321.22	13.25	8.91	25.69	2.88
3.5	1605.50	176.93	7.88	8.22	20.45	2.46
4.5	7400.40	649.08	12.73	0.94	143.33	13.71
5.5	8534.70	404.24	11.84	1.70	176.58	10.72
6.5	9496.30	356.55	11.98	1.76	202.82	8.57
7.5	9489.65	239.00	9.59	1.24	203.63	5.72
8.5	8282.55	1427.88	9.93	0.90	166.85	32.37
9.5	9340.38	1075.26	9.72	0.35	199.89	24.63

	As 188.979 nm		Cd 228.802 nm		Pb 220.353 nm		Cr 205.560 nm	
	Det. Limit (ppm)		Det. Limit (ppm)		Det. Limit (ppm)		Det. Limit (ppm)	
	0.31		**0.01**		**0.00**		**0.01**	
Depth (cm)	As (ppm)	SD	Cd (ppm)	SD	Pb (ppm)	SD	Cr (ppm)	SD
0.5	1.34	0.14	0.00	0.00	0.00	0.00	0.22	0.05
1.5	0.84	0.04	0.00	0.00	0.00	0.00	0.16	0.03
2.5	1.49	0.24	0.00	0.00	0.00	0.00	0.23	0.14
3.5	1.01	0.18	0.00	0.00	0.00	0.00	0.07	0.01
4.5	6.69	0.60	0.07	0.01	0.93	0.15	0.30	0.08
5.5	8.25	0.39	0.08	0.00	1.26	0.15	0.25	0.04
6.5	9.43	0.53	0.09	0.01	1.50	0.10	0.18	0.02
7.5	9.93	0.33	0.09	0.01	1.69	0.09	0.21	0.04
8.5	8.01	1.53	0.08	0.02	1.22	0.41	0.15	0.05
9.5	10.13	1.32	0.09	0.01	1.95	0.37	0.20	0.04

BH2: Exchangeable Phase

	Fe 238.863 nm		Ca 315.887 nm		Mn 293.305 nm	
	Det. Limit (ppm)		Det. Limit (ppm)		Det. Limit (ppm)	
	0.32		**0.17**		**0.37**	
Depth (cm)	Fe (ppm)	SD	Ca (ppm)	SD	Mn (ppm)	SD
0.5	0.00	0.00	3199.78	2341.15	105.64	22.71
1.5	0.00	0.00	797.13	24.51	45.45	3.13
2.5	0.00	0.00	1087.70	98.24	73.61	28.19
3.5	0.00	0.00	1002.32	21.41	71.51	24.27
4.5	0.00	0.00	907.79	91.06	45.15	2.45
5.5	0.00	0.00	1037.92	27.15	59.75	1.20
6.5	0.00	0.00	1000.02	54.14	67.39	3.11
7.5	0.00	0.00	1009.69	28.37	85.08	18.95
8.5	0.00	0.00	921.77	32.07	79.86	17.19
9.5	0.00	0.00	952.62	17.37	75.85	0.46

	As 188.979 nm		Cd 228.802 nm		Pb 220.353 nm		Cr 205.560 nm	
	Det. Limit (ppm)		Det. Limit (ppm)		Det. Limit (ppm)		Det. Limit (ppm)	
	0.44		**0.03**		**0.14**		**0.02**	
Depth (cm)	As (ppm)	SD	Cd (ppm)	SD	Pb (ppm)	SD	Cr (ppm)	SD
0.5	0.00	0.00	0.06	0.03	0.00	0.00	0.00	0.00
1.5	0.00	0.00	0.00	0.00	0.00	0.00	0.00	0.00
2.5	0.00	0.00	0.04	0.03	0.00	0.00	0.00	0.00
3.5	0.00	0.00	0.04	0.03	0.00	0.00	0.00	0.00
4.5	0.00	0.00	0.04	0.01	0.00	0.00	0.00	0.00
5.5	0.00	0.00	0.03	0.01	0.00	0.00	0.00	0.00
6.5	0.00	0.00	0.02	0.00	0.00	0.00	0.00	0.00
7.5	0.00	0.00	0.05	0.03	0.00	0.00	0.00	0.00
8.5	0.00	0.00	0.03	0.03	0.00	0.00	0.00	0.00
9.5	0.00	0.00	0.01	0.00	0.00	0.00	0.00	0.00

BH2: Oxide Phase

	Fe 253.681 nm		Ca 315.887 nm		Mn 293.305 nm	
	Det. Limit (ppm)		Det. Limit (ppm)		Det. Limit (ppm)	
	0.69		**0.28**		**0.01**	
Depth (cm)	Fe (ppm)	SD	Ca (ppm)	SD	Mn (ppm)	SD
0.5	32792.63	3914.83	4571.39	2322.26	516.10	50.63
1.5	24979.63	2400.33	1571.43	129.37	258.62	26.60
2.5	33776.21	5958.96	2211.39	545.08	363.71	75.77
3.5	34978.22	1596.00	2091.78	111.73	401.39	24.08
4.5	14121.13	601.44	748.78	34.00	154.90	7.57
5.5	18150.59	498.18	923.65	30.36	245.65	8.22
6.5	18707.96	910.00	883.39	57.40	310.23	19.41
7.5	18562.55	906.01	971.32	43.70	378.09	18.18
8.5	15850.52	286.03	898.96	18.90	341.78	7.47
9.5	16551.12	521.61	1028.64	29.64	410.96	11.08

	As 188.979 nm		Cd 228.802 nm		Pb 220.353 nm		Cr 205.560 nm	
	Det. Limit (ppm)		Det. Limit (ppm)		Det. Limit (ppm)		Det. Limit (ppm)	
	0.22		**0.01**		**0.05**		**0.03**	
Depth (cm)	As (ppm)	SD	Cd (ppm)	SD	Pb (ppm)	SD	Cr (ppm)	SD
0.5	15.84	2.37	1.83	0.24	151.86	23.15	131.87	18.19
1.5	12.19	1.34	1.50	0.17	139.94	15.72	128.44	13.67
2.5	16.76	2.05	2.21	0.40	222.78	46.55	199.62	38.15
3.5	16.67	0.95	2.37	0.15	231.46	16.34	216.29	12.30
4.5	6.14	0.43	0.79	0.03	78.86	4.31	75.66	3.65
5.5	8.07	0.31	1.06	0.02	102.89	2.53	100.98	2.73
6.5	6.83	0.27	0.94	0.05	88.41	5.54	77.55	4.27
7.5	6.49	0.25	0.80	0.03	86.24	4.16	65.06	3.30
8.5	5.73	0.29	0.70	0.03	78.85	1.54	51.91	0.88
9.5	4.88	0.49	0.76	0.01	83.51	1.93	49.67	1.45

BH2: AVS Phase

	Fe 238.863 nm		Ca 315.887 nm		Mn 293.305 nm	
	Det. Limit (ppm)		Det. Limit (ppm)		Det. Limit (ppm)	
	0.63		**0.19**		**0.09**	
Depth (cm)	Fe (ppm)	SD	Ca (ppm)	SD	Mn (ppm)	SD
0.5	1099.37	117.05	27649.02	32776.60	18.90	1.29
1.5	891.32	147.76	269.32	70.33	12.60	1.87
2.5	1268.55	461.18	994.45	665.07	16.50	5.75
3.5	1387.49	49.73	267.61	9.58	18.67	0.42
4.5	739.57	111.18	148.43	16.68	10.30	1.35
5.5	880.26	56.71	675.12	213.62	12.78	0.77
6.5	963.03	83.12	160.61	21.57	13.85	1.13
7.5	929.57	189.25	879.23	699.47	13.04	3.24
8.5	922.77	17.31	193.50	17.42	13.36	0.30
9.5	782.52	15.85	185.58	4.02	11.77	0.28

	As 188.979 nm		Cd 228.802 nm		Pb 220.353 nm		Cr 205.560 nm	
	Det. Limit (ppm)		Det. Limit (ppm)		Det. Limit (ppm)		Det. Limit (ppm)	
	0.05		**0.02**		**0.02**		**0.02**	
Depth (cm)	As (ppm)	SD	Cd (ppm)	SD	Pb (ppm)	SD	Cr (ppm)	SD
0.5	0.51	0.07	0.03	0.02	0.50	0.17	3.03	0.47
1.5	0.43	0.03	0.04	0.00	0.52	0.12	2.80	0.62
2.5	0.78	0.42	0.05	0.04	1.08	0.65	4.63	2.65
3.5	0.90	0.05	0.08	0.01	1.39	0.09	5.70	0.34
4.5	0.37	0.07	0.03	0.00	0.35	0.07	2.42	0.48
5.5	0.56	0.12	0.05	0.01	0.51	0.08	2.88	0.38
6.5	0.46	0.14	0.04	0.00	0.41	0.04	2.53	0.22
7.5	0.30	0.09	0.02	0.02	0.37	0.19	2.02	0.81
8.5	0.37	0.03	0.02	0.00	0.34	0.03	2.19	0.06
9.5	0.36	0.10	0.00	0.00	0.26	0.02	1.83	0.12

BH2: Org#1 Phase

	Fe 238.863 nm		Ca 315.887 nm		Mn 293.305 nm	
	Det. Limit (ppm)		Det. Limit (ppm)		Det. Limit (ppm)	
	0.41		**0.08**		**0.04**	
Depth (cm)	Fe (ppm)	SD	Ca (ppm)	SD	Mn (ppm)	SD
0.5	174.52	44.41	0.00	0.00	0.00	0.00
1.5	159.80	19.41	0.00	0.00	0.00	0.00
2.5	186.81	13.74	0.00	0.00	0.00	0.00
3.5	206.19	48.97	0.00	0.00	0.00	0.00
4.5	124.62	7.35	0.00	0.00	0.00	0.00
5.5	173.76	10.91	0.00	0.00	0.00	0.00
6.5	154.92	10.90	0.00	0.00	0.00	0.00
7.5	176.96	9.01	0.00	0.00	0.00	0.00
8.5	144.20	4.07	0.00	0.00	0.00	0.00
9.5	137.77	10.16	0.00	0.00	0.00	0.00

	As 197.197 nm		Cd 228.802 nm		Pb 220.353 nm		Cr 267.716 nm	
	Det. Limit (ppm)		Det. Limit (ppm)		Det. Limit (ppm)		Det. Limit (ppm)	
	0.35		**0.00**		**0.10**		**0.01**	
Depth (cm)	As (ppm)	SD	Cd (ppm)	SD	Pb (ppm)	SD	Cr (ppm)	SD
0.5	2.78	0.69	0.23	0.01	0.00	0.00	2.00	0.55
1.5	1.83	0.36	0.19	0.01	0.00	0.00	1.85	0.23
2.5	2.57	0.67	0.20	0.01	0.00	0.00	1.87	0.25
3.5	2.63	0.23	0.21	0.02	0.00	0.00	2.02	0.11
4.5	1.59	0.16	0.16	0.02	0.00	0.00	1.82	0.18
5.5	2.04	0.32	0.22	0.00	0.00	0.00	2.04	0.09
6.5	1.86	0.42	0.21	0.04	0.00	0.00	1.83	0.17
7.5	1.78	0.21	0.19	0.02	0.00	0.00	1.91	0.18
8.5	0.80	0.42	0.18	0.01	0.00	0.00	1.59	0.04
9.5	1.57	0.41	0.18	0.02	0.00	0.00	1.77	0.10

BH2: Org#2 Phase

	Fe 253.681 nm		Ca 315.887 nm		Mn 293.305 nm	
	Det. Limit (ppm)		Det. Limit (ppm)		Det. Limit (ppm)	
	1.41		**0.70**		**0.03**	
Depth (cm)	Fe (ppm)	SD	Ca (ppm)	SD	Mn (ppm)	SD
0.5	19015.35	3330.88	41372.31	49139.71	202.74	32.21
1.5	15209.72	2579.23	748.31	110.76	153.37	23.06
2.5	22481.14	8054.92	1021.05	442.56	201.92	66.49
3.5	23278.88	2869.53	874.94	82.90	206.17	22.18
4.5	14290.93	1037.49	543.53	19.01	135.24	6.15
5.5	17726.27	865.20	694.46	42.28	172.11	7.21
6.5	18866.94	1533.50	727.93	51.66	189.20	13.80
7.5	20248.97	1356.29	747.72	49.11	200.66	13.50
8.5	17607.34	504.12	681.85	16.24	173.50	4.02
9.5	19748.73	552.42	864.44	41.40	198.19	7.35

	As 188.979 nm		Cd 228.802 nm		Pb 220.353 nm		Cr 205.560 nm	
	Det. Limit (ppm)		Det. Limit (ppm)		Det. Limit (ppm)		Det. Limit (ppm)	
	0.11		**0.01**		**0.01**		**0.03**	
Depth (cm)	As (ppm)	SD	Cd (ppm)	SD	Pb (ppm)	SD	Cr (ppm)	SD
0.5	0.59	0.06	0.07	0.02	5.77	0.67	46.65	7.61
1.5	0.79	0.51	0.05	0.03	5.40	1.14	40.23	7.28
2.5	2.04	0.70	0.07	0.04	10.97	5.25	62.95	22.67
3.5	1.58	0.27	0.06	0.02	11.05	1.53	64.84	7.65
4.5	1.60	0.14	0.08	0.05	6.43	0.80	40.11	3.19
5.5	1.43	0.39	0.00	0.00	8.45	0.73	51.34	2.54
6.5	1.79	0.18	0.00	0.00	7.75	0.87	53.66	4.42
7.5	1.95	0.41	0.00	0.00	8.07	0.61	56.29	3.92
8.5	2.16	0.52	0.00	0.00	6.61	0.45	49.09	1.58
9.5	1.66	0.32	0.00	0.00	7.17	0.28	55.51	1.58

BH2: Pyrite Phase

	Fe 238.863 nm		Ca 315.887 nm		Mn 293.305 nm	
	Det. Limit (ppm)		Det. Limit (ppm)		Det. Limit (ppm)	
	1.06		**0.87**		**0.06**	
Depth (cm)	Fe (ppm)	SD	Ca (ppm)	SD	Mn (ppm)	SD
0.5	2106.60	353.31	57.81	20.14	7.12	0.66
1.5	2410.36	466.04	13.22	1.84	5.39	1.06
2.5	4545.79	1585.24	21.75	5.33	9.18	3.21
3.5	5267.33	638.80	17.77	3.31	9.89	1.41
4.5	3861.95	243.42	14.62	1.99	6.67	0.57
5.5	5817.78	225.88	18.57	5.91	7.94	0.27
6.5	5371.62	378.17	14.07	1.30	5.43	0.38
7.5	5777.46	367.95	18.88	4.24	4.81	0.37
8.5	5683.99	125.42	14.66	1.37	3.64	0.07
9.5	6556.64	194.32	17.63	1.41	3.35	0.04

	As 188.979 nm		Cd 228.802 nm		Pb 220.353 nm		Cr 205.560 nm	
	Det. Limit (ppm)		Det. Limit (ppm)		Det. Limit (ppm)		Det. Limit (ppm)	
	0.31		**0.01**		**0.00**		**0.01**	
Depth (cm)	As (ppm)	SD	Cd (ppm)	SD	Pb (ppm)	SD	Cr (ppm)	SD
0.5	1.44	0.17	0.03	0.01	0.00	0.00	1.04	0.41
1.5	2.32	0.60	0.03	0.01	0.00	0.00	0.24	0.05
2.5	5.12	2.03	0.05	0.02	0.00	0.00	0.53	0.15
3.5	5.70	0.89	0.06	0.01	0.00	0.00	0.44	0.10
4.5	3.80	0.21	0.04	0.01	0.00	0.00	0.38	0.07
5.5	5.62	0.22	0.06	0.00	0.00	0.00	0.48	0.11
6.5	4.75	0.43	0.05	0.00	0.00	0.00	0.39	0.02
7.5	4.55	0.47	0.04	0.00	0.00	0.00	0.50	0.11
8.5	3.42	0.09	0.03	0.00	0.00	0.00	0.39	0.02
9.5	2.80	0.04	0.02	0.00	0.00	0.00	0.41	0.03

MI1: Exchangeable Phase

	Fe 238.863 nm		Ca 315.887 nm		Mn 293.305 nm	
	Det. Limit (ppm)		Det. Limit (ppm)		Det. Limit (ppm)	
	0.68		**1.17**		**1.18**	
Depth (cm)	Fe (ppm)	SD	Ca (ppm)	SD	Mn (ppm)	SD
0.5	0.00	0.00	1884.35	244.67	77.49	4.06
1.5	0.00	0.00	1201.95	84.77	82.64	0.52
2.5	0.00	0.00	1050.07	50.34	107.20	2.03
3.5	0.00	0.00	1381.20	207.31	121.95	3.16
4.5	0.00	0.00	1318.95	52.17	132.38	1.80
5.5	0.00	0.00	1249.88	49.22	114.22	3.12
6.5	0.00	0.00	1222.15	31.04	95.82	1.84
7.5	0.00	0.00	1174.80	184.10	97.29	2.46
8.5	0.00	0.00	1102.71	146.31	86.37	7.68
9.5	0.00	0.00	1096.28	14.58	52.54	6.23

	As 188.979 nm		Cd 228.802 nm		Pb 220.353 nm		Cr 205.560 nm	
	Det. Limit (ppm)		Det. Limit (ppm)		Det. Limit (ppm)		Det. Limit (ppm)	
	0.40		**0.03**		**0.17**		**0.03**	
Depth (cm)	As (ppm)	SD	Cd (ppm)	SD	Pb (ppm)	SD	Cr (ppm)	SD
0.5	0.00	0.00	0.00	0.00	0.00	0.00	0.00	0.00
1.5	0.00	0.00	0.00	0.00	0.00	0.00	0.00	0.00
2.5	0.00	0.00	0.00	0.00	0.00	0.00	0.00	0.00
3.5	0.00	0.00	0.00	0.00	0.00	0.00	0.00	0.00
4.5	0.00	0.00	0.00	0.00	0.00	0.00	0.00	0.00
5.5	0.00	0.00	0.00	0.00	0.00	0.00	0.00	0.00
6.5	0.00	0.00	0.00	0.00	0.00	0.00	0.00	0.00
7.5	0.00	0.00	0.00	0.00	0.00	0.00	0.00	0.00
8.5	0.00	0.00	0.00	0.00	0.00	0.00	0.00	0.00
9.5	0.00	0.00	0.05	0.02	0.00	0.00	0.00	0.00

MI1: Oxide Phase

	Fe 253.681 nm		Ca 315.887 nm		Mn 293.305 nm	
	Det. Limit (ppm)		Det. Limit (ppm)		Det. Limit (ppm)	
	3.03		**0.69**		**0.08**	
Depth (cm)	Fe (ppm)	SD	Ca (ppm)	SD	Mn (ppm)	SD
0.5	14163.43	375.24	1331.46	212.63	372.23	90.99
1.5	13848.31	207.58	893.99	133.48	334.35	21.28
2.5	13387.89	369.95	743.60	3.66	249.19	2.44
3.5	18294.82	471.06	1091.73	44.76	348.21	10.75
4.5	20318.17	613.72	970.83	26.71	368.48	12.23
5.5	20515.18	956.01	984.43	72.68	344.01	29.50
6.5	19853.71	323.43	910.02	20.65	336.10	2.07
7.5	20294.16	340.42	1047.39	6.45	451.23	7.33
8.5	17657.75	404.52	985.25	25.92	439.32	17.64
9.5	13809.35	295.56	986.14	18.03	440.63	4.97

	As 188.979 nm		Cd 228.802 nm		Pb 220.353 nm		Cr 205.560 nm	
	Det. Limit (ppm)		Det. Limit (ppm)		Det. Limit (ppm)		Det. Limit (ppm)	
	0.40		**0.05**		**1.59**		**0.13**	
Depth (cm)	As (ppm)	SD	Cd (ppm)	SD	Pb (ppm)	SD	Cr (ppm)	SD
0.5	5.78	0.32	0.38	0.02	69.53	47.65	27.80	1.12
1.5	4.82	0.28	0.25	0.01	25.43	1.89	26.52	0.48
2.5	5.31	0.34	0.32	0.02	30.02	9.92	26.82	0.61
3.5	8.11	0.49	0.46	0.03	29.14	1.13	34.09	1.01
4.5	7.44	0.38	0.41	0.01	27.89	1.58	37.30	1.25
5.5	7.65	0.78	0.45	0.06	28.36	1.70	37.35	1.98
6.5	8.48	0.54	0.47	0.01	37.33	2.58	37.17	0.66
7.5	9.32	0.20	0.51	0.01	39.02	1.45	37.59	1.17
8.5	9.40	0.38	0.50	0.02	39.51	0.87	33.74	0.97
9.5	8.55	0.29	0.41	0.02	34.57	0.45	26.83	0.66

MI1: AVS Phase

	Fe 238.863 nm		Ca 315.887 nm		Mn 293.305 nm	
	Det. Limit (ppm)		Det. Limit (ppm)		Det. Limit (ppm)	
	2.06		**0.15**		**0.05**	
Depth (cm)	Fe (ppm)	SD	Ca (ppm)	SD	Mn (ppm)	SD
0.5	1894.20	276.80	20748.92	11041.26	60.23	48.13
1.5	1648.25	77.04	1819.95	1287.50	19.49	5.14
2.5	1385.79	473.80	1013.67	590.27	13.28	3.47
3.5	2114.53	81.73	465.73	98.18	19.12	0.72
4.5	2194.15	78.59	259.97	19.56	20.64	0.58
5.5	2284.46	252.25	639.10	243.32	22.98	2.97
6.5	2202.03	61.20	276.19	15.58	21.03	0.63
7.5	1807.21	773.72	832.31	533.92	17.93	6.82
8.5	2310.83	56.55	351.64	41.18	22.10	0.39
9.5	2000.13	162.97	313.78	60.06	18.77	1.29

	As 188.979 nm		Cd 228.802 nm		Pb 220.353 nm		Cr 205.560 nm	
	Det. Limit (ppm)		Det. Limit (ppm)		Det. Limit (ppm)		Det. Limit (ppm)	
	0.20		**0.01**		**0.21**		**0.05**	
Depth (cm)	As (ppm)	SD	Cd (ppm)	SD	Pb (ppm)	SD	Cr (ppm)	SD
0.5	0.37	0.14	0.02	0.00	0.22	0.27	2.84	0.66
1.5	0.30	0.04	0.02	0.00	0.00	0.00	2.41	0.10
2.5	0.35	0.09	0.02	0.02	0.13	0.05	2.11	0.84
3.5	0.54	0.04	0.06	0.00	0.41	0.07	3.42	0.15
4.5	0.48	0.08	0.07	0.00	0.52	0.09	3.58	0.15
5.5	0.53	0.06	0.06	0.01	0.85	0.04	3.76	0.51
6.5	0.47	0.07	0.07	0.01	0.84	0.24	3.61	0.18
7.5	0.46	0.18	0.05	0.04	0.75	0.47	2.93	1.39
8.5	0.61	0.13	0.08	0.01	0.59	0.05	3.73	0.13
9.5	0.48	0.05	0.03	0.01	0.35	0.04	3.24	0.34

MI1: Org#1 Phase

	Fe 238.863 nm		Ca 315.887 nm		Mn 293.305 nm	
	Det. Limit (ppm)		Det. Limit (ppm)		Det. Limit (ppm)	
	3.39		**0.30**		**0.26**	
Depth (cm)	Fe (ppm)	SD	Ca (ppm)	SD	Mn (ppm)	SD
0.5	261.29	40.83	0.00	0.00	0.00	0.00
1.5	217.03	6.01	0.00	0.00	0.00	0.00
2.5	205.81	27.16	0.00	0.00	0.00	0.00
3.5	216.70	44.93	0.00	0.00	0.00	0.00
4.5	245.65	8.11	0.00	0.00	0.00	0.00
5.5	278.60	20.03	0.00	0.00	0.00	0.00
6.5	262.71	15.02	0.00	0.00	0.00	0.00
7.5	258.68	8.74	0.00	0.00	0.00	0.00
8.5	245.70	13.26	0.00	0.00	0.00	0.00
9.5	225.83	4.61	0.00	0.00	0.00	0.00

	As 197.197 nm		Cd 228.802 nm		Pb 220.353 nm		Cr 267.716 nm	
	Det. Limit (ppm)		Det. Limit (ppm)		Det. Limit (ppm)		Det. Limit (ppm)	
	1.19		**0.06**		**0.91**		**0.15**	
Depth (cm)	As (ppm)	SD	Cd (ppm)	SD	Pb (ppm)	SD	Cr (ppm)	SD
0.5	1.77	0.48	0.21	0.03	0.00	0.00	0.24	0.06
1.5	1.79	0.34	0.21	0.03	0.00	0.00	0.47	0.22
2.5	2.03	0.33	0.24	0.01	0.00	0.00	0.76	0.14
3.5	2.91	0.44	0.28	0.01	0.00	0.00	0.72	0.03
4.5	2.73	0.62	0.32	0.01	0.00	0.00	0.98	0.10
5.5	3.12	0.19	0.27	0.01	0.00	0.00	0.68	0.08
6.5	3.16	0.32	0.29	0.03	0.00	0.00	0.85	0.13
7.5	3.89	0.40	0.31	0.01	0.00	0.00	0.97	0.07
8.5	2.98	0.13	0.30	0.01	0.00	0.00	0.99	0.08
9.5	2.45	0.58	0.27	0.00	0.00	0.00	0.68	0.14

MI1: Org#2 Phase

	Fe 253.681 nm		Ca 315.887 nm		Mn 293.305 nm	
	Det. Limit (ppm)		Det. Limit (ppm)		Det. Limit (ppm)	
	11.18		**3.94**		**0.41**	
Depth (cm)	Fe (ppm)	SD	Ca (ppm)	SD	Mn (ppm)	SD
0.5	24725.25	1611.31	14930.54	11055.00	294.62	67.74
1.5	24992.05	817.85	8901.92	7223.91	227.34	6.62
2.5	21614.60	184.45	2386.78	48.02	196.58	2.86
3.5	25902.19	460.37	2831.35	88.52	235.87	4.09
4.5	25058.20	968.35	2716.54	83.18	231.62	9.03
5.5	23237.26	1472.78	3408.66	752.98	221.93	13.30
6.5	23988.33	1044.20	2715.49	61.62	222.58	6.58
7.5	25514.45	679.87	2995.36	69.35	238.58	5.02
8.5	24336.42	847.44	2718.64	79.55	223.62	7.89
9.5	22139.64	328.84	2467.87	31.20	193.19	3.70

	As 188.979 nm		Cd 228.802 nm		Pb 220.353 nm		Cr 205.560 nm	
	Det. Limit (ppm)		Det. Limit (ppm)		Det. Limit (ppm)		Det. Limit (ppm)	
	0.73		**0.11**		**0.42**		**0.14**	
Depth (cm)	As (ppm)	SD	Cd (ppm)	SD	Pb (ppm)	SD	Cr (ppm)	SD
0.5	1.07	0.43	0.00	0.00	2.92	0.29	79.90	4.55
1.5	1.37	0.32	0.00	0.00	2.41	0.09	81.40	3.88
2.5	0.76	0.58	0.00	0.00	2.66	0.39	65.92	0.28
3.5	1.28	0.32	0.13	0.02	5.81	0.47	79.68	1.81
4.5	1.64	0.15	0.00	0.00	5.28	0.61	76.74	2.78
5.5	1.09	0.11	0.00	0.00	7.39	1.06	73.31	4.72
6.5	0.00	0.00	0.00	0.00	8.55	1.42	75.08	2.25
7.5	1.20	0.60	0.12	0.03	10.80	1.50	79.82	2.45
8.5	1.47	0.24	0.00	0.00	8.00	0.55	75.66	3.01
9.5	1.42	0.47	0.00	0.00	4.44	0.32	67.73	0.91

MI1: Pyrite Phase

	Fe 238.863 nm		Ca 315.887 nm		Mn 293.305 nm	
	Det. Limit (ppm)		Det. Limit (ppm)		Det. Limit (ppm)	
	0.92		**0.90**		**0.04**	
Depth (cm)	Fe (ppm)	SD	Ca (ppm)	SD	Mn (ppm)	SD
0.5	2732.88	304.63	39.56	5.10	10.00	1.22
1.5	2037.58	54.82	30.50	3.53	4.22	0.28
2.5	1473.61	51.93	38.70	8.74	2.63	0.18
3.5	1992.10	13.94	33.99	3.00	3.66	0.08
4.5	1891.08	57.34	32.28	6.16	3.10	0.05
5.5	1674.43	95.02	37.33	9.21	3.16	0.26
6.5	1510.91	6.08	29.05	1.90	2.75	0.06
7.5	1848.11	20.66	49.66	14.82	3.98	0.17
8.5	1520.39	14.99	30.38	1.45	2.98	0.03
9.5	1204.49	11.92	29.77	4.57	2.14	0.12

	As 188.979 nm		Cd 228.802 nm		Pb 220.353 nm		Cr 205.560 nm	
	Det. Limit (ppm)		Det. Limit (ppm)		Det. Limit (ppm)		Det. Limit (ppm)	
	0.32		**0.01**		**0.10**		**0.01**	
Depth (cm)	As (ppm)	SD	Cd (ppm)	SD	Pb (ppm)	SD	Cr (ppm)	SD
0.5	3.11	0.30	0.03	0.00	0.00	0.00	0.45	0.10
1.5	2.98	0.07	0.03	0.00	0.00	0.00	0.35	0.02
2.5	3.08	0.07	0.04	0.00	0.00	0.00	0.48	0.19
3.5	5.58	0.08	0.07	0.00	0.00	0.00	0.38	0.02
4.5	5.26	0.31	0.07	0.00	0.00	0.00	0.39	0.07
5.5	4.07	0.16	0.05	0.00	0.00	0.00	0.44	0.10
6.5	3.40	0.20	0.03	0.00	0.00	0.00	0.34	0.01
7.5	3.98	0.09	0.04	0.00	0.00	0.00	0.63	0.15
8.5	3.29	0.04	0.03	0.00	0.00	0.00	0.39	0.03
9.5	2.64	0.04	0.03	0.00	0.00	0.00	0.37	0.10

MI2: Exchangeable Phase

	Fe 238.863 nm		Ca 315.887 nm		Mn 293.305 nm	
	Det. Limit (ppm)		Det. Limit (ppm)		Det. Limit (ppm)	
	0.68		**1.17**		**1.18**	
Depth (cm)	Fe (ppm)	SD	Ca (ppm)	SD	Mn (ppm)	SD
0.5	0.00	0.00	1703.47	31.71	44.69	12.11
1.5	0.00	0.00	1576.77	56.96	91.60	4.34
2.5	0.00	0.00	1185.55	250.64	147.65	34.22
3.5	0.00	0.00	1688.73	155.46	279.27	72.59
4.5	0.00	0.00	1497.40	58.08	307.40	15.60
5.5	0.00	0.00	1722.82	9.01	398.15	1.28
6.5	0.00	0.00	1709.41	53.31	438.05	17.45
7.5	0.00	0.00	1490.50	257.39	326.01	125.96
8.5	0.00	0.00	1438.23	233.68	270.35	93.23
9.5	0.00	0.00	1639.91	77.93	287.21	12.51

	As 188.979 nm		Cd 228.802 nm		Pb 220.353 nm		Cr 205.560 nm	
	Det. Limit (ppm)		Det. Limit (ppm)		Det. Limit (ppm)		Det. Limit (ppm)	
	0.40		**0.03**		**0.17**		**0.03**	
Depth (cm)	As (ppm)	SD	Cd (ppm)	SD	Pb (ppm)	SD	Cr (ppm)	SD
0.5	0.00	0.00	0.17	0.02	0.22	0.04	0.00	0.00
1.5	0.00	0.00	0.11	0.02	0.00	0.00	0.00	0.00
2.5	0.00	0.00	0.05	0.01	0.00	0.00	0.00	0.00
3.5	0.00	0.00	0.05	0.01	0.36	0.11	0.00	0.00
4.5	0.00	0.00	0.00	0.00	0.00	0.00	0.00	0.00
5.5	0.00	0.00	0.04	0.01	0.37	0.10	0.00	0.00
6.5	0.00	0.00	0.00	0.00	0.00	0.00	0.00	0.00
7.5	0.00	0.00	0.03	0.03	0.19	0.10	0.00	0.00
8.5	0.00	0.00	0.04	0.02	0.00	0.00	0.00	0.00
9.5	0.00	0.00	0.00	0.00	0.00	0.00	0.00	0.00

MI2: Oxide Phase

	Fe 253.681 nm		Ca 315.887 nm		Mn 293.305 nm	
	Det. Limit (ppm)		Det. Limit (ppm)		Det. Limit (ppm)	
	3.03		**0.69**		**0.08**	
Depth (cm)	Fe (ppm)	SD	Ca (ppm)	SD	Mn (ppm)	SD
0.5	15753.79	501.07	787.17	17.70	231.22	7.82
1.5	16170.72	613.75	964.97	81.95	265.22	14.16
2.5	13805.09	257.20	662.74	26.87	193.81	4.37
3.5	21109.83	327.87	932.97	20.89	315.69	6.05
4.5	18039.75	449.78	761.30	18.10	276.55	7.83
5.5	19491.42	407.01	817.76	7.44	335.12	2.04
6.5	20877.66	1134.54	851.34	41.80	376.71	22.96
7.5	19229.22	685.59	831.21	24.94	423.45	14.93
8.5	19333.58	401.32	914.27	20.99	549.01	12.03
9.5	19501.60	414.97	1262.93	295.54	608.93	32.58

	As 188.979 nm		Cd 228.802 nm		Pb 220.353 nm		Cr 205.560 nm	
	Det. Limit (ppm)		Det. Limit (ppm)		Det. Limit (ppm)		Det. Limit (ppm)	
	0.40		**0.05**		**1.59**		**0.13**	
Depth (cm)	As (ppm)	SD	Cd (ppm)	SD	Pb (ppm)	SD	Cr (ppm)	SD
0.5	8.10	0.30	0.16	0.03	21.36	0.15	37.18	1.25
1.5	7.04	0.62	0.18	0.01	22.58	0.84	34.80	1.37
2.5	6.53	0.58	0.22	0.01	17.98	0.41	29.09	0.39
3.5	9.65	1.15	0.26	0.01	24.35	0.10	41.41	0.97
4.5	8.55	0.53	0.20	0.02	20.79	1.70	33.62	0.63
5.5	8.98	0.41	0.26	0.02	20.52	0.05	36.09	0.71
6.5	9.00	0.19	0.24	0.01	20.45	1.08	37.93	2.11
7.5	8.35	0.48	0.21	0.02	20.04	0.71	33.95	1.15
8.5	9.22	0.41	0.22	0.01	20.70	0.45	33.33	0.46
9.5	10.23	0.36	0.34	0.02	21.71	1.18	34.67	0.44

MI2: AVS Phase

	Fe 238.863 nm		Ca 315.887 nm		Mn 293.305 nm	
	Det. Limit (ppm)		Det. Limit (ppm)		Det. Limit (ppm)	
	2.06		**0.15**		**0.05**	
Depth (cm)	Fe (ppm)	SD	Ca (ppm)	SD	Mn (ppm)	SD
0.5	2225.12	289.43	180.96	9.39	19.62	2.31
1.5	2323.85	121.55	1473.34	1067.08	21.58	0.94
2.5	1558.94	640.21	642.21	591.34	14.78	5.15
3.5	3012.60	128.53	236.54	15.03	28.67	0.51
4.5	2447.97	322.28	184.71	22.29	24.42	2.55
5.5	2524.73	93.96	186.20	8.08	26.66	1.08
6.5	2612.10	71.89	168.31	12.00	27.93	0.85
7.5	2135.29	906.89	808.49	748.04	23.55	9.43
8.5	3050.89	145.35	254.14	16.64	33.51	1.05
9.5	3212.43	332.58	201.52	11.21	36.57	2.82

	As 188.979 nm		Cd 228.802 nm		Pb 220.353 nm		Cr 205.560 nm	
	Det. Limit (ppm)		Det. Limit (ppm)		Det. Limit (ppm)		Det. Limit (ppm)	
	0.20		**0.01**		**0.21**		**0.05**	
Depth (cm)	As (ppm)	SD	Cd (ppm)	SD	Pb (ppm)	SD	Cr (ppm)	SD
0.5	0.30	0.06	0.03	0.02	0.00	0.00	3.64	0.59
1.5	0.26	0.13	0.00	0.00	0.00	0.00	3.54	0.23
2.5	0.26	0.09	0.00	0.00	0.00	0.00	2.38	1.09
3.5	0.38	0.09	0.02	0.00	0.00	0.00	4.52	0.19
4.5	0.42	0.11	0.01	0.00	0.00	0.00	3.50	0.54
5.5	0.29	0.06	0.02	0.01	0.00	0.00	3.52	0.13
6.5	0.36	0.05	0.00	0.00	0.00	0.00	3.55	0.11
7.5	0.41	0.13	0.01	0.01	0.00	0.00	2.80	1.24
8.5	0.56	0.14	0.01	0.00	0.00	0.00	4.07	0.22
9.5	0.32	0.06	0.05	0.01	0.23	0.03	4.16	0.55

MI2: Org#1 Phase

	Fe 238.863 nm		Ca 315.887 nm		Mn 293.305 nm	
	Det. Limit (ppm)		Det. Limit (ppm)		Det. Limit (ppm)	
	3.39		**0.30**		**0.26**	
Depth (cm)	Fe (ppm)	SD	Ca (ppm)	SD	Mn (ppm)	SD
0.5	265.31	17.64	0.00	0.00	0.00	0.00
1.5	231.38	51.00	0.00	0.00	0.00	0.00
2.5	189.11	31.05	0.00	0.00	0.00	0.00
3.5	317.66	16.24	0.00	0.00	0.00	0.00
4.5	227.14	11.98	0.00	0.00	0.00	0.00
5.5	330.40	9.42	0.00	0.00	0.00	0.00
6.5	297.19	10.91	0.00	0.00	0.00	0.00
7.5	271.43	16.09	0.00	0.00	0.00	0.00
8.5	259.56	22.54	0.00	0.00	0.00	0.00
9.5	427.58	16.48	0.00	0.00	0.00	0.00

	As 197.197 nm		Cd 228.802 nm		Pb 220.353 nm		Cr 267.716 nm	
	Det. Limit (ppm)		Det. Limit (ppm)		Det. Limit (ppm)		Det. Limit (ppm)	
	1.19		**0.06**		**0.91**		**0.15**	
Depth (cm)	As (ppm)	SD	Cd (ppm)	SD	Pb (ppm)	SD	Cr (ppm)	SD
0.5	2.06	0.42	0.34	0.01	0.00	0.00	1.04	0.15
1.5	2.66	0.31	0.36	0.04	0.00	0.00	0.89	0.04
2.5	1.97	0.38	0.30	0.01	0.00	0.00	0.74	0.18
3.5	2.53	0.44	0.45	0.02	0.00	0.00	0.99	0.22
4.5	1.33	0.45	0.29	0.02	0.00	0.00	0.70	0.11
5.5	1.87	0.27	0.34	0.01	0.00	0.00	0.75	0.05
6.5	2.00	0.10	0.35	0.02	0.00	0.00	0.77	0.10
7.5	2.46	0.49	0.26	0.00	0.00	0.00	0.71	0.04
8.5	1.77	0.75	0.28	0.00	0.00	0.00	0.65	0.03
9.5	1.42	0.29	0.27	0.02	0.00	0.00	0.46	0.09

MI2: Org#2 Phase

	Fe 253.681 nm		Ca 315.887 nm		Mn 293.305 nm	
	Det. Limit (ppm)		Det. Limit (ppm)		Det. Limit (ppm)	
	11.18		**3.94**		**0.41**	
Depth (cm)	Fe (ppm)	SD	Ca (ppm)	SD	Mn (ppm)	SD
0.5	29493.94	878.91	2772.00	39.90	245.55	6.35
1.5	29831.89	439.91	3237.30	328.21	249.26	4.31
2.5	25657.20	941.06	2700.63	413.79	215.88	7.08
3.5	36370.95	258.76	3330.37	21.63	304.88	2.20
4.5	28588.83	1088.51	2579.35	39.24	240.15	8.61
5.5	29615.27	386.61	2738.24	44.04	250.32	2.52
6.5	29992.88	1669.14	2732.43	158.07	254.00	15.43
7.5	30346.98	1130.28	2659.82	98.92	253.78	9.44
8.5	30782.14	640.35	2813.65	45.13	259.85	5.04
9.5	32395.01	2305.45	2709.20	135.05	276.21	18.12

	As 188.979 nm		Cd 228.802 nm		Pb 220.353 nm		Cr 205.560 nm	
	Det. Limit (ppm)		Det. Limit (ppm)		Det. Limit (ppm)		Det. Limit (ppm)	
	0.73		**0.11**		**0.42**		**0.14**	
Depth (cm)	As (ppm)	SD	Cd (ppm)	SD	Pb (ppm)	SD	Cr (ppm)	SD
0.5	0.00	0.00	0.00	0.00	1.62	0.06	85.01	1.08
1.5	0.00	0.00	0.00	0.00	1.56	0.10	86.38	2.28
2.5	0.00	0.00	0.00	0.00	1.54	0.28	74.51	2.66
3.5	0.00	0.00	0.00	0.00	2.08	0.06	105.06	1.06
4.5	0.00	0.00	0.00	0.00	1.65	0.36	82.32	3.17
5.5	0.00	0.00	0.00	0.00	1.80	0.27	87.09	1.70
6.5	0.00	0.00	0.00	0.00	1.39	0.40	88.33	5.01
7.5	0.00	0.00	0.00	0.00	1.81	0.24	88.14	3.18
8.5	0.00	0.00	0.00	0.00	1.61	0.37	88.36	2.17
9.5	0.00	0.00	0.00	0.00	1.95	0.24	92.07	5.94

MI2: Pyrite Phase

	Fe 238.863 nm		Ca 315.887 nm		Mn 293.305 nm	
	Det. Limit (ppm)		Det. Limit (ppm)		Det. Limit (ppm)	
	0.92		**0.90**		**0.04**	
Depth (cm)	Fe (ppm)	SD	Ca (ppm)	SD	Mn (ppm)	SD
0.5	1017.50	32.39	36.58	12.96	2.65	0.24
1.5	1037.96	35.88	23.13	1.32	2.54	0.09
2.5	914.51	44.29	22.85	6.29	2.28	0.17
3.5	1131.57	24.15	27.55	3.42	2.74	0.08
4.5	857.48	96.89	19.23	6.44	2.11	0.41
5.5	981.07	8.01	20.65	3.62	2.38	0.07
6.5	847.49	52.68	16.03	1.62	2.03	0.15
7.5	813.06	42.56	17.84	3.99	1.91	0.15
8.5	1045.60	26.85	19.96	0.88	2.64	0.02
9.5	743.78	59.35	12.11	7.24	1.58	0.13

	As 188.979 nm		Cd 228.802 nm		Pb 220.353 nm		Cr 205.560 nm	
	Det. Limit (ppm)		Det. Limit (ppm)		Det. Limit (ppm)		Det. Limit (ppm)	
	0.32		**0.01**		**0.10**		**0.01**	
Depth (cm)	As (ppm)	SD	Cd (ppm)	SD	Pb (ppm)	SD	Cr (ppm)	SD
0.5	0.61	0.13	0.01	0.00	0.00	0.00	0.56	0.20
1.5	0.84	0.10	0.02	0.00	0.00	0.00	0.33	0.00
2.5	0.85	0.05	0.01	0.00	0.00	0.00	0.34	0.07
3.5	0.98	0.13	0.02	0.00	0.00	0.00	0.46	0.05
4.5	0.67	0.13	0.00	0.00	0.00	0.00	0.40	0.17
5.5	0.84	0.05	0.01	0.00	0.00	0.00	0.32	0.06
6.5	0.74	0.10	0.00	0.00	0.00	0.00	0.29	0.03
7.5	0.73	0.09	0.00	0.00	0.00	0.00	0.30	0.06
8.5	0.95	0.09	0.01	0.01	0.00	0.00	0.40	0.01
9.5	0.64	0.04	0.01	0.00	0.00	0.00	0.28	0.03

APPENDIX E

TOTAL SEDIMENT DIGESTS DATA ALL CORES

ER1: Total Digest

	Fe 253.681 nm		Ca 315.887 nm		Mn 293.305 nm	
	Det. Limit (ppm)		Det. Limit (ppm)		Det. Limit (ppm)	
	0.60		**0.29**		**0.03**	
Depth (cm)	Fe (ppm)	SD	Ca (ppm)	SD	Mn (ppm)	SD
0.5	35156.82	214.02	12058.73	47.59	531.48	6.90
1.5	31480.85	132.14	11181.51	50.78	396.18	0.37
2.5	23633.04	792.39	7465.68	253.52	339.26	3.32
3.5	25816.42	64.59	7925.06	236.87	338.91	4.49
4.5	24242.47	13.81	6702.85	120.68	322.38	2.09
5.5	29419.26	504.86	6790.18	415.66	351.10	2.03
6.5	37436.57	567.93	5831.94	10.16	371.26	7.29
7.5	37523.10	230.70	5774.54	20.40	389.40	1.68
8.5	42419.64	93.34	5541.40	40.35	434.48	2.16
9.5	48237.50	379.71	5353.49	65.70	467.24	0.50

	As 188.979 nm		Cd 228.802 nm		Pb 220.353 nm		Cr 205.560 nm	
	Det. Limit (ppm)		Det. Limit (ppm)		Det. Limit (ppm)		Det. Limit (ppm)	
	0.10		**0.01**		**0.06**		**0.02**	
Depth (cm)	As (ppm)	SD	Cd (ppm)	SD	Pb (ppm)	SD	Cr (ppm)	SD
0.5	13.30	2.06	0.91	0.03	35.01	2.94	67.61	0.39
1.5	8.34	0.22	0.71	0.03	39.38	0.41	56.48	0.60
2.5	5.60	0.08	0.63	0.04	116.13	28.30	46.14	4.79
3.5	5.43	0.12	0.76	0.02	32.88	0.63	41.84	0.81
4.5	5.89	0.73	0.76	0.03	32.72	0.41	42.39	0.54
5.5	8.73	0.28	0.93	0.02	43.63	0.43	50.72	0.22
6.5	11.22	0.96	0.99	0.06	57.24	0.54	66.70	1.04
7.5	10.96	0.15	1.23	0.04	63.16	0.35	66.93	0.31
8.5	14.53	0.24	1.52	0.05	75.03	0.94	75.19	0.26
9.5	15.36	0.57	1.39	0.03	77.35	0.68	84.83	0.31

ER2: Total Digest

	Fe 253.681 nm		Ca 315.887 nm		Mn 293.305 nm	
	Det. Limit (ppm)		Det. Limit (ppm)		Det. Limit (ppm)	
	0.60		**0.29**		**0.03**	
Depth (cm)	Fe (ppm)	SD	Ca (ppm)	SD	Mn (ppm)	SD
0.5	44055.07	392.75	6630.32	207.30	397.35	0.62
1.5	41177.38	689.72	5579.78	64.91	337.14	3.40
2.5	42063.01	181.10	5224.50	16.82	388.74	2.46
3.5	40050.00	605.63	5060.21	44.75	343.73	3.07
4.5	40227.71	646.77	4812.17	101.38	331.09	4.67
5.5	39024.75	198.74	4855.26	44.78	300.92	0.70
6.5	39615.31	77.39	5339.50	46.07	322.64	0.53
7.5	37124.89	8.05	5375.41	21.07	334.80	8.25
8.5	38119.16	318.29	5003.16	18.49	376.95	0.61
9.5	37250.68	4.68	4824.43	91.85	362.57	4.34

	As 188.979 nm		Cd 228.802 nm		Pb 220.353 nm		Cr 205.560 nm	
	Det. Limit (ppm)		Det. Limit (ppm)		Det. Limit (ppm)		Det. Limit (ppm)	
	0.10		**0.01**		**0.06**		**0.02**	
Depth (cm)	As (ppm)	SD	Cd (ppm)	SD	Pb (ppm)	SD	Cr (ppm)	SD
0.5	15.00	0.29	0.53	0.03	85.22	1.52	79.33	1.30
1.5	12.08	0.52	0.53	0.00	83.46	1.05	77.91	0.10
2.5	14.63	0.00	0.36	0.01	56.37	1.14	76.42	0.26
3.5	14.55	0.03	0.36	0.03	62.25	0.39	74.44	1.09
4.5	12.09	1.07	0.45	0.03	71.09	0.79	75.58	0.71
5.5	11.99	0.36	0.41	0.05	76.82	0.43	72.88	0.42
6.5	11.64	0.08	1.30	0.76	78.24	1.63	75.29	1.05
7.5	10.42	0.07	0.58	0.06	67.78	0.95	70.57	0.71
8.5	11.16	0.26	0.31	0.03	36.23	0.68	70.54	2.98
9.5	9.76	0.71	0.32	0.00	36.64	0.45	65.86	0.84

BH1: Total Digests

	Fe 253.681 nm		Ca 315.887 nm		Mn 293.305 nm	
	Det. Limit (ppm)		Det. Limit (ppm)		Det. Limit (ppm)	
	0.60		**0.29**		**0.03**	
Depth (cm)	Fe (ppm)	SD	Ca (ppm)	SD	Mn (ppm)	SD
0.5	74727.26	63.16	3510.05	31.99	1619.88	6.51
1.5	75341.10	695.97	3392.73	48.08	1658.68	22.11
2.5	76423.77	63.78	3501.80	17.64	1666.95	11.95
3.5	73231.05	140.54	3235.03	54.54	1476.28	6.75
4.5	72386.71	609.27	2986.89	4.63	1367.65	5.71
5.5	71024.56	228.68	2898.02	9.48	1356.62	5.82
6.5	65818.34	281.57	2949.91	61.93	1470.58	4.00
7.5	64004.08	419.84	2795.55	26.61	1442.93	5.94
8.5	66153.77	529.41	2970.61	40.26	1504.91	9.79
9.5	63827.56	219.93	3082.56	43.52	1465.59	1.17

	As 188.979 nm		Cd 228.802 nm		Pb 220.353 nm		Cr 205.560 nm	
	Det. Limit (ppm)		Det. Limit (ppm)		Det. Limit (ppm)		Det. Limit (ppm)	
	0.10		**0.01**		**0.06**		**0.02**	
Depth (cm)	As (ppm)	SD	Cd (ppm)	SD	Pb (ppm)	SD	Cr (ppm)	SD
0.5	47.43	0.17	0.74	0.01	109.30	0.59	302.09	0.86
1.5	47.75	0.93	0.76	0.03	109.26	1.17	308.26	5.09
2.5	48.01	0.66	0.75	0.00	109.34	0.44	308.92	1.12
3.5	43.99	0.60	0.73	0.03	104.77	0.88	289.90	1.58
4.5	42.45	0.58	0.77	0.03	108.49	0.80	284.07	1.52
5.5	40.14	0.77	0.77	0.01	109.27	0.61	257.14	2.01
6.5	38.40	0.74	0.72	0.03	98.95	0.81	194.67	0.50
7.5	39.26	0.19	0.79	0.01	100.56	0.35	185.54	0.50
8.5	40.25	0.45	0.77	0.00	100.87	0.85	187.23	2.68
9.5	40.78	0.19	0.84	0.02	94.53	0.41	152.60	1.14

BH2: Total Digests

	Fe 253.681 nm		Ca 315.887 nm		Mn 293.305 nm	
	Det. Limit (ppm)		Det. Limit (ppm)		Det. Limit (ppm)	
	0.60		**0.29**		**0.03**	
Depth (cm)	Fe (ppm)	SD	Ca (ppm)	SD	Mn (ppm)	SD
0.5	45792.48	976.35	10088.75	230.25	664.62	8.14
1.5	45698.24	329.89	8138.85	121.66	519.50	4.94
2.5	47659.19	270.04	7541.99	74.22	523.86	5.99
3.5	47931.88	153.28	7621.88	38.98	531.11	2.97
4.5	50177.95	634.97	6246.14	123.21	545.15	4.51
5.5	49372.17	98.59	6222.11	96.29	559.93	1.02
6.5	50152.30	89.01	6094.40	153.01	681.11	1.30
7.5	50099.54	236.84	6114.59	68.58	739.04	3.15
8.5	50080.06	38.08	6797.24	64.95	765.32	0.44
9.5	50979.41	568.69	7061.15	129.43	729.47	6.34

	As 188.979 nm		Cd 228.802 nm		Pb 220.353 nm		Cr 205.560 nm	
	Det. Limit (ppm)		Det. Limit (ppm)		Det. Limit (ppm)		Det. Limit (ppm)	
	0.10		**0.01**		**0.06**		**0.02**	
Depth (cm)	As (ppm)	SD	Cd (ppm)	SD	Pb (ppm)	SD	Cr (ppm)	SD
0.5	11.61	0.61	0.83	0.07	73.61	4.61	202.08	4.56
1.5	12.18	0.06	0.86	0.00	88.09	3.80	206.08	0.26
2.5	17.67	1.33	1.09	0.03	98.04	0.14	223.69	0.77
3.5	15.76	0.42	1.12	0.00	97.03	0.81	220.47	0.43
4.5	22.04	0.13	1.28	0.00	113.85	1.89	253.36	1.10
5.5	18.10	0.27	1.03	0.00	98.19	0.28	213.79	1.43
6.5	15.55	0.28	0.85	0.00	84.48	0.92	189.41	1.94
7.5	13.32	0.54	0.74	0.04	79.88	0.96	175.35	0.52
8.5	11.73	0.04	0.65	0.01	80.62	1.38	172.48	2.33
9.5	13.60	0.08	0.74	0.01	89.24	1.29	178.17	1.82

MI1: Total Digests

	Fe 253.681 nm		Ca 315.887 nm		Mn 293.305 nm	
	Det. Limit (ppm)		Det. Limit (ppm)		Det. Limit (ppm)	
	0.60		**0.29**		**0.03**	
Depth (cm)	Fe (ppm)	SD	Ca (ppm)	SD	Mn (ppm)	SD
0.5	54082.21	346.19	12079.27	153.16	885.17	3.46
1.5	47701.88	937.96	10500.72	255.29	656.39	10.98
2.5	43824.47	447.01	10339.76	177.41	613.56	1.13
3.5	43619.77	209.56	9507.97	63.09	682.72	3.36
4.5	45310.94	51.94	9381.58	73.95	786.43	1.06
5.5	47730.41	52.01	9318.08	21.09	784.17	13.16
6.5	47113.77	152.09	8465.70	332.40	757.01	1.04
7.5	48125.60	310.69	8360.72	17.08	756.43	3.44
8.5	41302.65	3195.26	9870.49	421.98	655.83	52.00
9.5	46541.80	219.86	8604.91	83.45	772.92	3.81

	As 188.979 nm		Cd 228.802 nm		Pb 220.353 nm		Cr 205.560 nm	
	Det. Limit (ppm)		Det. Limit (ppm)		Det. Limit (ppm)		Det. Limit (ppm)	
	0.10		**0.01**		**0.06**		**0.02**	
Depth (cm)	As (ppm)	SD	Cd (ppm)	SD	Pb (ppm)	SD	Cr (ppm)	SD
0.5	10.31	1.08	0.26	0.01	18.18	0.90	437.03	10.12
1.5	11.45	0.74	0.30	0.04	36.26	13.84	223.33	12.06
2.5	12.47	1.08	0.31	0.00	19.86	0.26	176.64	10.79
3.5	13.68	0.53	0.42	0.01	23.56	0.10	168.17	10.94
4.5	15.36	0.17	0.46	0.05	27.45	0.67	171.21	6.17
5.5	15.68	0.22	0.59	0.04	32.93	0.65	171.31	1.14
6.5	17.13	0.14	0.69	0.01	46.50	0.64	164.43	3.55
7.5	18.05	0.08	0.66	0.01	46.79	0.55	163.41	1.20
8.5	14.87	1.33	0.51	0.03	34.99	2.45	158.97	10.80
9.5	17.68	0.14	0.59	0.00	44.22	1.74	159.06	0.12

MI2: Total Digests

	Fe 253.681 nm		Ca 315.887 nm		Mn 293.305 nm	
	Det. Limit (ppm)		Det. Limit (ppm)		Det. Limit (ppm)	
	0.60		**0.29**		**0.03**	
Depth (cm)	Fe (ppm)	SD	Ca (ppm)	SD	Mn (ppm)	SD
0.5	47510.09	34.35	7434.46	111.65	603.71	1.00
1.5	45173.69	169.56	7743.97	188.49	516.12	0.91
2.5	47767.18	258.99	7265.53	43.34	645.00	4.03
3.5	50099.62	207.42	7615.45	174.02	736.25	5.06
4.5	49662.44	229.33	7176.78	20.12	818.78	1.89
5.5	50172.15	218.57	7376.43	102.34	910.93	1.41
6.5	51276.09	26.72	7353.82	44.61	939.77	0.00
7.5	50642.66	198.76	7573.07	44.02	987.75	5.62
8.5	49768.79	192.08	7704.41	1.80	1008.45	2.14
9.5	50819.84	254.50	7482.33	34.08	1089.59	3.35

	As 188.979 nm		Cd 228.802 nm		Pb 220.353 nm		Cr 205.560 nm	
	Det. Limit (ppm)		Det. Limit (ppm)		Det. Limit (ppm)		Det. Limit (ppm)	
	0.10		**0.01**		**0.06**		**0.02**	
Depth (cm)	As (ppm)	SD	Cd (ppm)	SD	Pb (ppm)	SD	Cr (ppm)	SD
0.5	8.00	0.27	0.22	0.04	18.02	0.05	161.72	1.13
1.5	8.60	0.84	0.34	0.17	16.89	0.00	161.28	0.07
2.5	8.00	0.62	0.24	0.02	17.95	0.10	163.40	1.20
3.5	8.15	0.01	0.20	0.00	18.06	0.32	164.86	1.02
4.5	10.01	0.06	0.18	0.04	17.20	0.29	161.50	0.71
5.5	11.18	0.54	0.21	0.01	17.15	0.32	159.13	0.94
6.5	11.34	0.75	0.21	0.03	17.31	0.12	162.29	0.43
7.5	11.34	0.21	0.20	0.03	16.78	0.11	162.04	0.13
8.5	10.01	0.07	0.17	0.02	16.73	0.30	160.01	0.64
9.5	11.53	0.16	0.27	0.03	17.95	0.40	161.02	1.05

APPENDIX F

TOTAL CARBON, NITROGEN, AND SULFUR DATA ALL CORES

ELIZABETH RIVER CORES

ER1						
Depth (cm)	%N	SD	%C	SD	%S	SD
0.5	0.117	0.005	2.003	0.089	0.566	0.015
1.5	0.101	0.002	1.822	0.072	0.462	0.005
2.5	0.146	0.007	2.126	0.138	0.541	0.014
3.5	0.062	0.008	1.591	0.057	0.303	0.046
4.5	0.067	0.009	1.352	0.064	0.466	0.063
5.5	0.132	0.000	2.019	0.009	1.103	0.020
6.5	0.103	0.002	1.782	0.060	0.878	0.035
7.5	0.142	0.001	2.153	0.071	1.248	0.013
8.5	0.175	0.004	3.286	0.224	1.577	0.047
9.5	0.154	0.003	2.494	0.036	1.661	0.003

ER2						
Depth (cm)	%N	SD	%C	SD	%S	SD
0.5	0.288	0.019	3.245	0.086	0.891	0.146
1.5	0.177	0.032	2.586	0.236	0.912	0.120
2.5	0.148	0.007	2.879	0.188	0.991	0.098
3.5	0.205	0.020	3.895	0.809	2.600	0.335
4.5	0.176	0.013	2.841	0.062	2.951	0.095
5.5	0.184	0.006	3.048	0.067	2.829	0.111
6.5	0.213	0.002	3.458	0.022	3.273	0.089
7.5	0.204	0.002	3.366	0.059	3.191	0.074
8.5	0.142	0.006	2.635	0.033	2.675	0.147
9.5	0.150	0.003	2.871	0.068	3.488	0.107

BALTIMORE HARBOR CORES

BH1						
Depth (cm)	%N	SD	%C	SD	%S	SD
0.5	0.329	0.006	5.030	0.002	0.507	0.002
1.5	0.309	0.006	4.587	0.106	0.454	0.003
2.5	0.292	0.008	4.490	0.063	0.415	0.026
3.5	0.285	0.004	4.325	0.047	0.432	0.005
4.5	0.241	0.000	3.790	0.038	0.730	0.031
5.5	0.213	0.001	2.771	0.060	1.548	0.050
6.5	0.236	0.003	3.552	0.030	1.508	0.105
7.5	0.227	0.005	3.197	0.031	1.351	0.055
8.5	0.217	0.001	2.755	0.032	1.854	0.103
9.5	0.218	0.001	2.888	0.088	1.755	0.098

BH2						
Depth (cm)	%N	SD	%C	SD	%S	SD
0.5	0.197	0.002	2.933	0.031	0.397	0.010
1.5	0.173	0.003	2.663	0.034	0.547	0.009
2.5	0.176	0.001	2.731	0.032	0.675	0.009
3.5	0.169	0.001	2.710	0.033	0.701	0.018
4.5	0.158	0.002	2.531	0.016	0.940	0.002
5.5	0.155	0.002	2.517	0.048	0.863	0.005
6.5	0.135	0.001	2.240	0.009	0.814	0.020
7.5	0.122	0.002	2.216	0.017	0.759	0.013
8.5	0.118	0.001	2.156	0.021	0.752	0.016
9.5	0.132	0.001	2.352	0.014	1.020	0.006

MARE ISLAND CORES

MI1						
Depth (cm)	%N	SD	%C	SD	%S	SD
0.5	0.120	0.010	1.460	0.090	0.360	0.070
1.5	0.110	0.002	1.460	0.030	0.560	0.010
2.5	0.120	0.001	1.550	0.010	0.480	0.030
3.5	0.110	0.001	1.400	0.020	0.410	0.020
4.5	0.110	0.004	1.540	0.080	0.370	0.010
5.5	0.130	0.003	1.740	0.020	0.530	0.030
6.5	0.130	0.001	1.730	0.020	0.500	0.004
7.5	0.140	0.003	2.000	0.070	0.600	0.020
8.5	0.110	0.002	1.550	0.020	0.540	0.020
9.5	0.100	0.001	1.440	0.020	0.360	0.020

MI2						
Depth (cm)	%N	SD	%C	SD	%S	SD
0.5	0.130	0.003	1.600	0.014	0.098	0.012
1.5	0.130	0.003	1.560	0.014	0.096	0.012
2.5	0.150	0.001	1.510	0.018	0.200	0.008
3.5	0.150	0.002	1.520	0.015	0.230	0.014
4.5	0.150	0.001	1.540	0.009	0.230	0.010
5.5	0.160	0.000	1.640	0.015	0.290	0.003
6.5	0.150	0.005	1.530	0.062	0.280	0.012
7.5	0.160	0.000	1.520	0.010	0.230	0.013
8.5	0.160	0.002	1.550	0.006	0.210	0.009
9.5	0.170	0.001	1.800	0.015	0.200	0.010

APPENDIX G

AVS AND PYRITE SULFIDE TO CALCULATED FE EQUIVALANTS ALL CORES

ELIZABETH RIVER CORES

ER1				
Depth (cm)	AVS Fe Equivalent (ppm)	AVS Fe Equivalent SD (ppm)	Pyrite Fe Equivalent (ppm)	Pyrite Fe Equivalent SD (ppm)
0.5	3.19	0.05	2180.45	97.89
1.5	0.80	0.06	2257.06	72.69
2.5	25.18	1.53	2577.05	171.92
3.5	61.46	6.21	3360.03	144.02
4.5	235.21	3.99	2808.98	117.61
5.5	911.55	45.35	4262.15	122.11
6.5	870.33	34.35	5238.66	161.86
7.5	1033.40	31.11	5860.73	29.92
8.5	384.40	27.95	6243.23	294.78
9.5	2903.09	23.53	7135.26	298.26

ER2				
Depth (cm)	AVS Fe Equivalent (ppm)	AVS Fe Equivalent SD (ppm)	Pyrite Fe Equivalent (ppm)	Pyrite Fe Equivalent SD (ppm)
0.5	6.51	0.24	7676.46	340.13
1.5	186.99	12.74	6116.05	173.02
2.5	668.90	48.26	6781.28	12.51
3.5	919.84	9.71	7394.59	260.26
4.5	549.87	14.24	10242.94	240.30
5.5	1230.99	5.55	8003.37	40.96
6.5	1225.21	16.28	8985.26	300.83
7.5	1231.06	34.28	9253.57	644.01
8.5	276.42	15.44	8984.57	476.39
9.5	493.25	2.11	8526.18	46.82

BALTIMORE HARBOR CORES

BH1				
Depth (cm)	AVS Fe Equivalent (ppm)	AVS Fe Equivalent SD (ppm)	Pyrite Fe Equivalent (ppm)	Pyrite Fe Equivalent SD (ppm)
0.5	47.35	3.81	3241.04	110.37
1.5	16.71	0.76	3519.47	155.89
2.5	12.45	0.27	2641.38	114.29
3.5	182.62	6.11	4471.64	101.32
4.5	1246.30	47.40	6589.54	80.53
5.5	1959.71	35.19	7835.50	512.40
6.5	3358.48	43.37	9226.45	429.56
7.5	3467.53	45.30	9050.68	155.40
8.5	3218.41	31.88	12021.44	887.77
9.5	3555.31	38.43	15723.15	249.99

BH2				
Depth (cm)	AVS Fe Equivalent (ppm)	AVS Fe Equivalent SD (ppm)	Pyrite Fe Equivalent (ppm)	Pyrite Fe Equivalent SD (ppm)
0.5	169.40	11.15	2149.06	77.04
1.5	676.99	48.37	2924.86	104.32
2.5	844.38	44.45	4080.71	146.23
3.5	1239.88	25.11	4404.36	178.16
4.5	1329.70	54.27	6343.96	16.34
5.5	1247.08	51.62	5867.73	34.24
6.5	894.96	46.90	5811.96	251.89
7.5	1410.39	12.91	6281.75	275.12
8.5	1061.00	53.79	6736.05	198.45
9.5	1132.12	25.82	7213.39	59.58

MARE ISLAND CORES

MI1				
Depth (cm)	AVS Fe Equivalent (ppm)	AVS Fe Equivalent SD (ppm)	Pyrite Fe Equivalent (ppm)	Pyrite Fe Equivalent SD (ppm)
0.5	1316.09	35.67	1506.14	10.24
1.5	1544.22	46.99	1599.26	17.12
2.5	1680.56	18.62	1615.70	31.16
3.5	3407.98	6.78	866.83	23.68
4.5	3953.88	27.65	1589.39	8.63
5.5	4630.26	49.72	1268.21	12.76
6.5	4434.12	45.05	1739.75	19.13
7.5	3416.57	38.14	2111.92	47.63
8.5	3081.65	41.70	1774.61	3.74
9.5	1977.52	41.15	1812.55	28.42

MI2				
Depth (cm)	AVS Fe Equivalent (ppm)	AVS Fe Equivalent SD (ppm)	Pyrite Fe Equivalent (ppm)	Pyrite Fe Equivalent SD (ppm)
0.5	37.10	0.62	1173.04	29.76
1.5	34.18	0.03	1145.09	42.61
2.5	181.64	3.80	1211.65	33.89
3.5	300.89	3.55	886.29	23.76
4.5	498.97	13.56	1060.62	22.24
5.5	583.99	15.52	1110.37	13.04
6.5	610.80	14.24	1186.14	1.13
7.5	491.27	5.12	1006.88	0.54
8.5	397.13	6.91	1025.16	5.99
9.5	668.53	17.71	1220.78	7.49

VITA

Brandon Gipson

Department of Ocean, Earth, and
Atmospheric Sciences
4600 Elkhorn Ave.
Norfolk, Va. 23529
757-683-4929

35260 Seacock Chaple Rd.
Zuni Va., 23898
(757)-647-8741

EDUCATION

Old Dominion University, Norfolk, Virginia
Master of Science, Ocean and Earth Sciences, December 2012
Concentration in Chemical Oceanography
GPA 3.59

Old Dominion University, Norfolk, Virginia
Bachelor of Science, Ocean and Earth Sciences, May 2007
Concentration in Geological Oceanography
Minor: Chemistry
GPA 3.4

WORK EXPERIENCE

Graduate Research Assistant **09/09 - 05/12**
Supervisor: Dr. Gregory Cutter
Old Dominion University, Norfolk, Virginia

Research Associate **04/08 - 08/09**
Supervisor: Dr. Gregory Cutter
Old Dominion University, Norfolk, Virginia

FIELD EXPERIENCE

Sea Going:

R/V Knorr- GEOTRACES: Nov.- Dec. 2011 GEOTRACES North Atlantic Zonal Transect Cruise, 35 days at sea

R/V Knorr- GEOTRACES: May 2009 GEOTRACES Intercalibration Pacific Cruise, 24 days at sea

R/V Knorr- GEOTRACES: June-July 2008 GEOTRACES Intercalibration Atlantic Cruise, 35 days at sea

SELECTED PUBLICATIONS

Zimmer, L., Gipson, B., Wurl, O., and Cutter, G.A. 2012. Distributions of nanomolar reactive phosphate and alkaline phosphatase across North Atlantic surface waters. Presented at the 2012 Ocean Sciences Meeting.

Gipson, B.R., and Cutter, G.A. 2012. A new phase speciation leaching procedure for determination of metals in both oxic and anoxic estuarine sediments. Presented at the 2012 Ocean Sciences Meeting.